University of Alberta

Phase Behaviour Prediction for Ill-Defined Hydrocarbon Mixtures

by

Nima Saber

A thesis submitted to the Faculty of Graduate Studies and Research
in partial fulfillment of the requirements for the degree of

Doctor of Philosophy
in
Chemical Engineering

Department of Chemical and Materials Engineering

©Nima Saber
Spring 2011
Edmonton, Alberta

Permission is hereby granted to the University of Alberta Libraries to reproduce single copies of this thesis and to lend or sell such copies for private, scholarly or scientific research purposes only. Where the thesis is converted to, or otherwise made available in digital form, the University of Alberta will advise potential users of the thesis of these terms.

The author reserves all other publication and other rights in association with the copyright in the thesis and, except as herein before provided, neither the thesis nor any substantial portion thereof may be printed or otherwise reproduced in any material form whatsoever without the author's prior written permission.

Abstract

Phase behaviour information is essential for the development and optimization of hydrocarbon resource production, transport and refining technologies. Experimental data sets for mixtures containing heavy oil and bitumen are sparse as phase behaviour data are difficult to obtain and cost remains prohibitive for most applications. A computational tool that predicts phase behaviours reliably for mixtures containing such ill-defined components, over broad temperature, pressure and composition ranges would play a central role in the advancement of bitumen production and refining process knowledge and would have favourable impacts on the economics and environmental effects linked to the exploitation of such ill-defined hydrocarbon resources.

Prior to this work, predictive computational methods were reliable for dilute mixtures of ill-defined constituents. To include a much wider range of conditions, three major challenges were addressed. The challenges include: creation of a robust and accurate numerical approach, implementation of a reliable thermodynamic model, and speciation of ill-defined constituents like Athabasca Bitumen Vacuum Residue (AVR). The first challenge was addressed by creating a novel computational approach based on a global minimization method for phase equilibrium calculations. The second challenge was tackled by proposing a thermodynamic model that combines the Peng-Robinson equation of state with group contribution and related parameter prediction methods. The speciation challenge was addressed by another research group at the University of Alberta.

Pseudo components they proposed were used to assign groups and estimate thermodynamic properties.

The new phase equilibrium computational tool was validated by comparing simulated phase diagrams with experimental data for mixtures containing AVR and n-alkanes. There is good qualitative and quantitative agreement between computed and experimental phase diagrams over industrially relevant ranges of compositions, pressures and temperatures. Mismatch was only observed over a limited range of compositions, temperatures and pressures. This computational breakthrough provides, for the first time, a platform for reliable phase behaviour computations with broad potential for application in the hydrocarbon resource sector. The specific computational results can be applied directly to solvent assisted recovery, paraffinic deasphalting, and distillation and refining processes for Athabasca bitumen a strategic resource for Canada.

Acknowledgment

My deepest gratitude goes to my family and above all, my parents for their love and support. I thank them for being a great encouragement in my life.

I am grateful for the help and guidance of my supervisor, Dr. John Shaw, whose patience, kindness, encouragement, and knowledge made the preparation of this thesis possible and kept me going. Under his supervision, I have gained an invaluable experience and for that I am forever in his debt.

I would also like to thank Dr. Marco Satyro (Department of Chemical and Petroleum Engineering, University of Calgary), Dr. Janet Elliott, Dr. Anthony Yeung, and Dr. Carolina diaz (now at Schlumberger) for their support and advice. I acknowledge Daniel E. Finkel for tips concerning the implementation of the DIRECT algorithm, Dr. Rafiqul Gani (Department of Chemical Engineering, Technical University of Denmark) for providing the latest version of the ProPred software, which was extremely helpful in applying group contribution methods to the molecular representations produced by Jeff Sheremata, and Dr. Jacek Gregorowicz (Polish Academy of Sciences) for providing computational data.

I had the pleasure of working with my colleagues (Mohammad Javad Amani, Jesus Amundarain, Nafiseh Dadgostar, Moïse Dion, Keivan Khaleghi, Merouane Khammar, Václav Laštovka, Brady Masik, Sepideh Mortazavi Manesh, Kasra Nikooyeh, Collins Obiosa-Maife, Ardalan Sadighian, Khanh Tran, Annemi Van Waeyenberghe, Cheng Xing, Bei Zhao, and Xiaohui Zhang) in the Petroleum Thermodynamic group. I am particularly thankful to my colleague Kasra Nikooyeh for reviewing the draft of this thesis and pointing out my grammatical mistakes and suggesting changes to make this work clearer. I would also like to thank Dr. Richard McFarlane (now at Alberta Research Council) for his valuable feedback and suggestions. I am also grateful to Mildred Becerra for her help and advice. I am thankful to Dr. Xiangyang Zou and Dr. Xiaohui Zhang for providing experimental phase behaviour data.

I am especially indebted to Dr. Jeff Sheremata (now at ConocoPhillips) for sharing his results and code on molecular representations for Athabasca bitumen and its residue.

I would like to thank Alberta Innovates, the Alberta Energy Research Institute (AERI), ConocoPhillips Canada Inc., Imperial Oil Resources, Kellogg Brown and Root Energy and Chemicals (KBR), Natural Sciences and Engineering Research Council of Canada (NSERC), NEXEN Inc., Shell Canada Ltd. Halliburton Energy Services, and Total E&P Canada for their financial support.

Table of Contents

List of Tables

List of Figures

Nomenclature

A	intermediate parameter based on equation of state parameter a
a or a(T)	temperature dependent equation of state energy parameter
a_c	parameter in Peng-Robinson Equation of State
B	intermediate parameter based on equation of state parameter b
b	equation of state co-volume parameter
d	equation of state parameter
e	equation of state parameter
F	amount of feed in mole
F(**x**)	tangent plane distance function (TPDF)
$f_i(m)$	function used in the estimation of parameter a (i = 1,2)
$\hat{f}_i$	fugacity of component i in the mixture
G	Gibbs free energy
K	vector of equilibrium factors
k_{ij}	binary interaction coefficient
M	number of first order groups in the method of Marrero and Gani
m	shape parameter
N	number of second order groups in the method of Marrero and Gani
N_c	number of components
N_g	number of different groups defined by the PPR78 method
N_j	number of functional groups of type j
N_p	number of phases
n	number of moles
O	number of third order groups in the method of Marrero and Gani

P	pressure
P_C	critical pressure
pc	contribution to critical pressure
P_r	reduced pressure
P^{sat}	saturation pressure
$Q(\beta)$	alternative function for three-phase equilibrium calculations
R	universal gas constant
S	total entropy
S	intermediate variable used in the estimation of parameters b and m
SG	specific gravity
T	temperature
T_b	boiling point temperature
T_C	critical temperature
tc	contribution to critical temperature
T_r	reduced temperature
U	total internal energy
V	total volume
v	molar volume
V_{Wj}	contribution of the j^{th} group to the van der Waals volume
$\mathbf{x}$	trial composition vector
x_i	mole fraction of component i
y_i	mole fraction of component i
Z	compressibility factor
$\mathbf{z}$	feed composition vector
Z_c	critical compressibility factor

z_i	mole fraction of component i in feed

Greek letters

α	temperature-dependent equation of state parameter
α_{ik}	fraction of molecule i occupied by group k for k_{ij} calculation
β	phase fraction
ε_i	(i=1) first and (i=2) second order contributions to acentric factor
μ	chemical potential
ω	acentric factor
δV_{WK}	correction to van der Waals volume
ϕ	fugacity coefficient
θ_1	normal boiling point
θ_2	specific gravity

Abbreviations

AVR	Athabasca vacuum residue
DIRECT	dividing rectangles
K	K-point, three-phase critical point
L	L-point, three-phase critical point
L	liquid
L1	lighter liquid phase
L2	denser liquid phase
LLV	liquid-liquid-vapour
LV	liquid-vapour

NMR	nuclear magnetic resonance
PPR78	predictive Peng-Robinson 78 method
PVT	pressure-volume-temperature
TPDF	tangent plane distance function
SARA	saturates-aromatics-resins-asphaltenes
SAFT	statistical associating fluid theory
SRK	Soave-Redlich-Kwong
TBP	true boiling curve
V	vapour
VAPEX	vapour extraction process
vdW	van der Waals

Chapter 1
Introduction

Phase behaviour measurement and prediction are of great importance in chemical and petroleum engineering applications. Successful design of chemical and petroleum processes, whether production, transport, refining or petrochemical in nature, depend on the correct prediction of phase behaviour and the estimation of thermodynamic properties such as phase composition and density, enthalpy, and heat capacity of pure fluids and mixtures. These properties are also key inputs for the development and optimization of process technologies. As Canada possesses among the largest hydrocarbon resource reserves in the world, advances in this area will have a significant impact on the country's economy. Due to the scale of the industry, even small improvements in the design of production and upgrading processes have large impacts on energy consumption, greenhouse gas emission and waste generation associated with these processes.

For mixtures containing heavy hydrocarbons and bitumen, thermodynamic properties and phase behaviour data are sparse, and will remain so because data are difficult to obtain experimentally. The materials themselves present challenges as do the conditions under which measurements are needed. Although significant advances have been made over the past two decades in measurement, costs remain prohibitive for most applications. The development of novel view-cells and accessories for experimental phase behaviour measurements allow researchers, for the first time, to tackle phase behaviour prediction for bitumen and heavy oil containing mixtures and to benchmark their computations against reliable phase behaviour data [1-2]. Although commercial simulators make phase behaviour prediction possible in a general sense, there are no methods available for heavy oil and bitumen phase behaviour prediction. A computational tool that can predict the phase behaviour using phase equilibrium calculations for such mixtures with sufficient precision for design applications can play a major role in the advancement of bitumen production and refining processes.

The available computational techniques for phase equilibrium calculations are well established, but do not guarantee convergence to correct phase behaviours. The possibility of false phase behaviour predictions is higher for bitumen and heavy oil containing mixtures as they exhibit complex phase behaviours, up to four or more phases in equilibrium, and complex patterns of phase behaviour with composition, temperature and pressure. Such numerical issues, arising even if the equation of state can provide correct phase behaviours, must be addressed through a computational approach based on analyses that provide both necessary and sufficient conditions for equilibrium, i.e. global as opposed to local phase stability analysis.

Furthermore, phase equilibrium calculations must be based on meaningful and accurate fluid characterizations, and an accurate equation of state or other Pressure-Volume-Temperature (PVT) models. Calculations for ill-defined hydrocarbons like bitumen and its constituents on their own or in mixtures with well defined components, such as n-alkanes, present numerous challenges due to the paucity of chemistry and other property information available from conventional characterizations. Cubic equations of state have been used widely to predict phase behaviour due to their performance and simplicity. All thermodynamic properties can be calculated using equations of state, an ideal gas heat capacity model, and fundamental thermodynamic relations. However, using cubic equations of state normally requires knowledge of two key parameters (energy parameter a, and co-volume b), which are difficult to obtain for heavy components irrespective of approach. Computationally, these parameters are based on critical temperatures, critical pressures, and the acentric factors, which are not available for heavy species due to thermal decomposition. Predicted phase behaviours, phase compositions, and other properties are sensitive to the values of these parameters.

There are several alternative approaches in the literature to calculate equation of state parameters that avoid the need for critical properties; however, only a couple of them are applicable to heavy hydrocarbons. One approach [3-5]

is to partition mixtures into molecularly defined pseudo components (based on ^{13}C NMR and other analytical data), and to apply group contribution methods to obtain equation of state parameters. For mixtures containing Athabasca Vacuum Residue (AVR), the parameters of the Peng-Robinson equation of state can be calculated reliably using Group Contribution theory. Another more conventional approach, which is not the focus of the current work, uses oil bulk properties, light ends analysis, distillation or simulated distillation data, to generate pseudo components and the associated compositions and critical properties required for an equation of state model [6-8]. This technique is widely used for systems including conventional oil, but fails to provide reliable predictions for heavy oil and bitumen containing mixtures.

The goal of the present work is to develop a predictive model and a modeling framework so that phase equilibria observed experimentally for heavy oil and bitumen containing mixtures can be predicted reliably and with sufficient accuracy for engineering design applications. The initial target applications include diluents addition, for transport, and de-asphalting. In prior work, the effect of multiphase equilibrium was not considered. Consequently, the results cannot be applied to mixtures where the percentage of heavy components exceeds ~ 10 wt.%. Key challenges in this work include:

1. development of a robust solution algorithm for multiphase behaviour, where false convergence and model mismatch remain issues in the current literature even for well defined binary mixtures.

2. ill-defined hydrocarbon speciation, where this project will build primarily upon prior and current work of others.

3. equation of state selection and parameter identification for identified species.

1.1 Thesis Outline

In addition to the current chapter (Chapter 1), which contains the introduction and literature review and explains the research goals, Chapters 2, 3, 4 and 5 are dedicated to the various portions of the research work and the combination of these compose a unified thesis. The individual chapters are in a paper format comprising an introduction, methodology, results and discussion, and conclusions. Each chapter contains its own nomenclature, abbreviation, and bibliography. The chapters are presented in a sequence according to the progress of the research.

Chapter 2, which is entitled "Rapid and Robust Phase Behaviour Stability Analysis Using Global Optimization", presents a reliable computational approach that is capable of handling multiphase equilibrium calculations for multicomponent mixtures. The proposed method converges to correct phase behaviours for several challenging examples evaluated using one to three orders of magnitude fewer function evaluations compared with other successful methods. This computational approach has the potential for use in a broad range of practical phase equilibrium calculation applications and addresses the numerical shortcomings involved in commercial simulators. The conventional numerical techniques used in commercial simulators are prone to failure even for simple mixtures of industrial importance making the engineering designs that are based on the results generated by such commercial simulators unreliable. The material in this chapter has been published in the Journal of Fluid Phase Equilibria (Saber, N., and Shaw, J. M. (2008) *Fluid Phase Equilibria*. 264 137-146).

While Chapter 2 aims at addressing the numerical issues involved in phase equilibrium calculations, Chapter 3 focuses on developing a reliable thermodynamic model. In this chapter, called "Toward Multiphase Equilibrium Prediction for Ill-Defined Asymmetric Hydrocarbon Mixtures", a group contribution based thermodynamic model is proposed to enable multiphase behaviour prediction for asymmetric mixtures that contain heavy components for which critical properties are not available. Liquid-liquid-vapour three-phase zones

for ternary mixtures containing n-decylbenzene and n-eicosane + light hydrocarbons provide illustrative test cases. The results are compared to experimental data and to modeling results obtained using other thermodynamic models available in the literature. The performance of group contribution computations is further tested by predicting the phase behaviour trends that are observed experimentally for such mixtures. The results show that the group contribution method developed by Marrero and Gani outperforms the other thermodynamic models by generating accurate phase behaviour and phase behaviour trend predictions for all cases evaluated. The results presented in this chapter have been published in the Journal of Fluid Phase Equilibria (Saber, N., and Shaw, J. M. (2009) *Fluid Phase Equilibria*. 285 73-82).

In Chapter 4, the new computational tool is further tested by generating phase diagrams for the mixture of AVR and n-decane. Computed phase behaviour results are based on the Peng-Robinson Equation of State where parameters are identified using the Marrero and Gani group contribution method [9] applied to pseudo components identified by Sheremata [10]. Binary interaction parameters are estimated using the PPR78 [11] method and a predictive correlation developed by Gao et al. [12]. The resulting phase diagrams are in broad agreement with available experimental data, including the pressure-temperature-composition placement of liquid-liquid and liquid-liquid-vapour regions. There is only a mismatch between the measured and predicted phase behaviour over the composition range 35 wt.% to 60 wt.% vacuum residue, where the predicted phase behaviour includes L1L2V and L1L2 phase behaviours not observed experimentally. Even with this limitation, these proof of concept computational results provide a significant advance over current practice for ill-defined hydrocarbons, in general, and provide an accurate phase behaviour model for deasphalting and other refining processes not previously available for Athabasca vacuum residue in particular. The title of this chapter is “On the Phase Behaviour of Athabasca Vacuum Residue + n-Decane” and has been published in the Journal of Fluid Phase Equilibria (Saber, N., and Shaw, J. M. (2010) *Fluid Phase Equilibria*. Accepted on 29-9-2010).

The thermodynamic model is then used to generate phase behaviour data and diagrams for mixtures of AVR + n-alkanes and results are discussed in Chapter 5. The predictions are in qualitative and quantitative agreement with measurements over a broad range of temperatures, pressures, and compositions. For the mixture of AVR + n-pentane, mismatch is observed for the composition range of ~40 to ~ 60 wt.% AVR, where the model is unable to predict a second LLV region at higher temperatures and pressures. Binary interaction coefficient values between residue pseudo components and n-alkanes are tuned based on a procedure that is introduced. Densities of two liquid phases present in the three-phase region are calculated and compared to the experimental data for the mixture of AVR + n-decane. The results presented in this chapter further proves the reliability of the proposed thermodynamic model and its potential to be employed as a universal heavy oil modeling tool. The title of this chapter is "On the Phase Behaviour of Athabasca Vacuum Residue + n-Alkanes". In Chapter 6, key conclusions drawn from this thesis are summarized and recommendations are made for future work.

1.2 Literature Review

1.2.1 Phase Equilibrium Calculations

Phase equilibrium calculations are perhaps the most important calculations in the petroleum industry and equations of state are the major thermodynamic models used in these calculations. Phase equilibrium calculations lead to determination of the composition and amount of oil and gas produced, pressure-temperature diagrams to determine the phases in reservoirs, solubility of solids in liquids, and solid deposition. These calculations are also an essential part of the simulation and optimization of chemical processes in the refining and petrochemical industry.

The fundamental thermodynamic relation for a N_c-component open system based on the first and the second laws is as follows:

$$dU = TdS - PdV + \sum_{i=1}^{Nc} \mu_i dn_i \tag{1.1}$$

where U is total internal energy, T is temperature, P is pressure, S is total entropy, V is total volume, and μ is chemical potential. Other extensive thermodynamic potentials and fundamental relations can be obtained by using different pairs of independent variables. For instance, if T and P are selected as the independent variables instead of S and V, Equation 1.1 can be rewritten in terms a new thermodynamic potential called Gibbs free energy. Equation 1.2 shows the fundamental relation in terms of temperature and pressure.

$$dG = -SdT + VdP + \sum_{i=1}^{Nc} \mu_i dn_i \tag{1.2}$$

From Equations 1.1 and 1.2, it follows that:

$$\mu_i = \left(\frac{\partial U}{\partial n_i}\right)_{S,V,n_{j\neq i}} = \left(\frac{\partial G}{\partial n_i}\right)_{T,P,n_{j\neq i}} \tag{1.3}$$

Based on Equation 1.3, the chemical potential is defined as the partial molar Gibbs energy. Consider a closed system consisting of two phases in equilibrium. Equation 1.2 can be applied to each phase and the closed system as a whole. The combination of these equations results in the basic phase equilibrium equations that consist of the equality of chemical potentials for each component in a mixture. For a N_c-component mixture of overall composition **z** in a two-phase equilibrium, a necessary condition of equilibrium is:

$$\mu_i^l = \mu_i^v,\ i = 1,2,\dots,N_c \tag{1.4}$$

The equilibrium condition in terms of chemical potentials can be replaced without loss of generality by:

$$\hat{f}_i^l = \hat{f}_i^v,\ i = 1,2,\dots,N_c \tag{1.5}$$

where l and v denote the liquid and the vapour phases respectively, and $\hat{f}_i$ is the fugacity of component i in the mixture. Let mixture mole fractions in the liquid and the vapour phases be **x** and **y** and the overall fraction of the vapour phase be β then a material balance for each component yields another N_c equations:

$$\beta y_i + (1-\beta)x_i = z_i,\ i = 1,2,\dots,N_c \tag{1.6}$$

Mole fractions in the liquid and the vapour phase must sum to unity, which yields the last equation:

$$\sum_{i=1}^{Nc}(y_i - x_i) = 0 \tag{1.7}$$

These equations thus yield $2N_c+1$ relations between $2N_c+3$ unknowns: **x**, **y**, temperature (T), pressure (P), and β. Two more specifications are required to define the phase equilibrium problem. The two most common specifications are the temperature and the pressure, which leads to classic flash calculations. The problem can be generalized to several phases in equilibrium. Suppose that the mixture of overall composition **z** can split into N_p phases at a certain pressure and temperature. According to the second law of thermodynamics, the Gibbs free energy at equilibrium has the lowest value in comparison with all possible states. The Gibbs free energy for the final multiphase multicomponent state can be expressed as:

$$\frac{G(\mathbf{n})}{RT} = \sum_{i=1}^{Nc}\sum_{j=1}^{Np} n_{ji} \ln \hat{f}_{ji}(y_j) \tag{1.8}$$

where **n** is a matrix of mole numbers with $N_c \times N_p$ elements, and $\hat{f}_{ji}$ is fugacity of component i in phase j. Here the optimization problem is expressed by Equation 1.9:

$$G(\mathbf{n}) \rightarrow \min$$

$$Subject \quad to: \quad n_i = \sum_{j=1}^{Np} n_{ji} \quad for \quad i = 1,2,...,Nc \tag{1.9}$$

$$where \quad 0 \le n_{ji} \le n_i \quad and \quad n_i = Fz_i$$

where F is moles of feed and **z** is feed mole fraction .

Computational approaches only based on equality of chemical potentials or local minimization of Gibbs free energy are likely to predict incorrect behaviours because Gibbs free energy can contain more than one minimum. This is particularly common for multiphase cases, or near critical points (K-points (L1=V+L2), L-points (L1=L2+V), ordinary (L=V)) where local and global Gibbs free energy minima are numerically similar [13-14]. False convergence or convergence to trivial roots or saddle points frequently occurs. Commercial process simulators as well as research tools are both prone to false convergence. These computational difficulties are due to the non-linear and potentially non-convex form of the objective functions employed, e.g. Gibbs free energy. In order to have a robust phase equilibrium calculation tool, a more reliable approach for phase equilibrium calculation should be employed. This approach consists of two major steps: phase stability analysis and flash calculations.

Flash calculations, including those employed by commercial process simulators, are based on local minimization of Gibbs free energy because global minimization methods are perceived to be computationally intensive. Further, local minimization methods normally converge to the global minimum of the Gibbs free energy with a good initialization. Michelsen [14-15] suggested that stability analysis results are an excellent starting point for flash calculations. Second order methods or successive substitution are normally reliable if the global minimum of the Tangent Plane Distance Function (TPDF) is obtained from the stability analysis [15-18]. However, the use of compositions corresponding to TPDF global minima to initialize flash calculations does not guarantee convergence to correct phase behaviours and compositions. A second stability test

should be performed to validate the correctness of flash calculations. Stability analysis is the necessary and sufficient condition for phase equilibrium and its robustness is *the* key to successful phase behaviour and phase composition prediction.

Baker et al. [13] demonstrated the practical application of the tangent plane condition of Gibbs in phase equilibrium calculations and Michelsen [14] proposed a computational approach based on minimizing the tangent plane distance. Phase stability analysis is performed using the tangent plane criterion. A mixture at a specified temperature T, pressure P, and feed composition **z** is stable if and only if the distance between the Gibbs free energy surface and the tangent plane associated with this surface at the feed composition is greater than zero except at the feed composition. In other words, if the tangent plane lies completely below the Gibbs surface, then the phase is stable. The Gibbs free energy graph for the binary mixture of methane and hydrogen sulphide is shown in Figure 1.1. Feed 1 is unstable as the tangent line at the feed composition crosses the Gibbs curve. On the other hand, feed 2 is stable because it lies completely below the Gibbs surface. If the minimization process results in negative values for the TPDF, denoted by F(**x**), the phase is unstable. The objective function for phase stability, subject to the mass balance constraint, is given by:

$$\begin{aligned} &\min F(\mathbf{x}) = \sum_i x_i (\ln x_i + \ln \phi_i(\mathbf{x}) - \ln z_i - \ln \phi_i(\mathbf{z})) \\ &\textit{subject to}: \ \sum_i x_i = 1 \qquad 0 \le x_i \le 1 \end{aligned} \tag{1.10}$$

where $\phi_i(\mathbf{x})$ and $\phi_i(\mathbf{z})$ are the fugacity coefficients of component i at compositions **x** and **z** respectively. Composition vector **z** is the feed composition and composition vector **x** is the test composition. Equation 1.10 can be converted to an unconstrained minimization by eliminating one component through:

$$x_{N_c} = 1 - \sum_{i=1}^{N_c - 1} x_i \tag{1.11}$$

This conversion reduces the dimensions of the numerical domain by one and the N_c-1 independent composition variables become bounded and unconstrained. If the TPDF is non-negative for all values of **x**, then the feed is stable and its composition corresponds to the global minimum of the Gibbs free energy. Otherwise, the composition **x** at the global minimum of the TPDF is used as initialization for flash calculations.

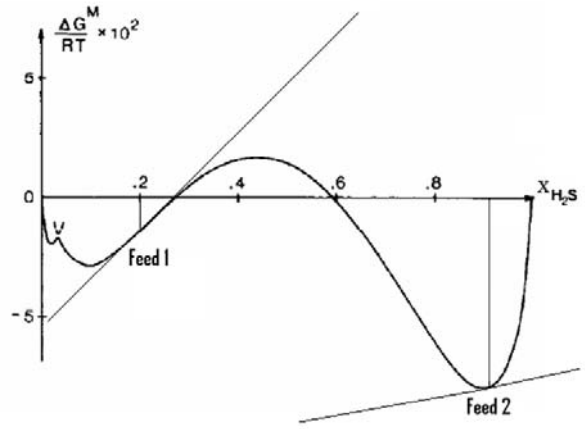

Figure 1.1. Gibbs free energy diagram for binary mixture of methane and hydrogen sulphide

With the introduction of the tangent plane criterion for phase stability evaluation [13-14], many approaches have been proposed to address the robustness and speed of the calculations involved in phase equilibrium calculations. Wakeham and Stateva have published [19] a general and critical review of the available numerical solutions for the determination of phase stability. The first approaches suggested were based on local minimization methods. These stationary point methods are applied to find the global minimum of TPDF by performing local minimizations for several initial points. There is no guarantee that the global minimum of TPDF can be located using such methods. Global optimization methods, however, have been found to be the most reliable approach for identifying the global minimum in the TPDF. The most important aspect of a global optimization algorithm is how it balances global versus local searches. Emphasis on global search increases the number of function evaluations significantly while emphasis on local search decreases the number of function

evaluations. Nonetheless, emphasis on local search also decreases the reliability of the resulting solution.

Sun and Seider [20], who used global optimization for the first time, tried to locate all stationary points for the tangent plane distance function (TPDF) using homotopy-continuation. Their approach tends to be computationally intensive and there is no theoretical guarantee that all the stationary points can be located. The Newton interval method in combination with generalized bisection was suggested by Hua et al. [21-23]. This approach requires interval arithmetic to find the roots of the equations resulting from the objective function's differentiation. The possibility of the presence of multiple solutions in an interval can cause numerical issues. This method also requires significant computational effort for multicomponent mixtures. Simulated annealing, which employs random searches in the computational domain, was used by Pan and Firoozabadi [24]. For the simulated annealing approach, the number of function evaluations is high due to an emphasis on global search, and computational outcomes are dependent on the selection of parameters employed in their algorithm. Balogh et al. [25], suggested another random-search approach. Again, there are several adjustable parameters employed that can affect computational outcomes and lead the algorithm to an incorrect solution. Elhassan et al. [26] proposed the use of the Area method for phase stability. This method requires modification and generalization to apply it to multiphase multicomponent cases. In a recent paper, Balogh et al. [27] applied some modifications and proposed a new generalization of the Area method based on the convex hull principal. Tunneling, used in both flash and stability analysis, was proposed by Nichita et al. [28-29]. This method is robust but the computational intensity and reliability are dependent on initial estimates. In a recent paper, Bonilla-Petriciolet et al. [30] compared the performance of a number of stochastic approaches and concluded that simulated annealing was the most reliable of the methods tested. However, all of these approaches involve large numbers of function evaluations. Yushan and Zhihong [31] used Lipschitz optimization to avoid use of starting points and knowledge of objective function gradients in their calculations. However, their approach has two major problems.

First, it does not lend itself to intuitive generalization for cases with more than two components. Second, the determination or estimation of Lipschitz constant, which is required for the optimization procedure, is not trivial. Jones et al. [32] proposed the DIviding RECTangles (DIRECT) approach that does not require case based constants or initial guesses and can be applied to any number of components. DIRECT is a deterministic method that provides a good balance between local and global search where local and global searches are not separated. A combination of both is used during all iterations. As a consequence, the number of function evaluations tends to be reduced for challenging examples without a concomitant reduction in reliability vis-à-vis other global optimization approaches.

For a mixture with feed composition **z**, if the stability analysis shows that the mixture is unstable, flash calculations are performed to identify the nature of equilibrium phases and compositions corresponding to the minimum of Gibbs free energy. Flash calculations can be performed using the global minimization methods as well, but due to the slow nature of these methods, local minimization methods are preferred instead. These local methods are usually based on solving the non-linear system of equations resulting from differentiating Equation 1.8, which leads to the classical approach based on the equality of chemical potentials or fugacities. The most common method for solving the two-phase flash is successive substitution combined with Newton's method for solving the Rachford-Rice equation [33]. The equilibrium factors, **K**, can be calculated assuming the mixture is an ideal solution, which means that fugacity coefficients are composition independent:

$$K_i = \frac{\phi_i^l(T,P)}{\phi_i^v(T,P)} \tag{1.12}$$

The Rachford-Rice equation, shown below, is then solved using the Newton method in the inner loop of the algorithm to find the value of the vapour fraction, β.

$$g(\beta) = \sum_{i=1}^{Nc} \frac{z_i(K_i - 1)}{1 - \beta + \beta K_i} = 0 \tag{1.13}$$

Liquid and vapour mole fractions are subsequently calculated using the following equations:

$$x_i = \frac{z_i}{1 - \beta + \beta K_i} \tag{1.14}$$

$$y_i = \frac{K_i z_i}{1 - \beta + \beta K_i} \tag{1.15}$$

The fugacity coefficients are then updated in the outer loop using the calculated mole fractions, and equilibrium conditions are checked for convergence. Despite being the simplest and safest approach, successive substitution is the most expensive method from a computational point of view. Successive substitution is a robust method, but it is typically slow to converge in critical regions. Mehra et al. [18] suggested an acceleration scheme to reduce the number of iterations and made the calculations less intensive. Higher order methods are also applied to flash calculations [15-16,34-36]. These methods usually involve a full Newton minimization and require calculation of the Jacobian matrix. To calculate the Jacobian matrix, fugacity derivatives with respect to mole numbers should be calculated. This was the main reason for the unpopularity of these methods in the past because partial composition derivatives of thermodynamic properties were considered unavailable. Newton-based methods therefore were expensive as they required numerical differentiation, which increases the complexity and cost of calculations. Quasi-Newton methods have gained considerable popularity starting with the work of Boston and Britt [37]. Minimization-based and derivative-free methods have also been investigated [38-40].

Several methods have also been proposed in the literature to make multiphase flash calculations more robust and reliable, but the subject has received much less attention than the two-phase calculations. The three-phase

flash based on successive substitution and the objective function proposed by Michelsen [34] remains the most reliable approach when coupled with a robust stability analysis. As mentioned above, the inner loop of the successive substitution algorithm runs on the assumption that the mixture is an ideal solution. For multiphase flash calculations, the classic Rachford-Rice equation is replaced with another objective function that was proposed by Michelsen [34]. This alternative formulation, Equations 1.16 and 1.17, facilitates the computational procedure and safeguards convergence.

$$Q(\beta) = \sum_{j=1}^{N_p} \beta_j - \sum_{i=1}^{N_c} z_i ln E_i \tag{1.16}$$

$$E_i = \sum_{k=1}^{N_p} \frac{\beta_k}{\phi_{ik}} \tag{1.17}$$

where **β** is the vector of phase fractions, **z** is the vector of feed composition, and ϕ_{ik} is the fugacity coefficient of component i in phase k. The phase fractions at equilibrium are given by the vector **β** that minimizes Q, subject to the following constraints:

$$\beta_j \geq 0, \qquad j = 1,2, \dots, N_p \tag{1.18}$$

The mole fractions in the individual phases are then calculated using Equation 1.19:

$$y_{ij} = \frac{z_i}{E_i \phi_{ij}} \tag{1.19}$$

It can be proven that Q is a strictly convex function with a minimum that is unique [34,41]. Therefore, any local minimization method, e.g. Newton's method with linesearch, is well suited for locating the minimum.

1.2.2 Thermodynamic Model

A thermodynamic model provides the necessary relationships between thermodynamic properties and can be used in combination with fundamental relations to generate all the properties required to perform phase equilibrium calculations. The most common thermodynamic models are equations of state and among them cubic equations of state are the most popular.

1.2.2.1 Cubic Equations of State

Cubic equations of state are mathematical expressions that relate pressure, volume, and temperature. These equations are modified formats of the van der Waals (vdW) equation of state. Equations 1.20 and 1.21 represent a general form for a cubic equation of state [42]:

$$P = \frac{RT}{v - b} - P_{att}(T, v) \tag{1.20}$$

$$P_{att}(T, v) = \frac{a}{v(v + d) + e(v - d)} \tag{1.21}$$

In the above equations, a, b, d, and e are equation of state parameters, which can be constants or function of temperature and fluid properties such as acentric factor; R is the universal gas constant. Cubic equations of state are perhaps the most frequently used equations for practical applications. Although they are not the most accurate thermodynamic models, they provide the best balance between accuracy, reliability, simplicity, and speed of computation. They also have the advantage of representing multiple phases with the same model. Furthermore, the predicted phase diagrams only include those arising in nature. For example, the van der Waals equation of state predicts 5 of the 6 possible binary phase behaviour types arising for hydrocarbon containing mixtures. The Peng-Robinson equation of state predicts all six and no others [43].

1.2.2.2 Peng-Robinson Equation of State

The Peng-Robinson cubic equation of state was developed during the 1970s and quickly became one of the most popular thermodynamic models especially in the oil and gas industry. This equation does not introduce any additional parameters beyond the original two presented in the van der Waals equation of state; however, it includes two major modifications [44]. The energy parameter, "a", considered a constant in the vdW model, was selected to be temperature dependent through the alpha function. Here, alpha was introduced following the same procedure used in the Soave-Redlich-Kwong (SRK) equation of state for defining a temperature dependant function [45]. As shown by Equations 1.22a, b and c, this function depends on the values of acentric factor (ω) and critical temperature (T_c):

$$a = a_c \alpha(T) \tag{1.22a}$$

$$a_c = \frac{0.45724 R^2 T^2}{p_c}$$

$$\alpha = \left[1 + (0.37464 + 1.54226\omega - 0.26992\omega^2)\left(1 - \left(\frac{T}{T_c}\right)^{\frac{1}{2}}\right)\right]^2 \tag{1.22b}$$

(1.22c)

The second modification of Peng and Robinson to the van der Waals equation of state is related to the critical compressibility factor (Z_c). Peng and Robinson recognized that the Z_c from the SRK equal to 1/3 was not very close to Z_c of typical hydrocarbons. They proposed to modify the equation of state to achieve the more reasonable value of 0.3074 for Z_c, which was much closer to that for typical hydrocarbons. Equation 1.23 shows the Peng-Robinson equation of state:

$$P = \frac{RT}{v - b} - \frac{a(T)}{v(v + b) + b(v - b)} \tag{1.23}$$

The second parameter of the Peng-Robinson equation of state is a function of critical temperature T_c and critical pressure P_c and can be calculated as follows:

$$b = \frac{0.07780RT_c}{P_c} \tag{1.24}$$

1.2.2.3 SAFT Equation of State

Statistical associating fluid theory (SAFT) was developed by Chapman et al. [46-47] using perturbation theory. The model based on this theory uses a Taylor series expansion of a property of a fluid around known properties of a reference fluid such as an ideal gas. The SAFT equation of state captures the effects of non-spherical, chain like molecular shape and molecular association.

In SAFT, molecules are considered to be made up of a specific number of segments attached together to form chains. These chains can be associated with each other through an unconstrained number of sites. In this equation, the Helmholtz energy is used as the fundamental fluid property and an ideal gas is used as the reference fluid. The SAFT equation can be expressed in terms of residual Helmholtz energy.

The SAFT model has been used successfully for a number of systems including: pure alkanes and mixture of alkanes, gas solubility in alkanes, methanol, acetic acid, asphaltenes, and polymer solutions. However, the group contribution methods associated with this equation of state are not well defined and are limited to vapour-liquid equilibrium and simple mixtures. Furthermore, phase behaviour types not occurring in nature are frequently predicted for this equation of sate. Because of the shortcomings of other major alternatives, in this work, we have chosen to use cubic equations of state as a basis for calculation.

1.2.2.4 Thermodynamic Property Calculations

The previously mentioned objective functions, i.e. TPDF and Gibbs free energy, are not explicitly defined with respect to mole fractions and physical properties. As a result, the selected cubic equation of state should be solved in

order to find the molar volume or compressibility factor, which is necessary to calculate fugacity coefficients. Here, the Peng-Robinson equation of state, Equation 1.23, is chosen to demonstrate the procedure. For a multicomponent mixture, the equation of state parameters, a and b, are calculated using the van der Waals mixing rules:

$$a = \sum_i \sum_j x_i x_j (a_i a_j)^{1/2} (1 - k_{ij}) \tag{1.25}$$

$$b = \sum_i x_i b_i \tag{1.26}$$

where x_i is the mole fraction of component i in the mixture, k_{ij} is the binary interaction parameter between component i and component j, and a_i and b_i are the Peng-Robinson parameters of the pure component i and are calculated using Equations 1.22a-c and Equation 1.24. Once these parameters are determined for the mixture, the compressibility factor can be obtained by solving the following equation which is another form of the Peng-Robinson equation of state:

$$Z^3 + (B-1)Z^2 + (A - 3B^2 - 2B)Z - AB + B^2 + B^3 = 0 \tag{1.27}$$

where, $Z = \frac{Pv}{RT}$, $A = \frac{aP}{R^2T^2}$, and $B = \frac{bP}{RT}$

The above equation can yield either one or three real roots, but only one should be used to calculate fugacity coefficient in the next step. The criterion to choose among these roots is developed by Michelsen [14-15]. The root, which results in lower value of the Gibbs free energy, should be selected as the acceptable one. The fugacity coefficients can then be calculated using the following equations:

$$\ln\left(\frac{\hat{f}_i}{x_i P}\right) = \frac{b_i}{b}(Z-1) - \ln(Z-B) - \left(\frac{A}{2\sqrt{2}B}\right)\left(\frac{2}{a}\sum_{j=1}^{Nc} x_j (a_i a_j)^{1/2}(1-k_{ij}) - \frac{b_i}{b}\right)\ln\left[\frac{Z+(1+\sqrt{2})B}{Z+(1-\sqrt{2})B}\right] \tag{1.28}$$

$$\phi_i = \frac{\hat{f}_i}{x_i P} \tag{1.29}$$

where, $\hat{f}_i$ is the fugacity of component i, A and B are defined in Equation 1.27, a_i and b_i are parameters of the Peng-Robinson equation of state for component i, and a and b are parameters of the Peng-Robinson equation of state for the mixture.

At the end of the phase equilibrium calculations, the type of the generated phases (vapour, light liquid, or dense liquid phase) is determined by comparing the values of compressibility factor and mass density for each phase. The determination of phase type based on this approach becomes specifically challenging and even impossible close to critical points where the properties of two phases in equilibrium becomes identical. A more appropriate approach for such problematic cases is to follow the trend of predicted phase behaviours to decide which phases should coexist based on the location of the equilibrium result with respect to phase boundaries.

1.2.3 Parameter Identification

As indicated in the previous section, equations of state parameters depend on critical temperature, critical pressure, and acentric factor. These are the required pure component properties for solving two-parameter cubic equations of state. The accuracy of values for these properties can greatly affect the accuracy of the phase behaviour predictions. Critical properties of a component can be measured provided that the material is thermally stable at the critical conditions. Direct measurements are not possible for heavy hydrocarbons (heavier than C_{20}) due to thermal cracking. Determination of the acentric factor as defined by Equation 1.30 requires knowledge of the critical temperature and pressure[48-49].

$$\omega = -\log\left[\frac{P^{sat}}{P_c}\right]_{Tr=0.7} - 1 \tag{1.30}$$

If measurements for the saturation pressure at the reduced temperature of 0.7 are not available, acentric factor should be determined using available correlations.

1.2.3.1 Properties from Correlations

Many correlations have been developed to predict the critical properties. These correlations have a weak theoretical basis and should be considered empirical. Ideally, these correlations should be used only in the range of data on which they are based. Due to lack of experimental data for heavy components however, these correlations are sometimes used outside of this range.

The first class of correlations proposed in the literature is based on single properties such as carbon number, molar mass or normal boiling point. For very heavy hydrocarbons, the use of normal boiling point can become problematic due to the potential thermal reactions. The first widely accepted simple correlations are based on the normal boiling point and specific gravity (SG) as these properties are available for petroleum distillates. The general form of this class of correlations proposed by Riazi and Daubert [50] is as follows:

$$\theta = aT_b^n SG^m \tag{1.31}$$

In Equation 1.31, θ is the critical property of concern, T_b is the normal boiling point, SG is the specific gravity, and a, n and m are equation coefficients. This correlation has been adapted for a wide variety of hydrocarbon families by regression of the coefficients with experimental data for each family. This two-parameter correlation can only be used for non-polar hydrocarbons while a third parameter becomes necessary for hydrocarbons containing heteroatoms (S, O, N) and polar functional groups. To overcome this problem, Riazi and Daubert [51] proposed a new correlation as follows:

$$\theta = a.\exp(b\theta_1 + c\theta_2 + d\theta_1\theta_2).\theta_1^e\theta_2^f \tag{1.32}$$

In Equation 1.32, θ is the critical property of concern, θ_1 is the normal boiling point, θ_2 is the specific gravity, and a, b, c, d, e and f are equation coefficients. Other pairs of properties such as boiling point and carbon-to-hydrogen ratio can

also be used in correlations provided by Riazi and Daubert. This equation works slightly better than other correlations suggested in the literature [52-53]. While Equation 1.32 predicts critical temperatures for n-alkanes very well, it shows significant deviations for sulphur containing and aromatic compounds. The same is true for prediction of critical pressures.

1.2.3.2 Group Contribution Methods

Group contribution methods for estimation of critical properties are based on molecular composition and structure. A molecular structure is divided into a set of functional groups whose properties have been regressed and comprise a data bank. The contributions of these functional groups are then summed to estimate a certain parameter or property. These methods can provide better results than correlations based on bulk properties as they intrinsically include molecular interactions. However, these methods are also developed by regression of data for components with low and measurable critical properties. Therefore, for heavy hydrocarbons, these correlations should be used outside the range of the data on which they are based.

The group contribution concept is based on two assumptions: 1. Intermolecular forces depend primarily on the bonds between the atoms of a molecule and on the nature of the atoms. These forces determine the values of the properties of interest; 2. Contributions of functional groups do not depend on their arrangements or their neighbours. The number and type of functional groups are normally assumed in advance and their contributions are obtained by fitting available experimental data. The most popular GC methods found in the literature to estimate critical properties are the method of Joback and Reid [54], Constantinou and Gani [55], Wilson and Jasperson [56], Marrero and Pardillo [57], Marrero and Gani [9], and Coniglio et al. [58-60]. Some of the more widely used group contribution methods are briefly discussed here.

The first group contribution method discussed here is developed by Joback and Reid [54]. This method can estimate critical temperature, pressure, and

volume as well as other thermodynamic properties. In this method, two levels of contributions are considered without including the effects of molecular geometry. As a result, the method does not distinguish the critical properties of isomers. To estimate critical temperature, it is required to know the material normal boiling point. Therefore, this method has a shortcoming in the case of heavy hydrocarbons. Wilson and Jasperson [56] developed another group contribution method based on the number of rings, atoms, and groups. Their method also considered two levels of contributions. Due to its simplicity, the method of Wilson and Jasperson is incapable of distinguishing between the critical properties of isomers. Testing these methods for over three hundred molecules, Poling et al. [61] found that both group contribution methods have similar accuracy.

The group contribution method developed by Marrero and Gani [9] includes the effect of more complex groups. As a result, this method has the capacity to distinguish between the properties of isomers. This method can estimate critical properties as well as normal boiling and melting points and enthalpies for phase transitions. In their method, there is no requirement to know the normal boiling point and the estimation of critical pressure does not depend on critical temperature. Marrero and Gani considered three levels of group contribution. The first level of contributions includes 182 simple groups that are used to describe the entire molecule. A wide variety of organic compounds can be described using these groups. The second level consists of more complex groups that allow a better description of polyfunctional compounds and differentiation among isomers. Unlike first order groups, these groups can overlap when they have atoms in common. A total of 122 second order groups have been defined, but they are unable to provide a good representation of compounds with more than one ring in their structure. Therefore, a third level of contribution is required to better describe polycyclic systems such as fused aromatic and non-aromatic rings as well as rings joined together by chains. A total of 66 third order groups have been defined. The equations for estimating critical temperature (K) and pressure (bar) are as follows:

$$\exp\left(\frac{T_c}{231.239}\right) = \sum_i N_i (tc_i) + \sum_j M_j (tc_j) + \sum_k O_k (tc_k) \qquad (1.33)$$

$$(P_c - 5.9827)^{-\frac{1}{2}} - 0.108998 = \sum_i N_i (pc_i) + \sum_j M_j (pc_j) + \sum_k O_k (pc_k) \qquad (1.34)$$

In the above equations, N_i, M_j, O_k are the numbers of the 1st, 2nd and 3rd order groups, respectively; tc_i, tc_j, tc_k are the 1st, 2nd and 3rd order group contributions to T_c; and pc_i, pc_j, pc_k are the 1st, 2nd and 3rd order group contributions to P_c.

The limiting value of critical pressure is 5.99 bar in the method of Marrero and Gani, which is higher than the 2.68 bar calculated from theoretical considerations by Tsonopoulos and Tan [62] for large n-paraffins. 2,000 compounds ranging from C_3 to C_{60} have been used to develop and evaluate this group contribution method. These compounds were drawn from the CAPEC database [63]. The error of estimating critical properties for this method is lower than the two previously mentioned methods. It seems that the Marrero-Gani group contribution method is the most reliable one to use for estimating critical properties. Unlike the other two methods, this method allows distinction between isomers, which is an additional advantage.

A number of group contribution methods have been developed to estimate the acentric factor [64-65]. One of these methods is developed by Constantinou, Gani and O'Connell [66]. Two levels of contributions are considered in this method. Second order contributions from more complex groups provide geometric considerations that may distinguish between some isomers. The group contribution method for estimating acentric factor is given in Equation 1.35.

$$\omega = 0.4085\left[\ln\left(\sum_i N_i \varepsilon_{1i} + A\sum_j M_j \varepsilon_{2j} + 1.1507\right)\right]^{\frac{1}{0.5050}} \qquad (1.35)$$

N_i and M_j in Equation 1.35 are the numbers of the 1st and 2nd order groups, ε_{1i} and ε_{2j} are the 1st and 2nd order group contributions to ω, and A is either 0 or 1 depending on whether or not there is a defined 2nd order contribution.

In another category of group contribution methods, instead of estimating critical properties and calculating the two cubic equation of state parameters, the group contribution methods are directly incorporated into the cubic equation of state. Coniglio et al. [58,60] have developed a group contribution-based form of the Peng-Robinson equation of state, which has acceptable performance for VLE calculations of heavy hydrocarbons. However, the extension of this method to multicomponent mixtures is not straightforward due to the many corrections introduced as pseudo structural increments. This method has been further refined and simplified by Crampon et al. [59]. Most of the specific structural increments are eliminated and more functional groups are included in the modified version. The simplified method was tested and observed deviations (~1 %) were within the range of the experimental uncertainties. This group contribution method considers a variety of classes of hydrocarbons including alkanes, naphtanes, alkylbenzenes, and polynuclear aromatics.

The estimation of the parameters is based on a linear sum of contributions. The co-volume parameter of the Peng-Robinson equation of state, b, is calculated based on a group contribution method developed by Bondi [67] for the van der Waals volume using methane as a reference. The equation for estimation of parameter b is shown below:

$$b = b_{CH4} \frac{\left(\sum_{j=1}^{7} V_{Wj} N_j + \sum_{j=1}^{3} \delta V_{Wk} I_k \right)}{V_{WCH_4}} \tag{1.36}$$

In the above equation, V_{Wj} is the contribution of the j^{th} group to the van der Waals volume and N_j is the number of groups of type j. δV_{WK}, represents a correction introduced by the method to special cases and I_k represents the number of corresponding occurrences. The methane co-volume b_{CH4} of Equation 1.36 has a value of 26.80 cm^3/mol and can be obtained from its critical properties. In the simplified version, the structural increments term, δV_{WK}, is eliminated.

The energy parameter of the Peng-Robinson equation of state, a, is temperature dependent and can be calculated using the following equation:

$$a(T) = a(T_b)\exp\left\{f_1(m)\left[1-\left(\frac{T}{T_b}\right)^{0.4}\right] - f_2(m)\left[1-\left(\frac{T}{T_b}\right)^{2.5}\right]\right\}$$

$$f_1(m) = 1.80546 \quad m + 0.21887 \tag{1.37}$$

$$f_2(m) = -0.11113 \quad m + 0.03502$$

In Equation 1.37, m, the characteristic of each compound, is a shape factor that can be calculated using group contribution methods and has a role similar to acentric factor [68]. This parameter is calculated using the expression shown below:

$$m = 0.23269S^{\left(\frac{1}{S^{0.6}}+0.5\right)} + 0.08781\ln(S) + 0.59180 \tag{1.38}$$

where S is an intermediate variable calculated based on group contributions:

$$S = \sum_{j=1}^{N_G} M_j N_j \tag{1.39}$$

In Equation 1.39, N_j is the number of occurrences of group j and M_j is its contribution to shape factor, m.

If the normal boiling point is not known or cannot be measured, it can be estimated by another group contribution method proposed by Coniglio et al. [58]. In Equation 1.37, $a(T_b)$ is the value of a(T) at the normal boiling temperature and can be estimated by iteration using the Peng-Robinson equation of state to match the vapour pressure at this temperature, i.e., 1 atm. The method is illustrated in Figure 1.2. In the proposed iterative algorithm, the variable a is replaced with A = a/(RT) for convenience. In addition, the chosen first estimation values for $A^{(1)}$ and β (Figure 1.2) facilitate convergence.

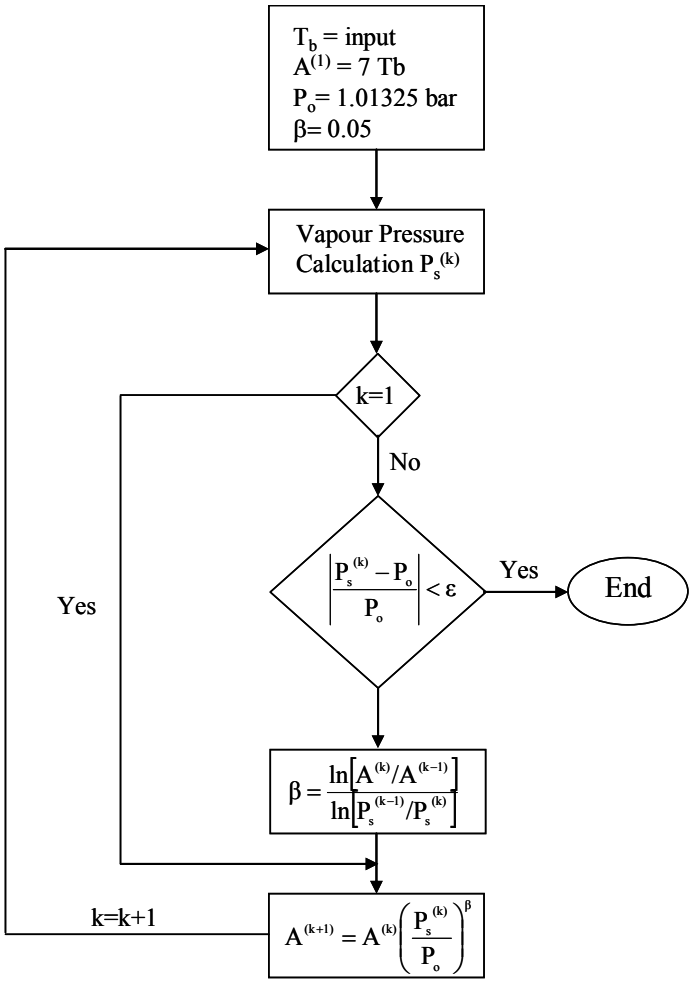

Figure 1.2. Flowchart for calculation of parameter a(T_b) [60].

The modified version of the group contribution method [59] includes 19 functional groups, which are shown in Table 1.1. The values for contributions to the van der Waals volumes V_j and the shape parameter m (M_j) are also tabulated in Table 1.1.

Table 1.1. Group contributions to the van der Waals volumes and the shape factor m [59]

Groups	V_j	M_j
Alkanes		
CH_3	13.67	0.085492
CH_2	10.23	0.082860
CH	6.78	0.047033
C	3.33	-0.028020

Groups	V_j	M_j
Naphthenes		
CH_2	10.23	0.062716
CH	6.78	0.034236
C	3.33	-0.010213
CH(ring/ring junction)	6.78	0.010039
C (ring/aromatic junction)	3.33	0.051147
Aromatic compounds		
CH	8.06	0.050476
C	5.54	0.071528
C condensed	4.74	0.013697
Aliphatic Alkanes		
=CH2	11.94	0.059938
=CH-	8.47	0.069836
=C<	5.01	0.060085
=C=	6.96	0.112156
=CH-aromatic ring	8.47	0.092399
Aliphatic Alkyls		
C	8.05	0.141491
CH	11.55	0.138136

This group contribution approach provided a significant improvement over application of the Peng-Robinson equation of state with the parameters being obtained from the critical properties of the compounds for n-alkanes up to n-triacontane and aromatics up to 1-phenylnaphthalene. Crampon et al. [69] tested the method using a database of more than 128 hydrocarbons including the mentioned compounds in addition to others such as fluorene and acenaphthene.

1.2.3.3 Binary Interaction Parameter Estimation

Binary interaction coefficients (k_{ij}) are adjustable empirical equation of state parameters that are introduced to improve the performance of mixing rules for mixtures. Most mixing rules for the energy parameters include one or more binary interaction parameters. These binary coefficients are normally calculated by fitting the phase equilibrium results of a specific equation of state to experimental vapour-liquid equilibrium data for a binary mixture. Therefore, binary interaction parameters are equation of state specific and not transferable from one equation of state to another. From a theoretical point of view, binary interaction parameters correct the equation of state energy parameter, a, to account for deviations from van der Waals forces [70]. The quality and accuracy of phase behaviour predictions depend strongly on the value of these coefficients [70-71].

Binary interaction parameters are not available for bitumen and heavy oil characterized by pseudo components as they cannot be obtained by regression of experimental data. One option is to set the binary interaction parameters equal to zero, but modeling mixture by setting all k_{ij} values to zero can result in significant deviations from experimental data. It should be mentioned that setting k_{ij} values to zero does not imply that the mixture is ideal. On the other hand, it has also been shown that poor k_{ij} tuning may lead to unreasonable phase behaviour or convergence failure [72-73]. Therefore, setting binary interaction parameters should be handled with special care.

Several correlations and approaches have been developed and proposed to estimate k_{ij} values for various equations of state. Most of these correlations have been generalized in terms of physical properties such as critical properties, acentric factor, or molecular weight [12,74-75]. Other methods are based on group contribution theory [11,76-79]. Two of the estimation methods used in the current research are discussed here.

For the Peng-Robinson equation of state, a generalized correlation that estimates k_{ij} values based on critical temperature and critical compressibility was proposed by Gao et al. [12] for binary mixtures of methane with n-paraffins up to n-decane as well as other simple hydrocarbons. This correlation considerably improved the quality of predictions for bubble point pressures and vapour phase compositions compared to setting k_{ij} values to zero. The correlation is shown in Equation 1.40.

$$k_{ij} = 1 - \left[\frac{2\left(Tc_i Tc_j\right)^{0.5}}{(Tc_i + Tc_j)}\right]^{\left(\frac{Zc_i + Zc_j}{2}\right)} \tag{1.40}$$

where T_c is the critical temperature and z_c is the critical compressibility factor.

Jaubert et al. [11,76-82] have developed a group contribution-based method called PPR78 to estimate temperature dependent binary interaction parameters (k_{ij}) for the Peng-Robinson equation of state. Most of the correlations for k_{ij} estimation are usually developed for a particular set of binary pairs, but this method is completely general as long as the molecules are composed of the defined functional groups. Additionally, only the critical properties and acentric factor are required. The PPR78 method relies on knowledge of the different forms of carbon present in molecules to estimate binary interaction coefficients. Group contributions, temperature, energy parameter (a_i), and co-volume (b_i) of the molecule are the necessary variables for k_{ij} calculations:

$$k_{ij}(T) = \frac{-\frac{1}{2}\left[\sum_{k=1}^{Ng}\sum_{l=1}^{Ng}(\alpha_{ik} - \alpha_{jk})(\alpha_{il} - \alpha_{jl})\, A_{kl}.\left(\frac{298.15}{T}\right)^{\left(\frac{B_{kl}}{A_{kl}} - 1\right)}\right] - \left(\frac{\sqrt{a_i(T)}}{b_i} - \frac{\sqrt{a_j(T)}}{b_j}\right)^2}{2\frac{\sqrt{a_i(T).\, a_j(T)}}{b_i.\, b_j}} \tag{1.41}$$

where T is the temperature, a_i and b_i are equation of state parameters, N_g is the number of different groups defined by the method (for the time being, 15 groups

are defined and N_g = 15), α_{ik} is the fraction of molecule i occupied by group k (occurrence of group k in molecule i divided by the total number of groups present in molecule i), and $A_{kl} = A_{lk}$ (where k and l are two different groups) are first contribution and $B_{kl} = B_{lk}$ are second contribution for interaction of k^{th} and l^{th} type groups ($A_{kk} = B_{kk} = 0$).

The fifteen groups defined so far are: group 1 = CH_3, group 2 = CH_2, group 3 = CH, group 4 = C, group 5 = CH_4 (i.e. methane), group 6 = C_2H_6 (i.e. ethane), group 7 = CH_{aro}, group 8 = C_{aro}, group 9 = $C_{\text{fused aromatic rings}}$, group 10 = $CH_{2,\text{ cyclic}}$, group 11 = CH_{cyclic}, group 12 = CO_2, group 13 = N_2, group 14 = H_2S, group 15 = -SH. The application of the above equation in equation of state calculations is straightforward despite the formidable appearance of it. The values of k_{ij} calculated by this method can be either positive or negative. This group contribution method can be of great advantage in predicting phase behaviour for asymmetric mixtures containing components for which binary interaction parameters are not available.

1.3 Challenges Associated with Heavy Oil and Bitumen Mixtures

Mixtures containing heavy oil or bitumen are usually not well defined and the first challenge that arises is how to characterize such mixtures. Characterization of molecules present in bitumen and heavy oil presents formidable experimental and theoretical challenges. Efforts are being made to define heavy oils in term of molecular structures of individual components, but the large number of distinct molecules present in heavy oil fractions makes this approach very challenging. Quantification of functional groups in molecules, and definition of mean molar mass, for boiling fractions, or whole crudes remain key challenges. For example, Jaffe et al. [83] identified more than 150 molecular substructures in petroleum residues. However, Sheremata et al. [10,84] proposed molecular representations for bitumen vacuum residue by building molecular models on the basis of just ten substructures, only seven of which were drawn from the work of Jaffe et al. [83]. Once these molecular representations are used, group contribution methods such as those developed by Marrero and Gani [9] or

Coniglio et al. [60] are likely to play a central role in phase behaviour and thermophysical property prediction. Group contribution methods have much to offer as many of the groups can be measured and quantified experimentally using more than one technique. Clearly over all molecular structures and molar masses remain ambiguous but there is greater agreement on the functional groups and the types of carbon they comprise, with the possible exception of asphaltenes. For asphaltenes, the situation is worse. There is little agreement on the nature of the molecular substructures they comprise. Pericondensed [85] and archipelago type molecular structures [84,86] have both been proposed for the same material.

Another approach to define heavy oil containing mixtures is characterization using oil bulk properties, distillation or simulated distillation data. This approach, typical of engineering calculations, relies on refinery style oil characterization where a true boiling point curve (TBP) is entered to help define the volatility behaviour of the fluid. The TBP curve is divided based on boiling point ranges where each range has a representative average boiling point and standard liquid density assigned to a pseudo component. Other information such as specific gravity, molecular weight, viscosity and other physical properties of the oil may be provided to the characterization package, and these data can be used to further refine the estimation of pseudo component physical properties. For bitumen and heavy oil, our particular focus here, much less data are available and conventional boiling range approximations are less robust. For example, more than 40 wt.% of Athabasca bitumen has nominal normal boiling points exceeding 525 ^{o}C. This means that even under vacuum the boiling temperature exceeds the temperature ranges at which most hydrocarbons are not reactive. Therefore, boiling ranges of these fractions are approximated using chromatographic techniques and extrapolated properties. Even with reliable boiling points, a challenge exists as correlations used to estimate critical properties are generally developed for lighter hydrocarbons. These relationships are applicable in the range of actual measurement, i.e. critical temperature up to 350 ^{o}C.

Beside characterization, there are other factors that can affect properties and phase behaviour predictions. Two of these factors are discussed here. Heavy crudes and bitumen usually contain aromatics and heteroatoms, while the available correlations for estimation of critical properties are usually based on data from the homologous series of n-paraffins. Only correlations that are based on the data from a large number of groups of molecules should be used for these mixtures (e.g. the group contribution method of Marrero and Gani). Another issue is the presence of a wide range of hydrocarbons from light distillates to heavy non-distillable residue in such mixtures, which makes them asymmetric mixtures. The asymmetry of heavy oil mixtures has a profound effect on phase behaviour, and liquid-liquid phase behaviour can occur even at low temperatures. Modeling these asymmetric mixtures based on van der Waals mixing rules can cause errors and other mixing rules may be required.

It should be mentioned that if the effect of the presence of solids is not included in the model, the reliable prediction of phase behaviour can only be extended up to the limit where precipitation/solidification at lower T is potentially an issue. A final challenge relates to polymorphic behaviour of relevant mixtures e.g. Athabasca Vacuum Residue (AVR) + n-alkane mixtures where density and enthalpy of mixing values depend on the thermal history of samples[87-88]. Care must be taken to ensure that the data sets and calculations address these issues.

1.4 Property Measurement and Prediction for AVR

Properties of mixtures comprising AVR will be used as a key test case for benchmarking and validating computational approaches adopted here. In this section, research directly related to the phase behaviour and thermophysical properties of AVR containing mixtures is discussed. Three distinct topics are addressed. The first topic concerns the molecular structure of AVR, which is the required input for group contribution methods. The second concerns previous attempts to predict the phase behaviour and thermodynamic properties of heavy hydrocarbon mixtures using group contribution approaches. Finally, phase behaviour and thermophysical property experimental data for mixtures containing

heavy hydrocarbons are discussed. These data will be used to assess the validity of predictions. Proper assessment of the precision and accuracy of the experimental results and their shortcomings are essential to the success of this work. For example, caution must be taken not to over fit low pressure bubble pressure data where the measurement error is large compared to the experimental values. Models developed here will not include solid phases. Such phases are expected to arise at low temperatures.

1.4.1 Molecular Structure of AVR

Defining the structure of heavy hydrocarbon fractions has been a challenging subject for researchers and research in this field continues to address the remaining issues. Experimental analytical data such as ^{13}C NMR test results, elemental composition, and apparent molecular weight in addition to high temperature simulated distillation data for heavy hydrocarbons are readily available in the literature.

Chung et al. [89] separated AVR into ten fractions by n-pentane supercritical fluid extraction. These fractions have been characterized in terms of physical and molecular properties. Sheremata et al. [10,84] have developed quantitative molecular representations of all ten fractions from supercritical separation of AVR. For these fractions, Sheremata et al. [10,84] proposed molecular representations using a Monte Carlo construction method. The optimized molecular representations of AVR proposed by Sheremata et al. [10,84] are consistent with the available ^{13}C NMR molecular structural information, molecular weight, aromaticity, and SARA fractionation data. It was found that six molecules were sufficient to represent each AVR fraction. Thus in his first contribution, Sheremata provided sixty molecular representations for AVR. More recently, he proposed a new smaller set of molecular pseudo components that are consistent with experimental simulated distillation data as well [10]. This achievement in characterization of AVR makes more reliable phase behaviour predictions possible. These molecular representations can be used as input data to

estimate the critical properties and equation of state parameters for mixtures containing AVR using group contribution methods.

1.4.2 Phase Behaviour Prediction of Athabasca Vacuum Residue

In the first attempt to model mixtures containing AVR, Mahmoodaghdam [90] used a group contribution method based equation of state to estimate the vapour pressure and density of AVR. A one-molecule-representation, available at the time for AVR, was used as the input for the group contribution theory proposed by Coniglio et al. [60]. This model failed to accurately predict the density and vapour pressure of AVR.

Van Waeyenberghe [5] used the simplified version of the group contribution method proposed by Coniglio et al. [59] devised for hydrocarbon mixtures along with the Peng-Robinson equation of state. In her work, the sixty molecular representations proposed by Sheremata et al. [84] were used. The effect of multiphase equilibrium was not considered in the model and calculations were performed based on vapour-liquid equilibrium. Results showed that the density and vapour pressure of dilute mixtures of Athabasca vacuum residue in n-decane could be modeled successfully (Figure 1.3), while the same properties for concentrated mixtures could not be accurately predicted (Figure 1.4). The objective of the mentioned study was to evaluate the potential of the computational approach, in a general sense, and to validate the model in the L1V region arising under dilute conditions in particular. As such, the model was a success based on the results in Figure 1.3. However, the results showed that vapour pressure predictions are sensitive to the presence of even small amounts of a second liquid phase.

a)

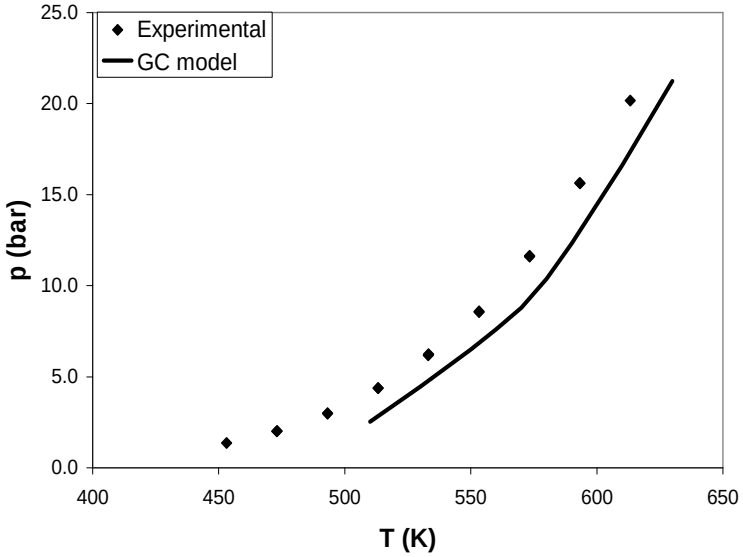

b)

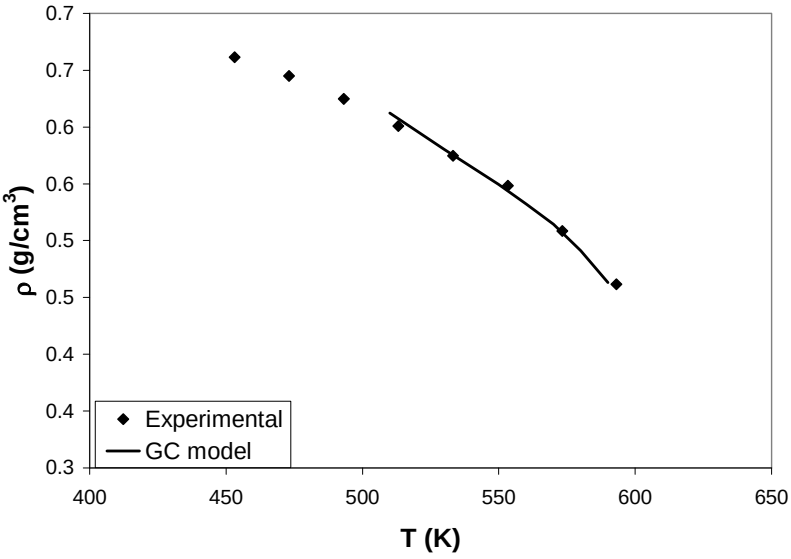

Figure 1.3. Vapour pressure (a) & Saturated liquid density (b) for AVR (10 wt.%) + n-decane. Reproduced with permission from [5]

a)

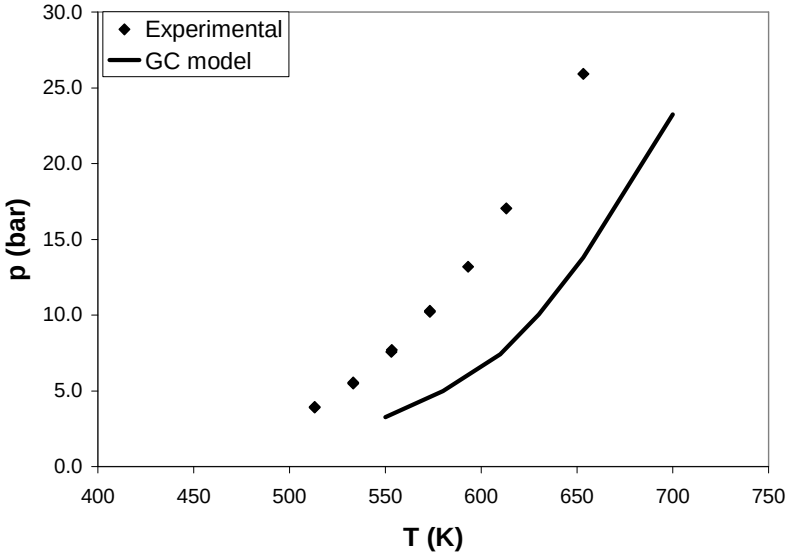

b)

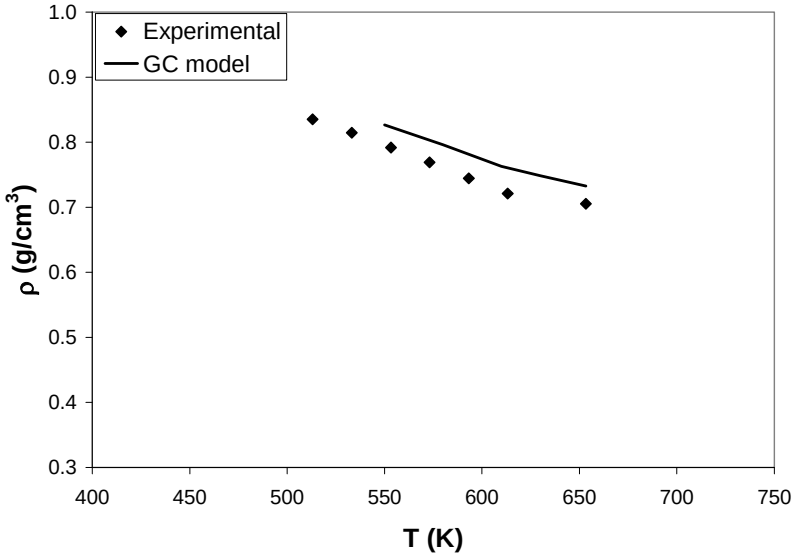

Figure 1.4. Vapour pressure (a) & Saturated liquid density (b) for AVR (50 wt.%) + n-decane. Reproduced with permission from [5]

Phase behaviour measurement data plotted in Figure 1.5 show that for a mixture of 10% AVR and n-decane, a second liquid phase is present over a wide range of temperature and pressures. The number of phases present in equilibrium increases as the percentage of AVR in the mixture is increased. This shows that for accurate modeling of the vacuum residue fluid properties in the absence of

solvents or at lower solvent concentrations, multiphase behaviour needs to be considered.

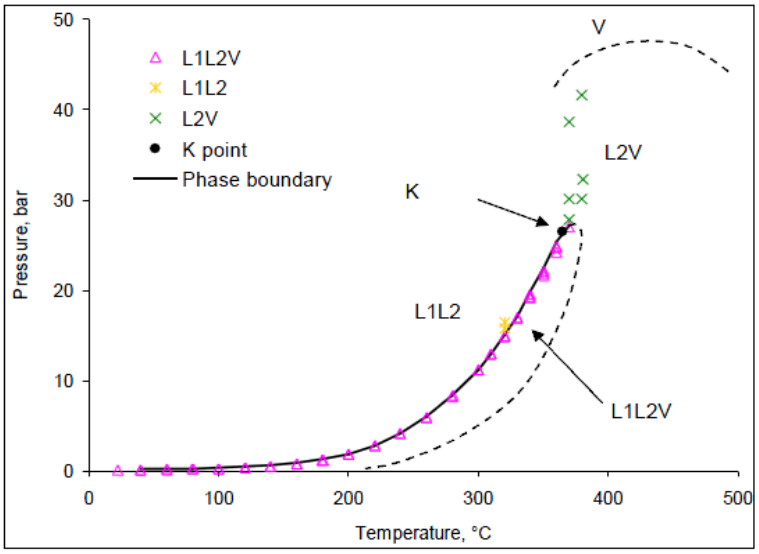

Figure 1.5. Phase diagram for the mixture of AVR (10 wt.%) + n-decane. Reproduced with permission from [91]

In a more recent work, McFarlane [4] showed that the phase behaviour, i.e.: vapour pressure and density, predictions can be improved by using alternative mixing rules for the co-volume parameter of the Peng-Robinson equation of state, Figure 1.6 and Figure 1.7. The group contribution method proposed by Marrero and Gani [9] was used in this study to estimate the critical properties for large and complex molecules present in the mixture. The sixty molecular representations of Sheremata et al. [84] were used as the input.

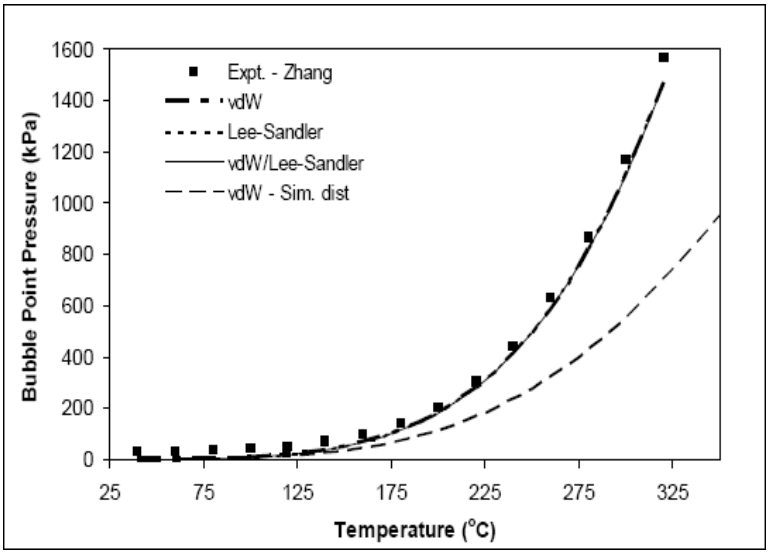

Figure 1.6. Comparison of measured bubble point pressures for 10.03 wt.% AVR mixture with n-decane (data of Zhang [91]) to predictions from the selected mixing rules. Reproduced with permission from [4]

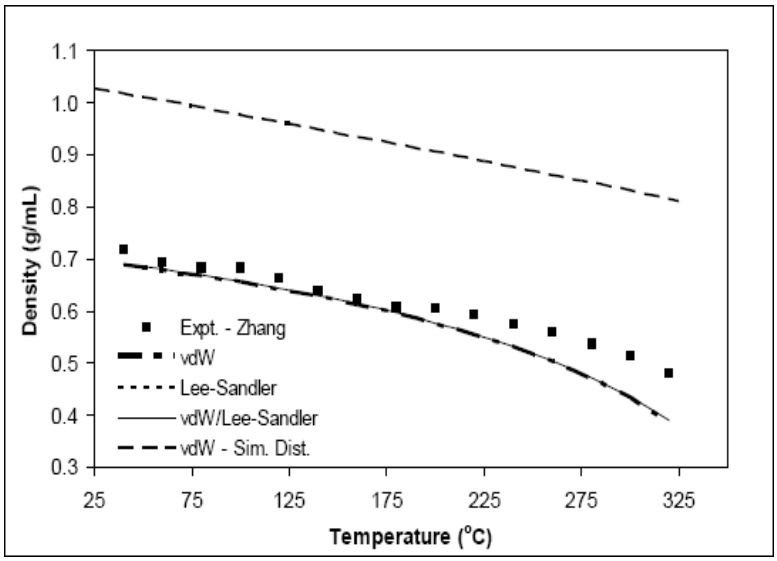

Figure 1.7. Comparison of measured liquid densities for 10.03 wt.% AVR mixture with n-decane (data of Zhang) to predictions from the selected mixing rules. Reproduced with permission from [4]

1.4.3 Phase Behaviour Measurements

Significant advances have been made over the past two decades in phase behaviour measurement techniques. These advances are reflected in the data made

possible through the development of novel view-cells and accessories for experimental phase behaviour measurements [1]. These developments allow researchers to benchmark their computations against reliable phase behaviour data for the first time.

The x-ray view cell apparatus developed by Shaw et al. [1-2] has been used to provide a visual image and record of phase behaviour of mixtures containing AVR and solvents such as n-decane. The phase behaviour is captured based on the difference in transparency of phases to x-ray emission. The apparatus is capable of determining number and nature of phases, phase volumes, and phase densities. In the current project, available vapour pressures and density data in addition to phase diagrams generated [91-93] using the x-ray view cell are utilized to validate the predicted phase behaviour.

1.5 Research Objectives

The predictive capability of previous works is limited to mixtures containing less than ~10 wt% heavy components and they show large deviation from experimental results in the case of higher heavy components concentration. This issue is going to be tackled in the current research by adding the effect of multiphase behaviour. This is a very important issue that should be solved because current prediction ability is far from being efficient for practical applications. For instance, consider the *in situ* bitumen recovery processes that are based on injection of solvents, e.g. VAPEX. Pure solvent enters the reservoir at solvent injection sites while farther from these sites the reservoir fluid consisting of pure bitumen remains undisturbed. The entire phase behaviour space can arise in the area affected by the solvent as the whole range of heavy oil/solvent composition exists. However, the current prediction ability is only limited to near solvent injection sites where the concentration of heavy components is low. The phase behaviour prediction should be extended to higher concentrations of heavy components in order to have successful optimization and development of bitumen production based on solvent injection.

Successful prediction of the phase behaviour of mixtures containing heavy oil and bitumen by creating a very reliable and robust computational tool is the ultimate goal of the current research project. As these mixtures are ill-defined, the common methods currently available are not applicable and new thermodynamic approaches, like group contribution theory, should be used to achieve the goal. The numerical method used for computations is also of great importance and, as a result, a very new and robust technique called global optimization is chosen to guarantee the correct results. Specific objectives include:

1. the generation and validation of a rapid and robust stability analysis algorithm

2. the generation and validation of a two-phase and three-phase flash calculation algorithm

3. the adaptation of thermodynamic models and benchmarking results obtained against experimental data. This work will include reliability testing of group contribution methods and other issues such as the impact of binary interaction parameters on computational outcomes

4. the generation of phase diagrams, e.g. P-T diagrams, for mixtures of AVR and n-alkanes using the created computational tool and comparing the results with available experimental data to refine the modeling

5. inclusion of the computational tool within a commercial simulator.

The present research project can be divided into three major parts. In the first part, a very robust and reliable computational tool for phase equilibrium calculations should be created. This computational tool should be able to handle multiphase equilibrium calculations. In this regard, a new computational approach based on global optimization methods is applied to the phase equilibrium calculations to guarantee the robustness of the algorithm. First, the stability analysis, which is *the* key to successful phase behaviour and phase composition prediction, is created. The two-phase flash and three-phase flash calculation algorithms are then added to complete the phase equilibrium calculations. This

robust and rapid computational approach has the potential for use in a broad range of practical phase equilibrium calculation applications where currently less reliable but rapid approaches are employed.

In the second part, a couple of group contribution theories, which are proven to be appropriate alternatives to avoid the use of measured values for critical properties of heavy components, are tested. The appropriateness of group contribution methods proposed by Crampon et al. [69] and Marrero and Gani [9] in combination with the Peng-Robinson equation of state as a basis for equilibrium calculations is evaluated by generating phase behaviour diagrams for asymmetric model mixtures. Liquid-liquid-vapour three-phase zones for ternary mixtures containing n-decylbenzene and n-eicosane + light hydrocarbons provide illustrative test cases and the results are compared to experimental data and to modeling results obtained using other thermodynamic models available in the literature. In this phase of the project, a reliable thermodynamic model that has the potential to predict the phase behaviour of mixtures containing ill-defined hydrocarbons such as bitumen and heavy oil is evaluated.

In the third part, the created computational tool is used to predict phase behaviours for AVR containing mixtures, such as AVR + n-decane and AVR + n-pentane. The predicted phase behaviour will be benchmarked against the available experimental data and the effect of addition of an extra phase will be investigated. The effect of different parameters of the thermodynamic model on the results is investigated and the model is refined, so that reliable predictions of the thermophysical properties of ill-defined hydrocarbon mixtures over a broad range of compositions and temperatures become possible.

1.6 References

[1] S. J. Abedi, H. Y. Cai, S. Seyfaie, and J. M. Shaw, *Fluid Phase Equilib.* **160** (1999) 775-781.

[2] J. M. Shaw and E. Behar, *Fluid Phase Equilib.* **209** (2003) 185-206.

[3] R. A. McFarlane, M. R. Gray, and J. M. Shaw, *Fluid Phase Equilib.* **293** (2010) 87-100.

[4] R. A. McFarlane, M.Sc. Thesis, University of Alberta, 2007.

[5] A. Van Waeyenberghe, M.Sc. Thesis, University of Alberta, 2006.

[6] M. A. Satyro and H. Yarranton, *Energy Fuels* **23** (2009) 3960-3970.

[7] G. N. Nji, W. Y. Svrcek, H. Yarranton, and A. A. Satyro, *Energy Fuels* **23** (2009) 366-373.

[8] G. N. Nji, W. Y. Svreek, H. W. Yarranton, and M. A. Satyro, *Energy Fuels* **22** (2008) 3559-3559.

[9] J. Marrero and R. Gani, *Fluid Phase Equilib.* **183** (2001) 183-208.

[10] J. M. Sheremata, Ph.D. Thesis, University of Alberta, 2008.

[11] S. Vitu, R. Privat, J. N. Jaubert, and F. Mutelet, *J. Supercrit. Fluids* **45** (2008) 1-26.

[12] G. H. Gao, J. L. Daridon, H. Saintguirons, P. Xans, and F. Montel, *Fluid Phase Equilib.* **74** (1992) 85-93.

[13] L. E. Baker, A. C. Pierce, and K. D. Luks, *SPEJ* **22** (1982) 731-742.

[14] M. L. Michelsen, *Fluid Phase Equilib.* **9** (1982) 1-19.

[15] M. L. Michelsen, *Fluid Phase Equilib.* **9** (1982) 21-40.

[16] M. L. Michelsen, *Fluid Phase Equilib.* **143** (1998) 1-12.

[17] M. L. Michelsen, *Comput. Chem. Eng.* **17** (1993) 431-439.

[18] R. K. Mehra, R. A. Heidemann, and K. Aziz, *Can. J. Chem. Eng.* **61** (1983) 590-596.

[19] W. A. Wakeham and R. P. Stateva, *Rev. Chem. Eng.* **20** (2004) 1-56.

[20] A. C. Sun and W. D. Seider, *Fluid Phase Equilib.* **103** (1995) 213-249.

[21] J. Z. Hua, J. F. Brennecke, and M. A. Stadtherr, *Fluid Phase Equilib.* **116** (1996) 52-59.

[22] J. Z. Hua, J. F. Brennecke, and M. A. Stadtherr, *Comput. Chem. Eng.* **22** (1998) 1207-1214.

[23] J. Z. Hua, R. W. Maier, S. R. Tessier, J. F. Brennecke, and M. A. Stadtherr, *Fluid Phase Equilib.* **158-160** (1999) 607-615.

[24] H. Q. Pan and A. Firoozabadi, *SPE Reservoir Evaluation Eng.* **1** (1998) 36-42.

[25] J. Balogh, T. Csendes, and R. P. Stateva, *Fluid Phase Equilib.* **212** (2003) 257-267.

[26] A. E. Elhassan, S. G. Tsvetkov, R. J. B. Craven, R. P. Stateva, and W. A. Wakeham, *Ind. Eng. Chem. Res.* **37** (1998) 1483-1489.

[27] J. Balogh, R. J. B. Craven, and R. P. Stateva, *Ind. Eng. Chem. Res.* **46** (2007) 1611-1631.

[28] D. V. Nichita, S. Gomez, and E. Luna, *Fluid Phase Equilib.* **194-197** (2002) 411-437.

[29] D. V. Nichita, S. Gomez, and E. Luna, *Comput. Chem. Eng.* **26** (2002) 1703-1724.

[30] A. Bonilla-Petriciolet, R. Vazquez-Roman, G. A. Iglesias-Silva, and K. R. Hall, *Ind. Eng. Chem. Res.* **45** (2006) 4764-4772.

[31] Z. Yushan and X. Zhihong, *Fluid Phase Equilib.* **162** (1999) 19-29.

[32] D. R. Jones, C. D. Perttunen, and B. E. Stuckman, *JOTA* **79** (1993) 157-181.

[33] J. Prausnitz, T. Anderson, E. Grens, C. Eckert, R. Hsieh, and J. O'Connell, *Computer Calculations for Multicomponent Vapor-Liquid and Liquid-Liquid Equilibria*. (Prentice-Hall, New Jersey, 1980).

[34] M. L. Michelsen, *Comput. Chem. Eng.* **18** (1994) 545-550.

[35] M. L. Michelsen, *Fluid Phase Equilib.* **158-160** (1999) 617-626.

[36] M. L. Michelsen, *Fluid Phase Equilib.* **30** (1986) 15-29.

[37] J. F. Boston and H. I. Britt, *Comput. Chem. Eng.* **2** (1978) 109-122.

[38] R. Gautam and W. D. Seider, *Aiche J.* **25** (1979) 991-999.

[39] R. Gautam and W. D. Seider, *Aiche J.* **25** (1979) 999-1006.

[40] J. Castillo and I. E. Grossmann, *Comput. Chem. Eng.* **5** (1981) 99-108.

[41] M. L. Michelsen and J. M. Mollerup, *Thermodynamic Models: Fundamentals & Computational Aspects*. (Tie-Line Publications, 2004).

[42] J. V. Sengers, R. F. Kayser, C. J. Peters, and H. J. J. White, *Equations of State for Fluids and Fluid Mixtures*, 1st ed. (Elsevier, 2000).

[43] P. H. Vankonynenburg and R. L. Scott, *Philosophical Transactions of the Royal Society of London Series a-Mathematical Physical and Engineering Sciences* **298** (1980) 495-540.

[44] D. Peng and D. B. Robinson, *Industrial & Engineering Chemistry Fundamentals* **15** (1976) 59-64.

[45] G. Soave, *Chem. Eng. Sci.* **27** (1972) 1197-1203.

[46] W. G. Chapman, K. E. Gubbins, G. Jackson, and M. Radosz, *Fluid Phase Equilib.* **52** (1989) 31-38.

[47] W. G. Chapman, K. E. Gubbins, G. Jackson, and M. Radosz, *Ind. Eng. Chem. Res.* **29** (1990) 1709-1721.

[48] K. S. Pitzer, *J. Am. Chem. Soc.* **77** (1955) 3427-3433.

[49] K. S. Pitzer, D. Z. Lippmann, R. F. Curl, C. M. Huggins, and D. E. Petersen, *J. Am. Chem. Soc.* **77** (1955) 3433-3440.

[50] M. R. Riazi and T. E. Daubert, *Hydrocarbon Process.* **60** (1980) 115-116.

[51] M. R. Riazi and T. E. Daubert, *Ind. Eng. Chem. Res.* **26** (1987) 755-759.

[52] M. G. Kesler and B. I. Lee, *Hydrocarbon Process.* **55** (1976) 153-158.

[53] C. H. Twu, *Fluid Phase Equilib.* **16** (1984) 137-150.

[54] K. G. Joback and R. C. Reid, *Chem. Eng. Commun.* **57** (1987) 233-243.

[55] L. Constantinou and R. Gani, *Aiche J.* **40** (1994) 1697-1710.

[56] G. M. Wilson, Jasperson, L.V., presented at the AIChE spring meeting, New Orleans, LA, 1996 (unpublished).

[57] J. Marrero-Morejon and E. Pardillo-Fontdevila, *Aiche J.* **45** (1999) 615-621.

[58] L. Coniglio and A. Nouviaire, *Ind. Eng. Chem. Res.* **40** (2001) 1781-1790.

[59] C. Crampon, L. Trassy, L. Avaullee, E. Neau, and L. Coniglio, *Fluid Phase Equilib.* **216** (2004) 95-109.

[60] L. Coniglio, L. Trassy, and E. Rauzy, *Ind. Eng. Chem. Res.* **39** (2000) 5037-5048.

[61] B. E. Poling, Prausnitz, J.M., O'Connell, J.P., *The Properties of Gases and Liquids*, 5th ed. (McGraw-Hill, New York, 2000).

[62] C. Tsonopoulos and Z. M. Tan, *Fluid Phase Equilib.* **83** (1993) 127-138.

[63] *Computer Aided Process-Product Engineering Center (CAPEC)*, Technical University of Denmark, Lyngby, 2000.

[64] B. X. Han and D. Y. Peng, *Can. J. Chem. Eng.* **71** (1993) 332-334.

[65] L. Constantinou, R. Gani, and J. P. Oconnell, *Fluid Phase Equilibria* **103** (1995) 11-22.

[66] L. Constantinou, R. Gani, and J. P. O'connell, *Fluid Phase Equilib.* **103** (1995) 11-22.

[67] A. Bondi, *Physical Properties of Molecular Crystals, Liquids and Glasses*. (John Wiley & Sons, New York, 1968).

[68] M. Rogalski, B. Carrier, and A. Peneloux, *Ind. Eng. Chem. Res.* **30** (1991) 1612-1617.

[69] C. Crampon, L. Trassy, L. Avaullee, E. Neau, and L. Coniglio, *Fluid Phase Equilib.* **216** (2004) 95-109.

[70] I. Polishuk, J. Wisniak, and H. Segura, *Fluid Phase Equilib.* **164** (1999) 13-47.

[71] I. Polishuk, *Fluid Phase Equilib.* **249** (2006) 198-199.

[72] H. Orbey and S. I. Sandler, *Modeling Vapor-Liquid Equilibria: Cubic Equations of State and Their Mixing Rules*. (Cambridge University Press, New York, 1998).

[73] K. S. Pedersen, P. Thomassen, and A. Fredenslund, *Chem. Eng. Sci.* **43** (1988) 269-278.

[74] H. Nishiumi, T. Arai, and K. Takeuchi, *Fluid Phase Equilib.* **42** (1988) 43-62.

[75] A. Kordas, K. Magoulas, S. Stamataki, and D. Tassios, *Fluid Phase Equilib.* **112** (1995) 33-44.

[76] J.-N. Jaubert and F. Mutelet, *Fluid Phase Equilib.* **224** (2004) 285-304.

[77] J.-N. Jaubert, S. Vitu, F. Mutelet, and J.-P. Corriou, *Fluid Phase Equilib.* **237** (2005) 193-211.

[78] F. Mutelet, S. Vitu, R. Privat, and J.-N. Jaubert, *Fluid Phase Equilib.* **238** (2005) 157-168.

[79] R. Privat, J.-N. Jaubert, and F. Mutelet, *Ind. Eng. Chem. Res.* **47** (2008) 2033-2048.

[80] S. Vitu, J.-N. Jaubert, and F. Mutelet, *Fluid Phase Equilib.* **243** (2006) 9-28.

[81] R. Privat, F. Mutelet, and J.-N. Jaubert, *Ind. Eng. Chem. Res.* **47** (2008) 10041-10052.

[82] R. Privat, J.-N. Jaubert, and F. Mutelet, *Ind. Eng. Chem. Res.* **47** (2008) 7483-7489.

[83] S. B. Jaffe, H. Freund, and W. N. Olmstead, *Ind. Eng. Chem. Res.* **44** (2005) 9840-9852.

[84] J. M. Sheremata, M. R. Gray, H. D. Dettman, and W. C. McCaffrey, *Energy Fuels* **18** (2004) 1377-1384.

[85] S. Zhao, L. S. Kotlyar, J. R. Woods, B. D. Sparks, K. Hardacre, and K. H. Chung, *FUEL* **80** (2001) 1155-1163.

[86] J. Murgich, J. A. Abanero, and O. P. Strausz, *Energy Fuels* **13** (1999) 278-286.

[87] M. Fulem, M. Becerr, M. D. A. Hasan, B. Zhao, and J. M. Shaw, *Fluid Phase Equilib.* **272** (2008) 32-41.

[88] A. B. Bazyleva, A. Hasan, M. Fulem, M. Becerra, and J. M. Shaw, *J. Chem. Eng. Data* **55** (2010) 1389-1397.

[89] K. H. Chung, C. M. Xu, Y. X. Hu, and R. N. Wang, *Oil Gas J.* **95** (1997) 66-69.

[90] E. Mahmoodaghdam, University of Alberta, 2002.

[91] X. Zhang, Ph.D. Thesis, University of Alberta, 2006.

[92] X. Y. Zou, Ph.D. Thesis, University of Toronto, 2003.

[93] Y. Maham, Zhang, X., Zabeti, P, Goodkey, J., Allain; M., Shaw, J. M., *Specific Partial Molar Volumes at Infinite Dilution and Volumes of Mixing for Athabasca Bitumen and Bitumen Vacuum Residue + Solvent Mixtures*, Asheville, North Carolina, 2006.

Chapter 2
Rapid and Robust Phase Behaviour Stability Analysis Using Global Optimization[1]

2.1 Introduction

Accurate and robust flash calculations are at the core of a broad range of chemical engineering design applications from pipelines to distillation columns, chemical reactors, and oil and gas production systems. Failure to predict phase equilibria correctly can adversely affect the technical feasibility of resulting designs, their economic viability, and their safety. Two broad classes of challenge arise. The first class of challenge is related to shortcomings in thermodynamic models themselves, i.e.: when the equations are solved correctly the wrong phase behaviour (number, nature, and composition of phases present) is predicted. This arises for binary and multicomponent mixtures alike and reflects inherent limitations in the equations of state or in the parameters regressed from available experimental data and employed in them for computations with specific mixtures. For example, the van der Waals equation of state does not predict Type VI phase behaviour, the phase behaviour of water + hydrocarbon binary mixtures [1], while the phase behaviour of anthracene + n-alkane mixtures is misspredicted due to inappropriate parameter selection [2]. The possible impact of solids on the number, nature and composition of phases present is also not normally included in equation of state models. Further elaboration of these important issues is beyond the scope of this contribution. The second class of challenge, addressed here, relates to tradeoffs between the robustness and the speed, measured in terms of the number of function evaluations, of computational techniques employed to solve for the number, nature and compositions of phases in equilibrium. A general and critical review of numerical solutions for the isothermal phase equilibrium problem and the determination of phase stability was published recently [3].

[1] This chapter with minor modifications has been published in the journal of Fluid Phase Equilibria: Saber, N., and Shaw, J. M. (2008) *Fluid Phase Equilibria*. 264 137-146

Below we provide an overview of global optimization methods for stability analysis, the focus of our work.

With the introduction of the tangent plane criterion for phase stability evaluation [4-6], many approaches have been proposed to address the robustness and speed of the calculations involved. Flash calculations, appearing in commercial process simulators, are based on local minimization because global minimization methods are perceived to be computationally intensive. Further, local minimization methods normally converge to the global minimum of Gibbs free energy with good initialization. Michelsen [5] suggested that stability test results provide an excellent starting point. Second order methods or successive substitution are normally reliable if the global minimum of the Tangent Plane Distance Function (TPDF) is obtained from stability analysis [7-10]. However, use of compositions corresponding to TPDF global minima to initialize flash calculations does not guarantee convergence to correct phase behaviours and compositions, as discussed below. A second stability test should be performed to validate the correctness of flash calculations. The robustness of the phase stability test is *the* key to successful phase behaviour and phase composition prediction.

Global optimization methods have been found to be the most reliable approach for identifying global minima in the TPDF. The most important aspect of a global optimization algorithm is how it balances global vs. local searches. Emphasis on global search increases the number of function evaluations significantly while emphasis on local search decreases the number of function evaluations, but decreases the reliability of the resulting solution. Sun and Seider [11], who used global optimization for the first time, tried to locate all stationary points for the tangent plane distance function (TPDF) using homotopy-continuation. Their approach tends to be computationally intensive and there is no theoretical guarantee that all the stationary points can be located. The Newton interval method in combination with generalized bisection was suggested by Hua et al. [12]. This approach is reliable, but requires interval arithmetic and also requires significant computational effort for multicomponent mixtures. Simulated

annealing (SA), which employs random searches in the computational domain, was used by Pan and Firoozabadi [13]. For the SA approach, the number of function evaluations is high due to an emphasis on global search, and computational outcomes are also dependent on the selection of parameters employed in their algorithm. Balogh et al. [14] suggested another random-search approach. Again, there are several adjustable parameters employed that can affect computational outcomes and lead the algorithm to an incorrect solution. Elhassan et al. [15] proposed the use of the Area method for phase stability. This method requires modification and generalization to apply it to multiphase multicomponent cases. In a recent paper, Balogh et al. [16] applied some modifications and proposed a new generalization of the Area method based on the convex hull principal. Tunneling, used in both flash and stability analysis, was proposed by Nichita et al. [17-18]. This method is robust but the computational intensity is dependent on initial estimates. In a recent paper, Bonilla-Petriciolet et al. [19] compared the performance of a number of stochastic approaches and concluded that simulated annealing was the most reliable of the methods tested. However, all of these approaches involve large numbers of function evaluations. Yushan and Zhihong [20] used Lipschitz optimization to avoid use of starting points and knowledge of objective function gradients in their calculations. However, there are two major problems with their approach. First, it does not lend itself to intuitive generalization for cases with more than two components. Second, the Lipschitz constant, which is required for the optimization procedure, cannot be determined or estimated easily. Jones et al. [21] proposed the DIviding RECTangles (DIRECT) approach that does not require case based constants or initial guesses and can be applied to any number of components. DIRECT is a deterministic method that also provides a good balance between local and global search where local and global searches are not separated. A combination of both is used during all iterations. As a consequence, the number of function evaluations tends to be reduced for challenging examples without a concomitant reduction in reliability vis-à-vis other global optimization approaches [21]. The DIRECT solution approach, not evaluated for phase stability analysis to date, was adopted

for the present work because it may have the potential to be fast enough for use in commercial simulators in lieu of less reliable local minimization methods currently employed.

2.2 DIRECT Optimization Algorithm

This method was proposed to resolve deficiencies related to Lipschitz optimization [21] and was created for cases with bounded domains and real-value objective functions. The Lipschitz constant can be considered as the weighting parameter balancing the emphasis between global and local searches. Standard Lipschitz methods have slow convergence as the value of this constant is usually large, which places emphasis on global search. By contrast, the DIRECT method uses all possible constants, during each iteration, and therefore operates at both the global and local search levels simultaneously. This is the main reason for the fast convergence of the method. The other modification is that sampling is done at central points instead of end points of intervals in order to prevent computational complexities arising in cases with many dimensions. The DIRECT method is guaranteed to converge to the global optimum eventually if the objective function is continuous or at least continuous in the neighbourhood of the global optimum and does not require the objective function to be Lipschitz continuous [21]. Key points related to the DIRECT method are briefly summarized here. For a detailed description of the method and proof of convergence see Jones et al. [21].

The first step in the DIRECT algorithm is to create a normalized computational space by transforming the domain into a unit imaginary domain called a hyper-cube (1×1…). The objective function is then evaluated at the centre of the hyper-cube (C) and then at points $C \pm a\mathbf{e}_i$, where 'a' is one third of the side length of the hyper cube, and '$\mathbf{e}_i$' is a unit vector with a one in the i^{th} position and zeros elsewhere. The normalized space is then subdivided into smaller rectangles with centres at points thus defined, with the "best" value of the function at the centre of the largest rectangle, as illustrated for a 2-D domain in Figure 2.1.

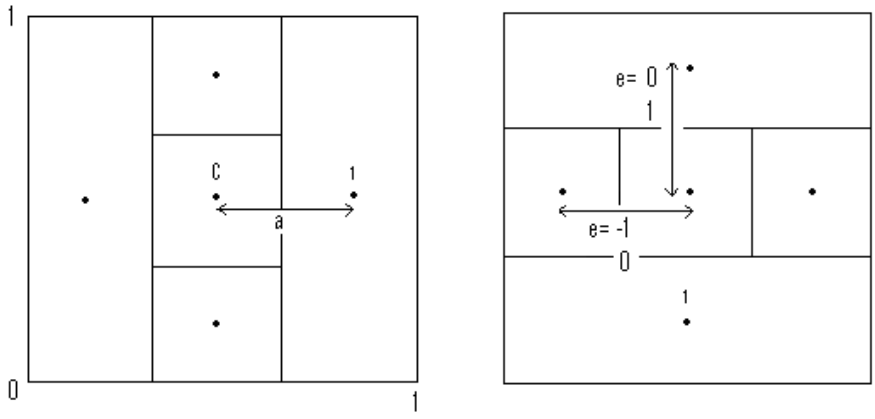

Figure 2.1. Two possible cases for the first division of the normalized space (1×1 hyper square) considering that the value at point 1 is the smallest

Following subdivision, rectangles which have the potential to contain the global optimum are identified and these are further subdivided into smaller rectangles. Rectangles are subdivided along their longest dimension; cubes are divided in all directions. During each iteration, the objective function can be called several times. The selection criteria for potentially optimal rectangles is defined by inequalities 2.1a and b. For a unit hyper-cube divided into m hyper-rectangles, $\mathbf{C}_i$ denotes the centre point of the i^{th} hyper-rectangle, and d_i denotes the distance from the centre point to the vertices and ε is a positive constant. A hyper-rectangle j is said to be potentially optimal if there exists a rate of change constant, $\tilde{L} > 0$, such that:

$$f(C_j) - \tilde{L}\, d_j \le f(C_i) - \tilde{L}\, d_i, \qquad \text{for all } i=1,\ldots,m \tag{2.1a}$$

$$f(C_j) - \tilde{L}\, d_j \le f_{\min} - \varepsilon \left| f_{\min} \right| \tag{2.1b}$$

ε, an optimization parameter, is set at 0.0001 for all calculations performed in this work as suggested by Jones et al. [21]. Condition 2.1b prevents the algorithm from becoming too local, where numerous function evaluations yield only small improvements. As a result, some smaller rectangles are not selected. Once potentially optimal rectangles are chosen, the algorithm divides them into smaller units following the rules described above. The process continues until a specified

number of iterations or function evaluations are performed or convergence within a specified tolerance is reached.

2.3 Phase Stability Objective Function

Phase stability analysis is performed using the tangent plane criterion. A mixture at a specified temperature T, pressure P, and feed composition $\tilde{z}$ is stable if and only if the distance between the Gibbs free energy surface and the tangent plane associated with this surface at the feed composition is greater than zero except at the feed composition. In other words, if the tangent plane lies completely below the Gibbs surface, then the phase is stable. If the optimization process results in negative values for the tangent plane distance function (TPDF), denoted by F($\tilde{x}$), the phase is unstable. The objective function for phase stability, subject to the mass balance constraint, is:

$$\begin{aligned} &\min F(\tilde{x}) = \sum_i x_i(\ln x_i + \ln \phi_i(\tilde{x}) - \ln z_i - \ln \phi_i(\tilde{z})) \\ &subject\ to: \ \sum_i x_i = 1 \qquad 0 \le x_i \le 1 \end{aligned} \tag{2.2}$$

where $\phi_i(\tilde{x})$ and $\phi_i(\tilde{z})$ are the fugacity coefficients of component i at compositions $\tilde{x}$ and $\tilde{z}$ respectively. Composition vector $\tilde{z}$ is the feed composition and composition vector $\tilde{x}$ is the test composition. Equation 2.2 can be converted to an unconstrained minimization by eliminating the mole fraction of one component in the trial phase:

$$x_N = 1 - \sum_{i=1}^{N-1} x_i \tag{2.3}$$

This reduces the dimensions of the hyper cube by one and the N-1 independent composition variables become bounded and unconstrained. If the TPDF is non-negative for all values of $\tilde{x}$, then the feed is stable and its composition corresponds to a global minimum of the Gibbs free energy. Otherwise, the composition, $\tilde{x}$ at the global minimum of the TPDF is used as a starting point for

flash calculations as this composition is always similar to the composition of one of the phases resulting from them. In the examples described below, either the Peng-Robinson [22] or the Soave-Redlich-Kwong equations of state [23] were used to evaluate component fugacities. However, the stability solution method is independent of the equation of state employed.

2.4 Flash Calculations

If the stability analysis shows that a mixture is unstable, flash calculations are performed to identify equilibrium phase natures and compositions corresponding to the global minimum of Gibbs free energy for a mixture with feed composition $\tilde{z}$. The Peng-Robinson [22] and the Soave-Redlich-Kwong equations of state [23] were used to calculate the thermodynamic properties and evaluate the fugacities appearing in the flash calculations. The two-phase flash calculations were performed using an accelerated successive substitution method suggested by Mehra et al. [9] and starting points identified using the DIRECT method as outlined above. This selection is arbitrary as according to Michelsen [5,7] flash calculation computational approaches tend to be robust as long as appropriate starting points are identified. Successive substitution is a robust method, but it is typically slow to converge in critical regions. Acceleration is used to reduce the number of iterations.

2.5 Results and Discussion

The efficiency and robustness of the DIRECT solution method for phase stability and phase equilibrium calculations is demonstrated using six benchmark examples drawn from the literature. Performance comparisons with other available approaches are made on the basis of function evaluations. Robustness comparisons are made on the basis of the correctness of phase behaviour and phase composition computations. Example 1, from Michelsen [5], concerns the phase behaviour of methane + hydrogen sulphide binary mixtures. The TPDF possesses several local minima and the mixture can exhibit both liquid-liquid and vapour-liquid behaviours for different feed compositions at the specified

temperature and pressure. Example 2, from Hua et al. [24], concerns methane + propane mixtures at high pressure. Example 3, from Hua et al. [12], concerns a ternary mixture for which the stability analysis is performed close to a critical point and a phase boundary. Example 4, from Nagarajan et al. [25], concerns an eight component mixture near a critical point that shows the efficiency of the method for a larger number of components. Example 5 concerns a nitrogen-rich light-hydrocarbon mixture comprising six components. This is another difficult case identified by Michelsen [7], which exhibits unexpectedly complicated phase behaviour based on the Soave-Redlich-Kwong equation of state. The phase equilibrium for this case is evaluated in the liquid-liquid region close to the three-phase boundary. Example 6 concerns a five component mixture from Bonilla-Petriciolet et al. [19].

2.5.1 Example 1: hydrogen sulphide (1) and methane (2)

The phase behaviour and phase compositions for this mixture were evaluated at T=190 K and P=40.53 bar using the Soave-Redlich-Kwong equation of state, with T_{C1}=373.2 K, P_{C1}=89.4 bar, ω_1=0.1, T_{C2}=190.6 K, P_{C2}=46.0 bar, ω_2=0.008, and the binary interaction coefficient, k_{12}=0.08. This challenging benchmark example was also treated by Michelsen [5,7], Hua et al. [24], Yushan and Zhihong [20], Balogh et al. [14], and Nichita et al. [18]. The hydrogen sulphide + methane binary mixture exhibits both liquid-liquid and vapour-liquid phase behaviour at the specified conditions. The TPDF at this temperature and pressure has several stationary points for compositions chosen here. For the equimolar mixture, there are five stationary points from which three are minima in the TPDF as shown in Figure 2.2.

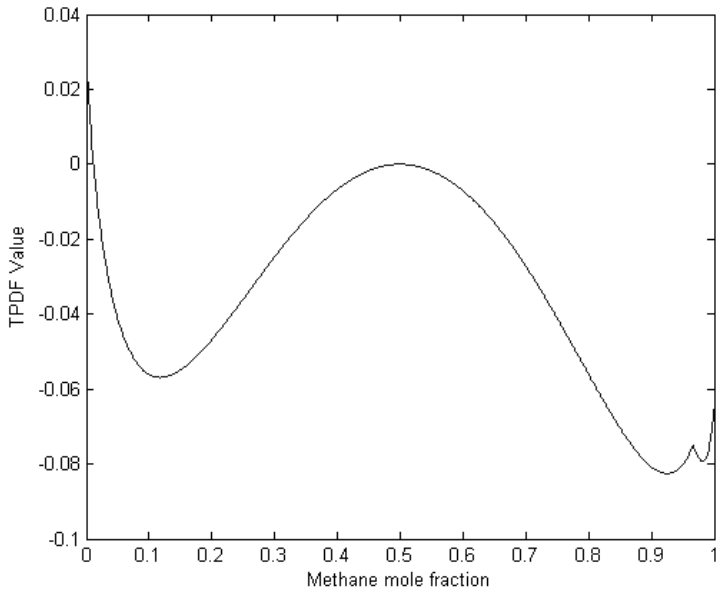

Figure 2.2. TPD function for equimolar mixture of H_2S/C_1

A stability analysis was performed for six different feed compositions as shown in Table 2.1. The first three mixtures are unstable while the latter three are stable. The composition associated with the global TPDF and objective function values obtained for the DIRECT approach and for the other methods are consistent with one another and are correct. However, the number of function evaluations for the DIRECT approach is three orders of magnitude lower than the Lipschitz [20] approach, two order of magnitude lower than Newton-interval [24] and stochastic methods [14], and one order of magnitude lower than conventional Tunneling [18].

Two-phase flash calculations were performed for the three unstable feed compositions using the composition at the global minimum of the TPDF for initialization. The flash calculations for these three cases converge to correct phase behaviours and compositions as shown in Table 2.2. Two cases exhibit liquid-liquid equilibrium; one case exhibits liquid-vapour equilibrium. Commercial simulators, Aspen HYSYS 2004.2 and VMGSim 3.1, converge to liquid-vapour phase behaviour for all three cases. The commercial simulators may not converge in some cases to the correct phase behaviours because the initialization is inappropriate, as pointed out by Michelsen [5]. To illustrate the

impact of initialization on flash calculation outcome, the local minimum of the TPDF at (0.0184, 0.9816) was also employed for the equimolar case. Convergence to the false phase behaviour and phase compositions predicted by the commercial simulators results. These false convergence results are shown in the last row of Table 2.2.

Table 2.1. Stability analysis for example 1 (binary mixture of H_2S/C_1 at P=40.53 bar and T=190K)

Feed Composition (z_1, z_2)	Composition of global minimum (x_1, x_2)	Objective function	Number of function evaluations				
			DIRECT	Lipschitz [20]	Interval Newton[24]	Tunneling [18]	Stochastic [14][a]
(0.0187, 0.9813)	(0.07669, 0.92331)	-3.9598×10^{-3}	75	24983	8438	645	3671
(0.888, 0.112)	(0.07918, 0.92082)	-2.4667×10^{-3}	51	26643	8396	630	3848
(0.5, 0.5)	(0.07461, 0.92539)	-8.2522×10^{-2}	67	24355	8406	696	3409
(0.0115, 0 .9885)	(0.0115, 0.9885)	0[b] (TS)[c]	113	-	5424	512	3584
(0.07, 0 .93)	(0.07, 0 .93)	0 (TS)	75	-	8504	-	3689
(0.89, 0.11)	(0.89, 0.11)	0 (TS)	89	-	8410	667	3862

[a] For the tuning parameters with the highest correct convergence success rate reported.

[b] The code returns TPD value less than 1×10^{-11}

[c] Trivial solution

Table 2.2. Two-phase flash calculation results for example 1 (binary mixture of H_2S/C_1 at P=40.53 bar and T=190 K)

Feed composition (z_1, z_2)	Phase 1 composition	Phase 2 composition	Phase 1 Compressibility factor (Z)	Phase 2 Compressibility factor (Z)
(0.0187,0.9813)	(0.0173,0.9827)	(0.0661,0.9339)	0.5348 (vapour)	0.1698 (liquid)
(0.888, 0.112)	(0.8886,0.1114)	(0.0797,0.9203)	0.0938 (liquid)	0.1630 (liquid)
(0.5,0.5) Initialization at global TPDF minimum	(0.8886,0.1114)	(0.0797,0.9203)	0.0938 (liquid)	0.1630 (liquid)
(0.5,0.5) Initialization at local TPDF minimum	(0.8874,0.1126)	(0.0189,0.9811)	0.0938 (liquid)	0.5314 (vapour)

2.5.2 Example 2: methane (1) and propane (2)

The phase behaviour and phase compositions for this mixture were evaluated at T=277.6 K and P=100 bar using the Soave-Redlich-Kwong equation of state. Parameters for methane (1) are given in the previous section, and those for propane (2) are T_{C2}=369.8 K, P_{C2}=42.5 bar, ω_2=0.152; k_{12}=0.029. Again, three feed compositions were considered as shown in Table 2.3. The first two compositions (near their L=V critical points) are unstable as the value of TPDF is negative, but the third overall composition is stable because the stability calculation converges to the feed composition. Stability results obtained using the DIRECT approach and three other available methods agree. For these cases as well, the DIRECT method requires one to three orders of magnitude fewer function evaluations than the conventional Tunneling [18], Newton-interval [24], and Lipschitz [20] approaches.

Table 2.3. Stability analysis for example 2 (binary mixture of C_1/C_3 at P=100 bar and T=277.6 K)

Feed Composition (z_1, z_2)	Composition of global minimum	Objective function	function evaluations			
			DIRECT	Lipschitz [20]	Interval Newton [24]	Tunneling [18]
(0.68, 0.32)	(0.77252,0.22748)	-3.3481×10^{-4}	39	94127	19986	1113
(0.73,0.27)	(0.65028,0.34972)	-2.9496×10^{-3}	55	107533	14768	1539
(0.4, 0.6)	(0.4, 0.6)	0[a] (TS)[b]	81	37899	2518	586

[a] The code returns TPD value less than 1×10^{-11}

[b] Trivial solution

Two-phase flashes were performed for the two unstable feed compositions using the composition at the global TPDF minimum as the starting point. Results, shown in Table 2.4, agree with expectation. From the similarity of compositions and the values of the compressibilities for the phases, both mixtures are near critical.

Table 2.4. Two-phase flash calculation results for example 2 (binary mixture of C_1/C_3 at P=100 bar and T=277.6 K)

Feed composition (z_1, z_2)	Phase 1 composition	Phase 2 composition	Phase 1 Compressibility factor (Z)	Phase 2 Compressibility factor (Z)
(0.68, 0.32)	(0.6583,0.3417)	(0.7657,0.2343)	0.4227	0.5370
(0.73,0.27)	(0.6583,0.3417)	(0.7657,0.2343)	0.4227	0.5370

2.5.3 Example 3: methane (1), ethane (2), and nitrogen (3)

This example, originally studied by Hua et al. [12], concerns a ternary mixture of methane, ethane, and nitrogen at T=270 K and P=76 bar. The Peng-Robinson equation of state is used with the methane properties given above, and T_{C2}=305.4 K, P_{C2}=48.8 bar, ω_2=0.098, T_{C3}=126.2 K, P_{C3}=33.9 bar, ω_3=0.04, and k_{12}=0.021, k_{13}=0.038, k_{23}=0.08. Three feeds were selected and their stability was evaluated. The stability results obtained for these cases are shown in Table 2.5.

The first feed composition is near the dew point locus, the second one is in the two-phase region close to the L=V critical point, and the third feed composition is in the single-phase region close to the L=V critical point. As expected, the first and second feeds are unstable while the third feed is stable. All of the methods evaluated are consistent with one another and are correct. Again the DIRECT method requires one to two orders of magnitude fewer function evaluations than the other methods reported in Table 2.5. Bonilla-Petriciolet et al. [19] report stability results for three additional stochastic methods that agree with the values reported here but simulated annealing is the most robust. The flash calculations for the two unstable phases, Table 2.6, also agree with one another and with expectation.

Table 2.5. Stability analysis for Example 3 (ternary mixture of $C_1/C_2/N_2$ at P=76 bar and T=270 K)

			function evaluations				
Feed Composition (z_1, z_2, z_3)	Composition of global minimum	Objective function	DIRECT	Interval Newton[12]	SA [19]	Tunneling [18]	Stochastic [14][C]
(0.1, 0.6, 0.3)	(0.06775, 0.79918, 0.13307)	-1.481×10^{-2}	329	5498	92422	3474	3938
(0.3,0.55, 0.15)	(0.24516,0.65803, 0.09681)	-1.169×10^{-3}	243	13421	92467	4831	10337
(0.38,0.54, 0.08)	(0.38,0.54, 0.08)	0[a] (TS)[b]	361	10207	91369	2929	3705

[a] The code returns TPD value less than 1×10^{-10}

[b] Trivial solution

[c] For the tuning parameters with the highest correct convergence success rate reported.

Table 2.6. Two-phase flash calculation results for example 3

Feed composition (z_1, z_2, z_3)	Phase 1 composition	Phase 2 composition	Phase 1 Compressibility factor (Z)	Phase 2 Compressibility factor (Z)
(0.1, 0.6, 0.3)	(0.1116,0.5204, 0.3680)	(0.0740,0.7782, 0.1478)	0.6142	0.2712
(0.3,0.55, 0.15)	(0.3130,0.5237, 0.1633)	(0.2512,0.6485, 0.1003)	0.4914	0.3135

2.5.4 Example 4: eight-component mixture

The stability of an eight-component mixture, NCG8, from Nagarajan et al. [25] was evaluated with the Peng-Robinson equation of state. The properties of the components are shown in Table 2.7, and the non-zero binary interaction coefficients are shown in Table 2.8.

Table 2.7. Properties of components for example 4 (eight-component mixture)

Component	Critical temperature (K)	Critical pressure (bar)	Acentric factor
C_1	190.6	45.99	0.008
C_2	305.4	48.83	0.098
C_3	369.8	42.44	0.152
nC_4	425.2	37.99	0.193
nC_5	469.6	33.73	0.251
nC_6	507.4	29.68	0.296
$C_{7\text{-}16}$	606.28	25.757	0.4019
C_{17+}	825.67	14.58	0.7987

Table 2.8. Binary interaction coefficients for example 4 (eight-component mixture)

	C_1	C_2	C_3
$C_{7\text{-}16}$	0.0500	0.0400	0.0100
C_{17+}	0.0900	0.0550	0.0100

A stability analysis and a flash calculation were performed at T=353 K and P=385 bar, which is near a L=V critical point for the feed composition selected. Composition data and results are shown in Table 2.9, and a computation comparison with Tunneling is shown in Table 2.10. The feed was found to be unstable. Nichita et al. [17] report compositions corresponding to a local minimum and the global minimum in the TPDF, and perform a two-phase flash calculation to obtain the composition of two phases corresponding to the global minimum of Gibbs free energy. The DIRECT method identifies the local

minimum with one order of magnitude fewer function evaluations than the Tunneling method, but this is the only case evaluated where the DIRECT method requires the same order of magnitude of function evaluations to arrive at the global TPDF minimum as another global search method. The phase compositions and objective function values reported in Table 2.9 and Table 2.10 differ slightly from those reported by Nichita et al. [17]. This arises due to small differences between the input properties employed in the two works. Nichita et al. [17] did not report pure component properties. The compressibility factors, for the two phases are also reported in Table 2.9. The values appear high given the proximity of a critical point. However, Nichita et al. [17] do not report compressibilities for this case.

Table 2.9. Composition results for example 4 (eight-component mixture)

				Two-phase flash	
Component	Feed composition	Stability Test (composition at local minimum)	Stability Test (composition at global minimum)	Phase 1 (Z=1.1624)	Phase 2 (Z=1.0224)
C_1	0.6883	0.7474	0.6139	0.6380	0.7276
C_2	0.0914	0.0913	0.0878	0.0902	0.0923
C_3	0.0460	0.0426	0.0477	0.0481	0.0444
nC_4	0.0333	0.0289	0.0365	0.0363	0.0309
nC_5	0.0139	0.0115	0.0159	0.0156	0.0125
nC_6	0.0152	0.0121	0.0178	0.0175	0.0134
$C_{7\text{-}16}$	0.0896	0.0585	0.1266	0.1164	0.0687
C_{17+}	0.0222	0.0077	0.0539	0.0377	0.0100

Table 2.10. Stability analysis for example 4 (the eight-component mixture near the critical point)

Conditions		Objective function	function evaluations	
T (K), P (bar)			DIRECT	Tunneling [17]
353, 385	Local minimum	-2.793×10^{-4}	5381	33642
	Global minimum	-4.87×10^{-4}	43239	35871

2.5.5 Example 5: nitrogen-rich light-hydrocarbon mixture

The stability of a six-component mixture comprising methane, ethane, propane, n-butane, n-pentane and nitrogen was studied by Michelsen [7]. This mixture with a composition noted in Table 2.13 exhibits unexpectedly complicated phase behaviour as modeled by the Soave-Redlich-Kwong equation of state. This equation of state predicts two separate 3-phase regions and six critical points using the pure component properties given above and non-zero binary interaction coefficients given in Table 2.11. At T=150.9 K and P=40.52 bar, the mixture is close to a LL-LLV 3-phase boundary but within a liquid-liquid region. The stability test took a large number of function evaluations to converge, Table 2.12, but a global minimum in the TPDF was identified which showed that the mixture was unstable. The subsequent flash calculations converged to LV phase behaviour. A second stability analysis was performed using the resulting vapour phase composition as the feed composition. A new global TPDF minimum was identified which showed that the LV result was unstable. A second flash calculation was then performed which converged to the stable solution, i.e.: liquid-liquid equilibrium. Both Aspen HYSYS 2004.2 and VMGSim 3.1, converge to the unstable LV phase behaviour. Convergence to the correct phase behaviour in this case is difficult as the difference between the values of the reduced Gibbs free energy ($\Delta G/RT$) for LL vs LV phase behaviour is 1.379×10^{-4}. This example shows that using compositions corresponding to the global minimum of the TPDF does not guarantee convergence to correct phase behaviours and highlights the importance of using stability analysis to verify the correctness of predicted phase behaviours and compositions.

Table 2.11. Binary interaction coefficients for example 5 (six-component mixture)

	C_1	C_2	C_3	nC_4	nC_5
N_2	0.02	0.06	0.08	0.08	0.08

Table 2.12. Stability analyses for example 5 (six-component mixture)

Conditions T (K), P (bar)		Objective function	function evaluations for DIRECT
150.9, 40.52	Stability Test 1	-1.132×10^{-2}	35027
	Stability Test 2	-3.275×10^{-4}	20063

Table 2.13. Feed and phase compositions for example 5 (six-component mixture)

			Two-phase flash based on stability test 1			Two-phase flash based on stability test 2	
	Feed	Stability Test 1, Global minimum	Phase 1 Z=0.5731	Phase 2 Z=0.1578	Stability Test 2, Global minimum	Phase 1 Z=0.1614	Phase 2 Z=0.1588
N_2	0.3040	0.7254	0.71569	0.2909	0.3764	0.3635	0.2535
C_1	0.5479	0.2723	0.2820	0.5564	0.5415	0.5448	0.5505
C_2	0.0708	0.0021	0.00216	0.0730	0.0478	0.0523	0.0865
C_3	0.0367	0.00013	0.00014	0.0379	0.0192	0.0218	0.0494
nC_4	0.0208	0.0000095	0.0000098	0.0215	0.0086	0.0100	0.0300
nC_5	0.0198	0.0000012	0.0000011	0.0204	0.0065	0.0076	0.0302

2.5.6 Example 6: light-hydrocarbon mixture

This mixture, comprising five light hydrocarbons (ethane, propane, n-butane, n-pentane and n-hexane), was studied by Bonilla-Petriciolet et al. [19]. The mixture is modeled using the Soave-Redlich-Kwong equation of state and pure component properties mentioned above. All interaction parameters were set to zero. Stability analysis and two-phase flash calculations were performed for two feed compositions, shown in Table 2.14 and Table 2.15, at T=390 K and P= 55.8 bar. The stability test results and phase composition values, Table 2.14 and Table 2.15, agree with the computations of Bonilla-Petriciolet et al. [19]. The compositions and values of the objective function differ slightly from those given by Bonilla-Petriciolet et al.[19], due to small differences between the sets of pure component properties employed in the two works. Two orders of magnitude fewer

function evaluations were required for the stability test using the DIRECT approach than for Very Fast Simulated Annealing (VFSA), Stochastic Differential Equations (SDE), Modified Direct Search Annealing (MDSA), or Simulated Annealing (SA) – Table 2.16. It should also be noted that the Very Fast Simulated Annealing algorithm converged to local minima during several calculation attempts.

Table 2.14. Feed and phase compositions for example 6 (light hydrocarbon mixture 1)

			Two-phase flash	
Component	Feed No. 1	Stability (composition at Global minimum)	Phase 1 (Z=0.4057)	Phase 2 (Z=0.3731)
C_2	0.401	0.3888	0.4038	0.3899
C_3	0.293	0.2925	0.2931	0.2926
nC_4	0.199	0.2045	0.1977	0.2040
nC_5	0.0707	0.0747	0.0698	0.0743
nC_6	0.0363	0.0395	0.0356	0.0391

Table 2.15. Feed and phase compositions for example 6 (light hydrocarbon mixture 2)

			Two-phase flash	
Component	Feed No. 2	Stability (composition at Global minimum)	Phase 1 (Z=0.3551)	Phase 2 (Z=0.4271)
C_2	0.387	0.4175	0.3849	0.4159
C_3	0.2925	0.2935	0.2924	0.2936
nC_4	0.2	0.1867	0.2009	0.1874
nC_5	0.074	0.0644	0.0747	0.0649
nC_6	0.0465	0.0378	0.0471	0.0382

Table 2.16. Stability analysis for the example 6 (light hydrocarbon mixture at 390 K & 55.8 bar)

	Objective function	function evaluations				
		DIRECT	MDSA	SA	VFSA	SDE
Feed 1	-1.5907×10^{-6}	3185	263980	266926	129534	565142
Feed 2	-2.0312×10^{-5}	3657	261723	266701	130395	814136

2.5.7 General Discussion

The number of function evaluations associated with global minimization methods is linked to how the balance between local and global searches is managed. Tunneling combines local optimization with a tunneling procedure to give a global aspect to a search that makes the search faster. DIRECT employs a combined local-global search during each iteration, where small constants ($\tilde{L}$) place an emphasis on local search and large constants place an emphasis on global search. For the Lipschitz method only large constants are used for optimization, which tends to slow searches. The efficiency of Tunneling is also affected by the initialization procedure that affects the speed of convergence, while the efficiency of stochastic methods and their reliability depend on the tuning of several parameters. The six examples above demonstrate the robustness and the efficiency of the DIRECT algorithm with respect to phase stability analysis and highlight the importance of stability analysis and the composition associated with the TPDF minimum in obtaining correct phase natures and compositions during subsequent flash calculations. The DIRECT algorithm converges to the global TPDF minimum for all cases evaluated. Stochastic methods, as a group, require two to three orders of magnitude more function evaluations than the DIRECT algorithm, and have only a statistical probability of convergence to global minima as demonstrated in example 6 for the Very Fast Simulated Annealing (VFSA) approach. Tunneling requires one order of magnitude more function evaluations than the DIRECT method in all but one case, example 4 (comprising eight components), where it converges faster than the DIRECT method. The DIRECT method is clearly affected more by dimensionality than Tunneling. However, there are numerous industrial applications, such as large-scale oil and gas reservoir simulations where the number of components is severely restricted because of the speed of calculations. In many cases practitioners are currently limited to ~ five components or pseudo components. The application of the

DIRECT method for such cases would improve the reliability of these simulations without introducing a significant additional computational cost.

The number of function evaluations for stationary point methods used in commercial phase equilibrium simulators to initiate flash calculations is typically one order of magnitude less than that needed for the DIRECT method. However, these algorithms may not converge to the global minimum of the TPDF as they are based on local minimization methods, and there is no guarantee that correct phase behaviours or phase compositions are obtained. The robustness of two typical process simulators, Aspen HYSYS 2004.2 and VMGSim 3.1 is summarized in Table 2.17, for examples 1-3 and 5-6 above. For example 4, required input data for the pseudo component is missing and calculations cannot be performed. Both simulators converge to false phase behaviours for mixtures of industrial interest notably methane + hydrogen sulphide (example 1), and nitrogen + light hydrocarbons (example 5), albeit at extreme conditions. These simulators appear to be prone to false convergence with respect to phase behaviour whenever the Gibbs free energy surface is non-convex. Given the importance of flash calculation precision and the efficiency and robustness of the DIRECT approach for flash calculation initialization, consideration should be given to including global search techniques in phase equilibrium simulators to increase their robustness. At a minimum, its introduction as an option or as an off-line check on the stability of predicted phase behaviour should be considered because phase behaviour result reliability is critical to the design of all industrial processes.

Table 2.17. Correctness of phase behaviour predicted by commercial simulators

		VMGSim 3.1	Aspen HYSYS2004.2
Example 1	Case 1	✓[a]	✓
	Case 2	×[b]	×
	Case 3	×	×
Example 2	Case 1	✓	✓
	Case 2	✓	✓
	Case 3	✓	✓
Example 3	Case 1	✓	✓
	Case 2	✓	✓
	Case 3	✓	✓
Example 4		-[c]	-
Example 5		×	×
Example 6	Case 1	✓	✓
	Case 2	✓	✓

[a] converges to the correct solution
[b] converges to false phase behaviour
[c] Required input parameters for pseudo component are not available

2.6 Conclusions

The robustness and the efficiency of the DIviding RECTangles (DIRECT) algorithm for phase stability analysis vis-à-vis other global minima search techniques is demonstrated using six challenging benchmark examples drawn from the literature. The DIRECT algorithm converges to the global TPDF minimum for all cases evaluated and uses significantly fewer function evaluations than Tunneling, the next fastest global minimization method for three of four cases evaluated. Stochastic methods, as a group, require two to three orders of magnitude more function evaluations than the DIRECT algorithm, and only have a statistical probability of convergence to global minima. Other approaches (Lipschitz and Newton Interval) also require large numbers of function evaluations. Identification of the global TPDF minimum during phase stability calculations does not guarantee the correctness of subsequent flash calculations if the calculations are based on local minimization approaches and stability analysis should be performed on flash calculation results to validate their correctness. The DIRECT method handles stability analysis for multicomponent mixtures and near critical points in an efficient and reliable way, and does not require initialization or knowledge of TPDF gradients. Commercial simulators do not currently make use of global minimization to initiate flash calculations and to validate the

correctness of predicted phase behaviours and phase compositions. Commercial simulators are shown to converge to false phase behaviours even for mixtures of industrial importance. Incorporation of a fast global minimization algorithm such as DIRECT in process simulators would appear to be warranted.

2.7 Nomenclature

a	one third of the side length of the hyper-cube
C_i	centre point of the i^{th} hyper-rectangle
d_i	distance from the centre point to the vertices
$\mathbf{e}_i$	unit vector with a one in the i^{th} position
$F(\tilde{X})$	tangent plane distance function (TPDF)
$f(C_j)$	objective function value at centre point
G	Gibbs free energy
k	binary interaction coefficient
$\tilde{L}$	rate of change constant
N	number of components
P	pressure
P_C	critical pressure
R	universal gas constant
T	temperature
T_C	critical temperature
$\tilde{x}$	trial composition vector
Z	compressibility factor
$\tilde{z}$	feed composition vector

Greek letters

ε DIRECT minimization parameter

ω acentric factor

φ fugacity coefficient

Subscripts

i component index, and hyper-cube index

j hyper-cube index

2.8 Abbreviations

DIRECT	dividing rectangles
L	liquid
LL	liquid-liquid
LLV	liquid-liquid-vapour
LV	liquid-vapour
MDSA	modified direct search annealing
SA	simulated annealing
SDE	stochastic differential equations
V	vapour
VFSA	very fast simulated annealing

2.9 References

[1] P. H. Vankonynenburg and R. L. Scott, *Philos. Trans. R. Soc. London* **298** (1980) 495-540.

[2] D. Minicucci, X. Y. Zou, and J. M. Shaw, *Fluid Phase Equilib.* **194** (2002) 353-360.

[3] W. A. Wakeham and R. P. Stateva, *Rev. Chem. Eng.* **20** (2004) 1-56.

[4] L. E. Baker, A. C. Pierce, and K. D. Luks, *SPEJ* **22** (1982) 731-742.

[5] M. L. Michelsen, *Fluid Phase Equilibria* **9** (1982) 1-19.

[6] J. W. Gibbs, *Trans. Conn. Acad. Arts Sci.* **11** (1873) 382-404.

[7] M. L. Michelsen, *Fluid Phase Equilibria* **9** (1982) 21-40.

[8] M. L. Michelsen, *Comput. Chem. Eng.* **17** (1993) 431-439.

[9] R. K. Mehra, R. A. Heidemann, and K. Aziz, *CJChE* **61** (1983) 590-596.

[10] M. L. Michelsen, *Fluid Phase Equilib.* **143** (1998) 1-12.

[11] A. C. Sun and W. D. Seider, *Fluid Phase Equilib.* **103** (1995) 213-249.

[12] J. Z. Hua, R. W. Maier, S. R. Tessier, J. F. Brennecke, and M. A. Stadtherr, *Fluid Phase Equilib.* **158-160** (1999) 607-615.

[13] H. Q. Pan and A. Firoozabadi, *SPE Reservoir Evaluation Eng.* **1** (1998) 36-42.

[14] J. Balogh, T. Csendes, and R. P. Stateva, *Fluid Phase Equilib.* **212** (2003) 257-267.

[15] A. E. Elhassan, S. G. Tsvetkov, R. J. B. Craven, R. P. Stateva, and W. A. Wakeham, *Ind. Eng. Chem. Res.* **37** (1998) 1483-1489.

[16] J. Balogh, R. J. B. Craven, and R. P. Stateva, *Ind. Eng. Chem. Res.* **46** (2007) 1611-1631.

[17] D. V. Nichita, S. Gomez, and E. Luna, *Fluid Phase Equilib.* **194-197** (2002) 411-437.

[18] D. V. Nichita, S. Gomez, and E. Luna, *Comput. Chem. Eng.* **26** (2002) 1703-1724.

[19] A. Bonilla-Petriciolet, R. Vazquez-Roman, G. A. Iglesias-Silva, and K. R. Hall, *Ind. Eng. Chem. Res.* **45** (2006) 4764-4772.

[20] Z. Yushan and X. Zhihong, *Fluid Phase Equilib.* **162** (1999) 19-29.

[21] D. R. Jones, C. D. Perttunen, and B. E. Stuckman, *JOTA* **79** (1993) 157-181.

[22] D. Peng and D. B. Robinson, *I.&E.C. Fund.* **15** (1976) 59-64.

[23] G. Soave, *Chem. Eng. Sci.* **27** (1972) 1197-1203.

[24] J. Z. Hua, J. F. Brennecke, and M. A. Stadtherr, *Comput. Chem. Eng.* **22** (1998) 1207-1214.

[25] N. R. Nagarajan, A. S. Cullick, and A. Griewank, *Fluid Phase Equilib.* **62** (1991) 191-210.

Chapter 3
Toward Multiphase Equilibrium Prediction for Ill-Defined Asymmetric Hydrocarbon Mixtures[1]

3.1 Introduction

Reliable phase behaviour predictions using robust phase equilibrium calculations are essential in numerous chemical and petroleum engineering applications. Prediction of thermodynamic properties for mixtures containing diverse molecule sizes is of great importance and is a subject of both industrial and scientific interest. For mixtures containing small molecules like CO_2, nitrogen, methane in addition to large hydrocarbon molecules such as constituents of bitumen and heavy oil, thermodynamic properties and phase behaviour data are not usually available in the literature as they are difficult to obtain experimentally. Interpolation and extrapolation of sparse and incomplete data sets is necessary. Successful phase behaviour and phase composition prediction for mixtures including such ill-defined fluid constituents can play a major role in this field. However, formidable challenges must be faced.

There are two broad classes of challenge that should be addressed in order to guarantee reliable phase behaviour prediction for these mixtures: creation of a robust and accurate computational tool, and implementation of a reliable thermodynamic model. The first class of challenge relates to tradeoffs between the robustness and speed of computational techniques employed to solve for the number, nature and compositions of phases in equilibrium. This issue has been addressed in Chapter 2 in detail [1] and is discussed briefly here. Flash calculations, used for phase equilibrium calculations, are based on local minimization because global minimization methods are computationally intensive. Further, local minimization methods normally converge to the global minimum of Gibbs free energy with good initialization. Michelsen [2-4] correctly

[1] This chapter with minor modifications has been published in the journal of Fluid Phase Equilibria: Saber, N., and Shaw, J. M. (2009) *Fluid Phase Equilibria*. 285 73-82

suggested that stability test results are reliable initialization for flash calculations. However, use of compositions resulting from phase stability analysis to initialize flash calculations does not guarantee convergence to correct phase behaviours and compositions [1]. A second stability test should be performed to validate the correctness of flash calculation results. A robust stability analysis is the key to correct phase equilibrium calculations. To fulfill this need, in general, a very reliable and rapid stability test was created based on the global minimization method called DIRECT (Dividing Rectangles) [5]. For example, this stability analysis approach eliminates numerical shortcomings of commercial process simulators where flash calculations are prone to failure when the Gibbs free energy surface is non-convex.

The second class of challenge, which is the focus of this contribution, relates to shortcomings in thermodynamic models. Equations of state (EOS) are the most popular thermodynamic models that can be used for phase equilibrium calculations even at high pressures. Among these, cubic equations of state provide the best balance between accuracy, reliability, simplicity, and speed of computation. Further, they only predict phase diagrams arising in nature. It should be mentioned that small differences in equations of state structure and parameters may lead to significant differences with respect to phase behaviour prediction. For example, for methane + hexane binary mixtures, where in the low temperature liquid-vapour region numerous cubic EOS perform equivalently, the nature of predictions diverge in the critical region [6]. Not all of the cubic EOS predict the liquid-liquid-vapour and liquid-liquid phase behaviour observed experimentally. The Peng-Robinson equation of state (PR EOS) provides the most accurate results for this binary mixture. Although the accuracy of these predictions is dependent on knowledge of experimental equilibrium data, proper selection of the empirical functionalities of a reliable cubic equation of state like the Peng-Robinson EOS and binary interaction parameters enables prediction of complicated critical loci with a high degree of accuracy [7]. The limitations of cubic equations of state are evident as they do not account for factors like polarity, molecular shape, chain length, hydrogen bonds, and association, but they are able to correlate most of the

consequences of all these factors. However, the inherent limitations of a cubic equation of state do not warrant the employment of more complicated thermodynamic models. Besides the inconsistencies in phase behaviour prediction that can be introduced with more complex models, an inherent restriction, these models do not provide better results [8]. Cubic equations of state have been employed to predict the phase behaviour of asymmetric hydrocarbon mixtures such as gas condensates [8-9] and model reservoir fluids [10] and have the potential to be used for more complex mixtures. However, the problem of selecting an appropriate thermodynamic model becomes even more severe for mixtures containing heavier and ill-defined components where the critical properties are not normally available or where the molecular structure of molecules present and their molar mass distribution are both weakly defined. Development of group contribution methods [11-13] has addressed this issue to some extent, but the reliability of these methods in predicting multiphase behaviour warrants attention because most of these methods are based on parameters derived from vapour, liquid or liquid-vapour equilibrium data. Parameters appearing in most group contribution methods are obtained by regression of data for molecules with measurable critical properties. As a result, employing them for large molecules and for pseudo components is a stringent test of their reliability.

McFarlane [14] studied and compared the consistency of different group contribution methods including Joback and Reid [15], and Wilson-Jasperson [16] and found that the method of Marrero and Gani [11] generates the most consistent set of critical properties for mixtures containing heavy oil and bitumen. The group contribution based Peng-Robinson equation of state, developed by Coniglio et al. [13,17] and further simplified by Crampon et al. [12], was tested for the same mixtures and generated reasonable results [18]. Here, the performance of a mixed EOS model is compared to normal equations of state and the effect of binary interaction parameters is studied. The focus is on the three-phase region of phase diagrams for ternary asymmetric model mixtures containing n-eicosane and n-decylbenzene. These are among the largest components for which critical

properties are available in the literature, and they provide a good basis for comparison among thermodynamic models. Experimental phase diagrams with a focus on the three-phase region and retrograde behaviour for these mixtures have been generated [10,19-20]. Such mixtures are of great importance in practice and knowledge of the three-phase region can play a major role in assessing the reliability of calculations supporting process design and development. While vapour-liquid equilibrium has been studied and modeled successfully using equations of state and group contribution theory [21-23], the performance of the same models in the three-phase region has received much less attention. Multiphase equilibrium calculations are a rigorous test for a thermodynamic model. The objective of this contribution is to investigate differences among group contribution methods with respect to phase behaviour and phase composition prediction for asymmetric mixtures with large molar mass components and to create a reliable combination of group contribution theory and cubic equations of state as a basis for successful phase behaviour and phase composition predictions for bitumen and heavy oil applications.

3.2. Thermodynamic Model

The Peng-Robinson (PR) equation of state, Equation 3.1a, was selected for the current work.

$$P = \frac{RT}{v-b} - \frac{a(T)}{v(v+b)+b(v-b)} \tag{3.1a}$$

Parameters appearing in Equation 3.1a are calculated based on Equations 3.1b-f. The temperature dependencies shown in Equations 3.1d and 3.1e for the energy parameter, α, are used. The van der Waals mixing rules, Equations 1.25 and 1.26, are employed to calculate the equation of state parameters for mixtures.

$$a = a_c \alpha(T) \tag{3.1b}$$

$$a_c = \frac{0.45724 R^2 T_c^2}{p_c} \tag{3.1c}$$

$$\alpha = \left[1 + (0.37464 + 1.54226\omega - 0.26992\omega^2)(1 - (\frac{T}{T_c})^{\frac{1}{2}})\right]^2 \quad \text{for} \quad \omega \le 0.49 \qquad (3.1d)$$

$$\alpha = \left[1 + (0.3796 + 1.485\omega - 0.1644\omega^2 + 0.01667\omega^3)(1 - (\frac{T}{T_c})^{\frac{1}{2}})\right]^2 \quad \text{for } \omega > 0.49 \quad (3.1e)$$

$$b = \frac{0.07780RT_c}{p_c} \qquad (3.1f)$$

The only parameters that are adjustable are the binary interaction coefficients, k_{ij}s, which have a significant impact on the accuracy of the predicted phase behaviour. The PR equation of state is employed along with two group contribution (GC) methods, Crampon et al. [12] and Marrero and Gani [11], and these comprise the thermodynamic model. These two GC methods are discussed briefly below.

3.2.1 Group Contribution Method of Marrero and Gani

Marrero and Gani [11] estimate critical properties that are used to calculate equation of state parameters. This method includes three levels of group contribution and the effect of complex groups. The first level of contribution consists of small groups that can define the entire molecular structure. The second level consists of more complex groups and includes geometric considerations that can be used to distinguish isomers. The third level of contribution better describes polycyclic systems like fused aromatics. This method can estimate critical properties as well as normal boiling and melting points and enthalpies for phase transitions. The equations for estimating critical temperature (K) and pressure (bar) have the form:

$$\exp(\frac{T_c}{231.239}) = \sum_i N_i tc_i + \sum_j M_j tc_j + \sum_k O_k tc_k \qquad (3.2)$$

$$(P_c - 5.9827)^{-\frac{1}{2}} - 0.108998 = \sum_i N_i pc_i + \sum_j M_j pc_j + \sum_k O_k pc_k \qquad (3.3)$$

where N_i, M_j, O_k are the numbers of the 1st, 2nd and 3rd order groups, respectively; tc_i, tc_j, tc_k are the 1st, 2nd and 3rd order group contributions to T_c; and pc_i, pc_j, pc_k are the 1st, 2nd and 3rd order group contributions to P_c.

There are also group contribution methods that can be used to estimate the acentric factor, as the method of Marrero and Gani does not provide any information in this regard. The method used here was developed by Constantinou et al. [24]. Two levels of contributions are considered in this method. Second order contributions from more complex groups are linked to geometry and distinguish isomers. The group contribution method for estimating acentric factor is given in Equation 3.4:

$$\omega = 0.4085\left[\ln\left(\sum_i N_i\varepsilon_{1i} + A\sum_j M_j\varepsilon_{2j} + 1.1507\right)\right]^{\frac{1}{0.5050}} \tag{3.4}$$

N_i and M_j in Equation 3.4 are the numbers of the 1st and 2nd order groups, ε_{1i} and ε_{2j} are the 1st and 2nd order group contributions to ω, and A is either 0 or 1 depending on whether or not there is a defined 2nd order contribution.

3.2.2 Group Contribution Method of Crampon et al.

In this approach, instead of estimating critical properties and calculating the two cubic equation of state parameters, the group contributions are directly incorporated into the cubic equation of state. Coniglio et al. [13,17] developed this group contribution-based form of the PR equation of state. It was further refined and simplified by Crampon et al. [12]. This group contribution method considers a variety of hydrocarbons including alkanes, naphtanes, alkylbenzenes, and polynuclear aromatics.

Parameters of the corresponding chemical species are calculated through formulae accounting for weighted contributions of the different groups present. The co-volume parameter of the PR equation of state, b, is calculated based on a group contribution method developed by Bondi [25] for the van der Waals volume using methane as a reference, as shown in Equation 3.5:

$$b = b_{CH4}\frac{\left(\sum_{j=1}^{7} V_{Wj}N_j + \sum_{j=1}^{3}\delta V_{Wk}I_k\right)}{V_{WCH_4}} \tag{3.5}$$

where V_{Wj} is the contribution of the j^{th} group to the van der Waals volume and N_j is the number of groups of type j. δV_{WK}, represents a correction introduced for special cases and I_k represents the number of corresponding occurrences. The methane co-volume b_{CH4} has a value of 26.80 cm^3/mol and is obtained from its critical properties [17].

The energy parameter of the PR equation of state, a, is temperature dependent and is calculated using Equation 3.6:

$$a(T) = a(T_b)\exp\left\{f_1(m)\left[1-\left(\frac{T}{T_b}\right)^{0.4}\right] - f_2(m)\left[1-\left(\frac{T}{T_b}\right)^{2.5}\right]\right\}$$

$$f_1(m) = 1.80546 \quad m + 0.21887 \tag{3.6}$$

$$f_2(m) = -0.11113 \quad m + 0.03502$$

where m is a shape factor that can be calculated using group contribution methods and has a role similar to acentric factor. If the normal boiling point is not known or cannot be measured, it can be estimated by another group contribution method proposed by Coniglio et al. [17]. In Equation 3.6, $a(T_b)$ is the value of a(T) at the normal boiling temperature and can be estimated by iteration using the Peng-Robinson equation of state to match the vapour pressure at this temperature, i.e., 1 atm. The estimation of the parameters (a and b) is based on a linear sum of contributions.

3.3 Multiphase Equilibrium Calculations

Numerous computational techniques have been proposed to make multiphase equilibrium calculations more reliable. Baker [26] and Michelsen [2] showed that normal equilibrium conditions based on equality of chemical potentials cannot guarantee correct phase behaviour prediction because Gibbs free

energy can contain more than one minimum. They also proved that stability analysis is the necessary and sufficient condition for phase equilibrium. In other words, including phase stability analysis in multiphase equilibrium calculations is vital to the reliability of phase behaviour prediction.

With the introduction of the tangent plane criterion for phase stability evaluation [2,26], many approaches have been proposed to address the robustness and speed of the calculations involved. It has been proven that only methods based on global search in the domain of the tangent plane distance function provide reliable results. In this regard, a global minimization computational technique called DIRECT was adopted for the stability analysis [1], which provides a balance between reliability and computational speed. Two-phase flash calculations, based on successive substitution, generated correct phase behaviour predictions in combination with this stability analysis. In this work, the three-phase flash based on successive substitution and the objective function proposed by Michelsen [27] has been added to the equilibrium calculation package. The equilibrium calculations start with the stability analysis performed on a feed composition. If the stability analysis shows that the mixture is unstable, two-phase flash calculations are performed to identify equilibrium phase natures and compositions corresponding to the global minimum of Gibbs free energy. The stability analysis tests the results of the two-phase flash calculations and the three-phase flash calculations are performed if required. The results of each stability analysis are used to initialize the subsequent flash calculations. This multiphase equilibrium computational tool has been tested numerically for several challenging cases in the literature and provided both rapid and reliable phase behaviour predictions [1].

3.4 Results and Discussion

Results obtained from two hybrid thermodynamic models (Marrero and Gani + the PR EOS and Crampon et al. + the PR EOS) are presented and then discussed. In some cases, calculations were also performed using the PR equation of state and experimental critical properties. For other cases, additional

calculations are available in the literature. These provide additional bases for comparison and discussion.

The reliability of the thermodynamic models for phase behaviour prediction is tested using two types of model mixtures. The first type consists of a binary immiscible mixture containing n-decylbenzene to which an additional constituent, also immiscible with n-decylbenzene, is added. These mixtures were studied experimentally by Shaw et al. [10], who prepared phase diagrams with a focus on the three-phase region. The PR equation of state was also used by these authors to model the experimental data and to generate the three-phase region boundaries. The results obtained are qualitatively successful. The second type of mixture consists of an immiscible binary mixture comprising n-eicosane and ethane to which propane (miscible with both n-eicosane and ethane) or methane (miscible only with ethane) is added. The experimental three-phase equilibrium data for these latter cases were obtained by Gregorowicz et al. [19-20]. They modeled their experimental data using several equations of state including one version of SAFT and concluded that in general the PR equation of state with modified energy parameter values provides the best phase boundary predictions for these mixtures [8]. These mixtures are excellent test cases as they challenge the reliability of thermodynamic models both with respect to generating correct phase behaviours at specific compositions and with respect to phase behaviour trends that result from addition of a third component to a binary mixture. Luks [28] showed that addition of a third component to a binary mixture shifts the location of liquid-liquid-vapour (LLV) region and alters its size depending on the miscibility of the third component. Addition of a component miscible with either of the other components increases the miscibility of the mixture and causes the LLV zone to shrink and disappear at a tricritical point (T; L1=L2=V). This leads to LLV regions on the high temperature side of the binary LLV line. On the other hand, addition of an immiscible component increases the size of the three-phase zone and leads to three-phase zones on the low temperature side. A schematic of these phase behaviour trends is shown in Figure 3.1. The lines surrounding the LLV zones are critical loci (K; L1=V + L2 and L; L1=L2+V). Both of these

phase behaviour patterns are expected in heavy oil or bitumen + lighter oil or gas mixtures of industrial interest with applications from enhanced production to deasphalting to refining [29-30] in addition to more complex phase behaviours such as SLLV.

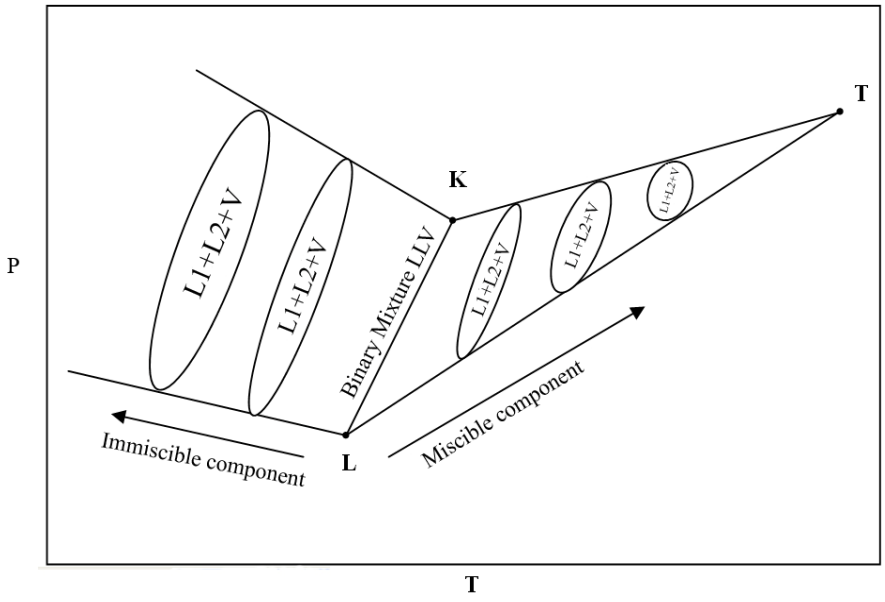

Figure 3.1. Schematic of phase behaviour trends expected upon addition of a third component to a binary mixture that exhibits LLV phase behaviour.

Each thermodynamic model is first tested by generating phase diagrams for model mixtures mentioned above at different sets of compositions and benchmarking the results against experimental data. If successful, the thermodynamic model is then used to create phase behaviour trends for these model mixtures and the results are compared to the trends observed experimentally. The results obtained with each thermodynamic model are discussed below.

3.4.1 The Peng-Robinson EOS (standard coefficients)

Shaw et al. [10] modeled mixtures containing n-decylbenzene using the PR EOS and experimental critical properties and acentric factors. They benchmarked the phase diagrams against experimental data for four different cases. Their calculations were repeated here using the same thermodynamic

model, input data, and binary interaction coefficients (k_{ij}) to generate the phase diagram for an additional set of compositions. The experimental three-phase (LLV) region and surrounding two-phase regions (L1V, L2V, L1L2) and critical points for this latter phase diagram are shown in Figure 3.2 A. The observed phases include a low-density liquid phase, L1, a denser liquid phase, L2, and a vapour phase V. Two critical points are found on the boundary of the three-phase region. At the L-point, L1 and L2 become critical in the presence of the vapour phase and at the K-point, L1 and V become critical in the presence of L2. The experimental phase boundary measurements are compared to the computed phase diagram in Figure 3.2 B. The estimated critical properties, the acentric factor, and the standard interaction coefficients between n-decylbenzene and other components are given in Table 3.1. The phase diagrams generated by Shaw et al. [10] and the phase diagram generated here agree with the experimental data qualitatively and the phase boundaries are within an acceptable range of error (~5 K and ~5 bar). The predicted liquid-liquid-vapour zones are shifted to lower pressures and temperatures, and their shapes, sizes and locations are approximately correct.

Although the standard Peng-Robinson equation of state is successful in predicting the phase diagrams for mixtures containing n-decylbenzene, it does not provide reliable results for mixtures containing n-eicosane. Gregorowicz and de Loos [8] used the Peng-Robinson EOS to model mixtures containing n-eicosane and found out that this thermodynamic model only generates reasonable results for such mixtures when modified versions of the energy parameter or mixing rules are employed. Our attempt to model the phase behaviour of these mixtures shows that phase equilibrium calculations based on the PR EOS + standard coefficients results in phase diagrams in which the three-phase zone is not present. The estimated critical properties, the acentric factor, and the standard interaction coefficients between n-eicosane and other components are given in Table 3.1. Binary interaction coefficient values for pairs of smaller molecules are 0. The unsuccessful prediction of phase diagrams indicates that the Peng-Robinson equation of state on its own is not a reliable thermodynamic model for phase

behaviour prediction for asymmetric mixtures in general even if constituents are well defined.

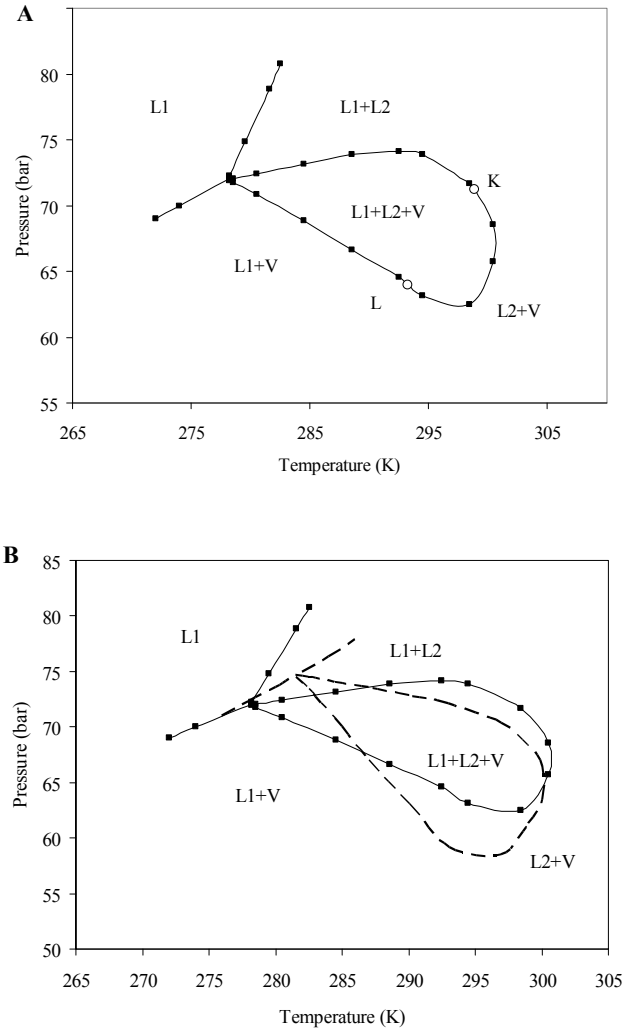

Figure 3.2. Phase boundaries for the ternary mixture of ethane (87.3 mole %), nitrogen (10 mole %), and n-decylbenzene (2.7 mole %). A) Measurements[10], B) Predictions (■, experimental data [10]; — — —, PR EOS with standard k_{ij}, acentric factor and experimental critical points for each consitituent).

Table 3.1. Physical and thermodynamic properties for n-decylbenzene and n-eicosane [8,10]

compound	molar mass	P_c (bar)*	T_c (K)*	acentric factor*	Standard k_{ij} for the PR EOS				
					N_2	CH_4	C_2H_6	CO_2	C_3H_8
n-decylbenzene	218.34	18.3 / 17.84	743 / 748.74	0.66 / 0.646	0.2	0.02	0.02	0.12	-
n-eicosane	282.55	11.74 / 12.55	768.42/ 766.28	0.8846 / 0.886	-	0.06468	0.02362	-	0.0159

* experimental values / values estimated using the Marrero and Gani method.

3.4.2 Group Contribution Based PR EOS: Method of Crampon et al.

The group contribution based PR EOS proposed by Crampon et al. [12] was also used to generate phase behaviour predictions for mixtures containing n-decylbenzene. The phase diagram shown in Figure 3.2 A comprises the first test case. Figure 3.3 A shows the predicted phase diagram using the standard values of binary interaction coefficients given in Table 3.1. The LLV zone is shifted to much lower temperatures and pressures and its shape and size are predicted incorrectly. Better results can be obtained by setting binary interaction coefficients to zero as shown in Figure 3.3 B, which shows that the values of these coefficients should be modified to generate more accurate phase behaviour predictions. The phase diagram shown in Figure 3.3 C is obtained using custom fit k_{ij} values given in Table 3.2. The k_{ij} values reported in Table 3.2 were then used for the same mixture, n-decylbenzene + ethane + nitrogen, with a different composition and the predicted phase behaviour is compared to the experimental data in Figure 3.4 A. Again, the LLV region is much bigger than the experimental one and it is shifted significantly to lower temperatures and pressures. While this set of calculations is not definitive, optimum interaction parameter values, k_{ij}, appear to require customization and may be mixture specific. This is an undesirable outcome that imposes significant barriers to the application of this approach for multiphase behaviour calculations where data sets are sparse and incomplete.

For the second test, k_{ij} values were tuned for mixtures containing carbon dioxide + ethane + n-decylbenzene instead of nitrogen. These values are reported

in Table 3.3. The value of the binary interaction coefficient between ethane and n-decylbenzene is slightly different from the value obtained for ternaries with nitrogen. Phase equilibrium calculations based on these k_{ij} values do not provide accurate LLV regions as illustrated in Figure 3.4 B and Figure 3.4 C. The method of Crampon et al. yields substantially poorer LLV phase behaviour prediction results than the standard PR EOS, for cases where the PR EOS works well, even with mixture and composition dependent interaction parameters. As a result, this approach is not recommended for phase behaviour prediction of asymmetric mixtures, and in the context of the present work this method was abandoned.

Table 3.2. Best fit binary interaction coefficients for the ternary mixture of C_2H_6, N_2, and n-decylbenzene - method of Crampon et al. [31]

	ethane	nitrogen
nitrogen	0.08	
n-decylbenzene	-0.06	-0.09

Table 3.3. Best fit binary interaction coefficients for C_2H_6 + CO_2 + n-decylbenzene - method of Crampon et al. [31]

	ethane	carbon dioxide
carbon dioxide	0.12	
n-decylbenzene	-0.05	-0.05

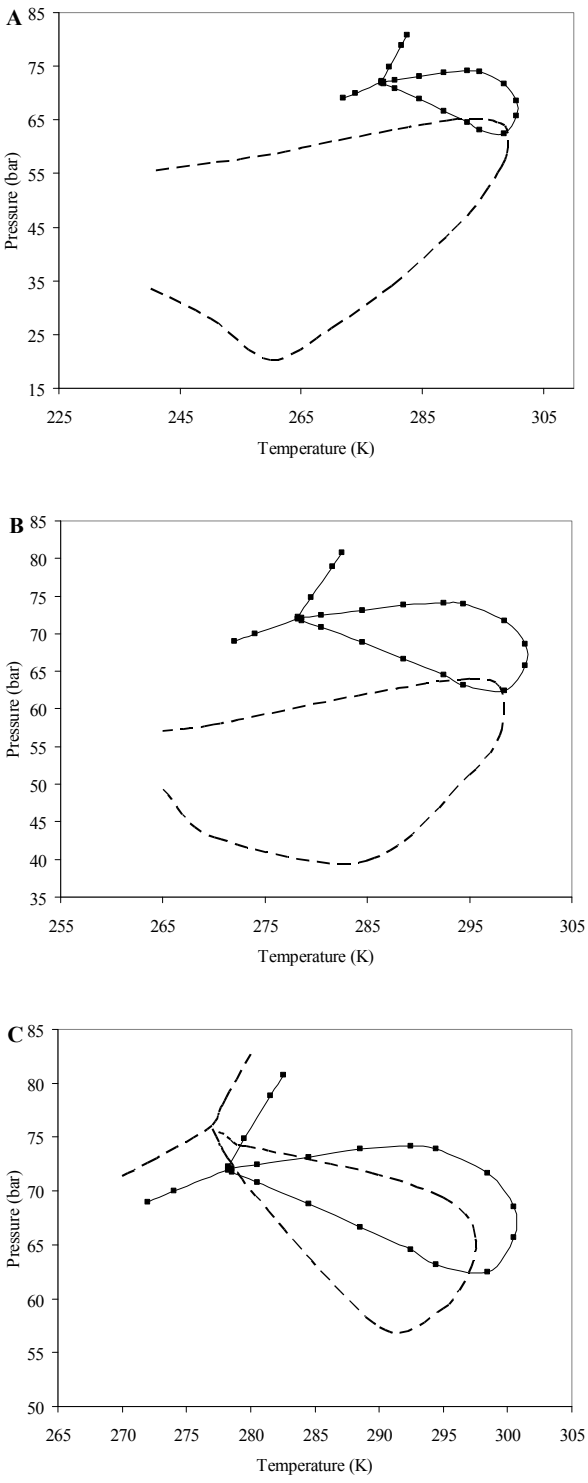

Figure 3.3. Measured and computed phase boundaries for a ternary mixture of ethane (87.3 mole %), nitrogen (10 mole %), and n-decylbenzene (2.7 mole %). Computations are for the Crampon et al. GC based PR EOS with A) standard k_{ij}; B) k_{ij}=0; C) k_{ij} shown in Table 3.2.

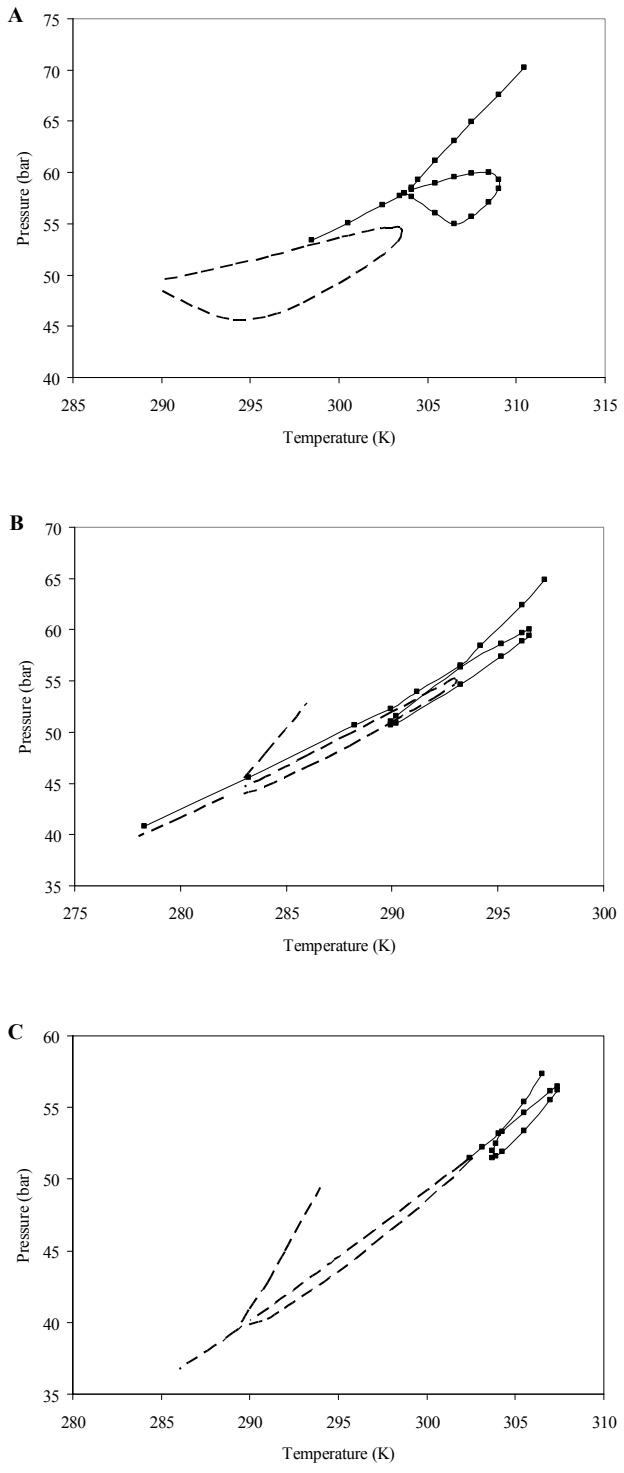

Figure 3.4. Phase boundaries (■, experimental data [10]; ▬ ▬ ▬, Crampon et al. GC based PR equation with modified k_{ij}) for: A) ethane (94.09 mole %), nitrogen (3.0 mole %), and n-decylbenzene (2.91 mole %). B) ethane (58.8 mole %), carbon dioxide (40.0 mole %), and n-decylbenzene (1.2 mole %). C) ethane (88.2 mole %), carbon dioxide (10.0 mole %), and n-decylbenzene (1.8 mole %).

3.4.3 Group Contribution Based PR EOS: Method of Marrero and Gani (MG)

The group contribution method developed by Marrero and Gani in combination with the PR EOS was selected as the second hybrid thermodynamic model for predicting phase diagrams for mixtures containing n-decylbenzene. The phase equilibrium calculations were performed using the standard values of binary interaction coefficients shown in Table 3.1 without further modification. The group contribution theory was used to estimate the critical properties and acentric factor of n-decylbenzene. These values are also shown in Table 3.1. For other constituents, critical properties and acentric factors that are available in the literature were used. The results are shown in Figure 3.5 A-D. As shown in Figure 3.5 A, this thermodynamic model provides the best estimate for the phase diagram in terms of size, shape and location of the LLV zone compared to the experimental data. The slope of the phase boundary between the L1L2 and L1 zones is better represented than with the standard PR EOS. For the cases shown in Figure 3.5 B-D, the computed phase boundaries are also in good qualitative and quantitative agreement with experiment.

Phase equilibrium calculations for ternary mixtures of ethane + propane + n-eicosane and ethane + methane + n-eicosane were also performed using the standard k_{ij} values given in Table 3.1. No attempt was made to modify k_{ij} values or to fit the interaction parameters to the experimental data. The critical properties and acentric factor of n-eicosane, estimated by the method of Marrero and Gani, are also shown in Table 3.1. Example experimental and computed three-phase zones are shown in Figure 3.6 A and B. The phase diagrams are well predicted qualitatively, i.e.: the nature of the phase behaviour is correct. Further, the shape of the LLV three-phase region is approximately the same as the experimental one, but the size is generally larger. The LLV zone and the critical loci are shifted to lower temperatures and pressures, but are still within an acceptable range of error. The modeling results have the same level of accuracy as those obtained by Gregorowicz and de Loos [8] who used modified versions of the PR EOS. So, while the standard PR EOS does not generate correct phase diagrams for these

mixtures, direct application of the Marrero and Gani group contribution method + the PR EOS and standard interaction parameters yields consistent phase behaviour predictions and allows us to lever the existing database of interaction parameters effectively. However, tuning k_{ij} values would certainly improve fits for the LLV zone. This result highlights the sensitivity of phase behaviour predictions to parameter values, in this case, the critical properties of the heavy component. This subject has been explored in detail for the van der Waals-like EOS [32]

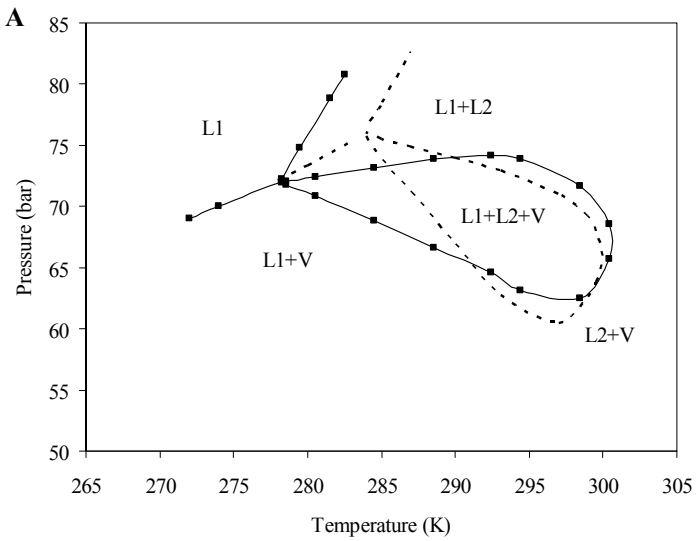

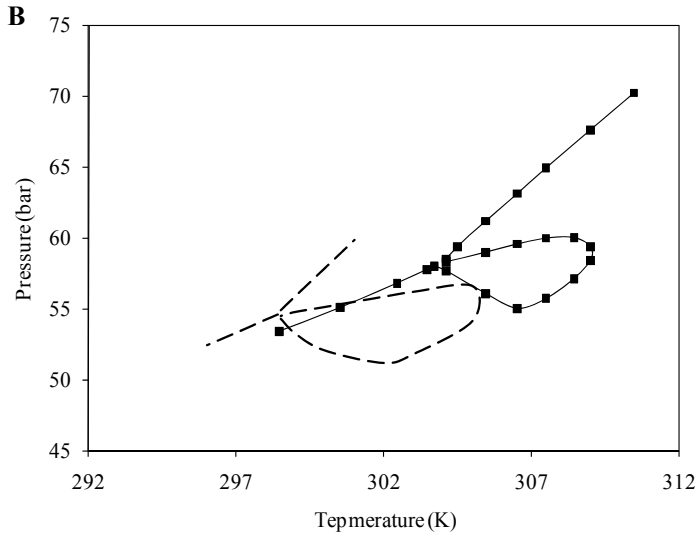

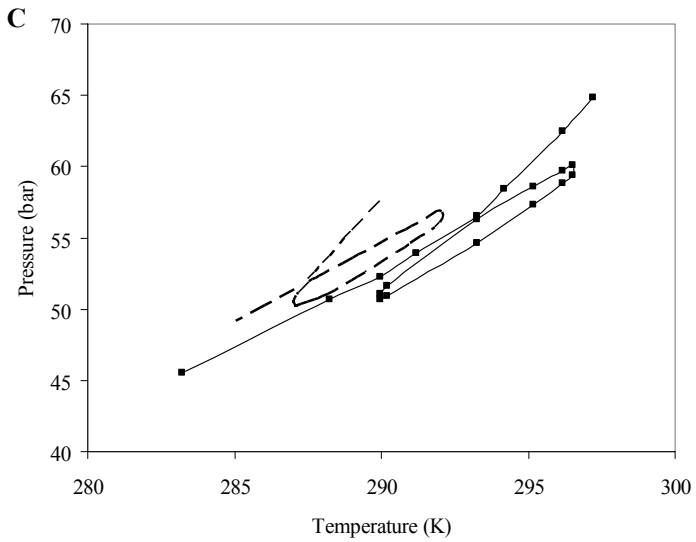

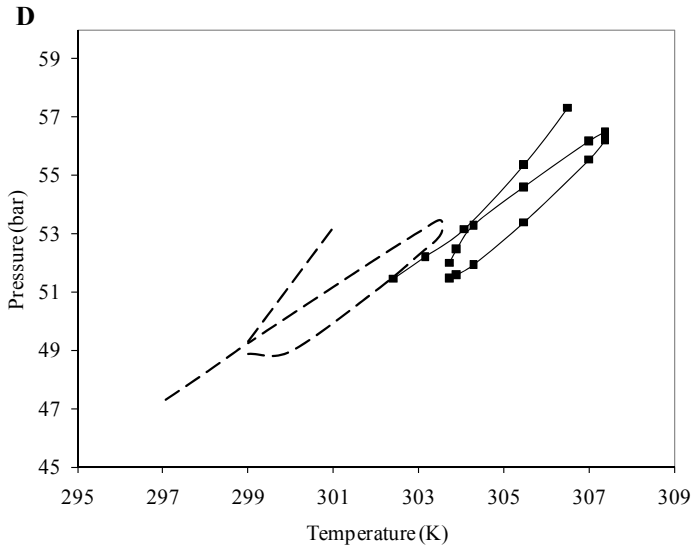

Figure 3.5. Experimental and predicted LLV phase boundaries for a selection of ternary mixtures containing n-decylbenzene (■, experimental data [10]; ▬ ▬ ▬, Marrero and Gani GC method with standard k_{ij}). A) ethane (87.3 mole %), nitrogen (10 mole %), and n-decylbenzene (2.7 mole %). B) ethane (94.09 mole %), nitrogen (3.0 mole %), and n-decylbenzene (2.91 mole %). C) ethane (58.8 mole %), carbon dioxide (40.0 mole %), and n-decylbenzene (1.2 mole %). D) ethane (88.2 mole %), carbon dioxide (10.0 mole %), and n-decylbenzene (1.8 mole %).

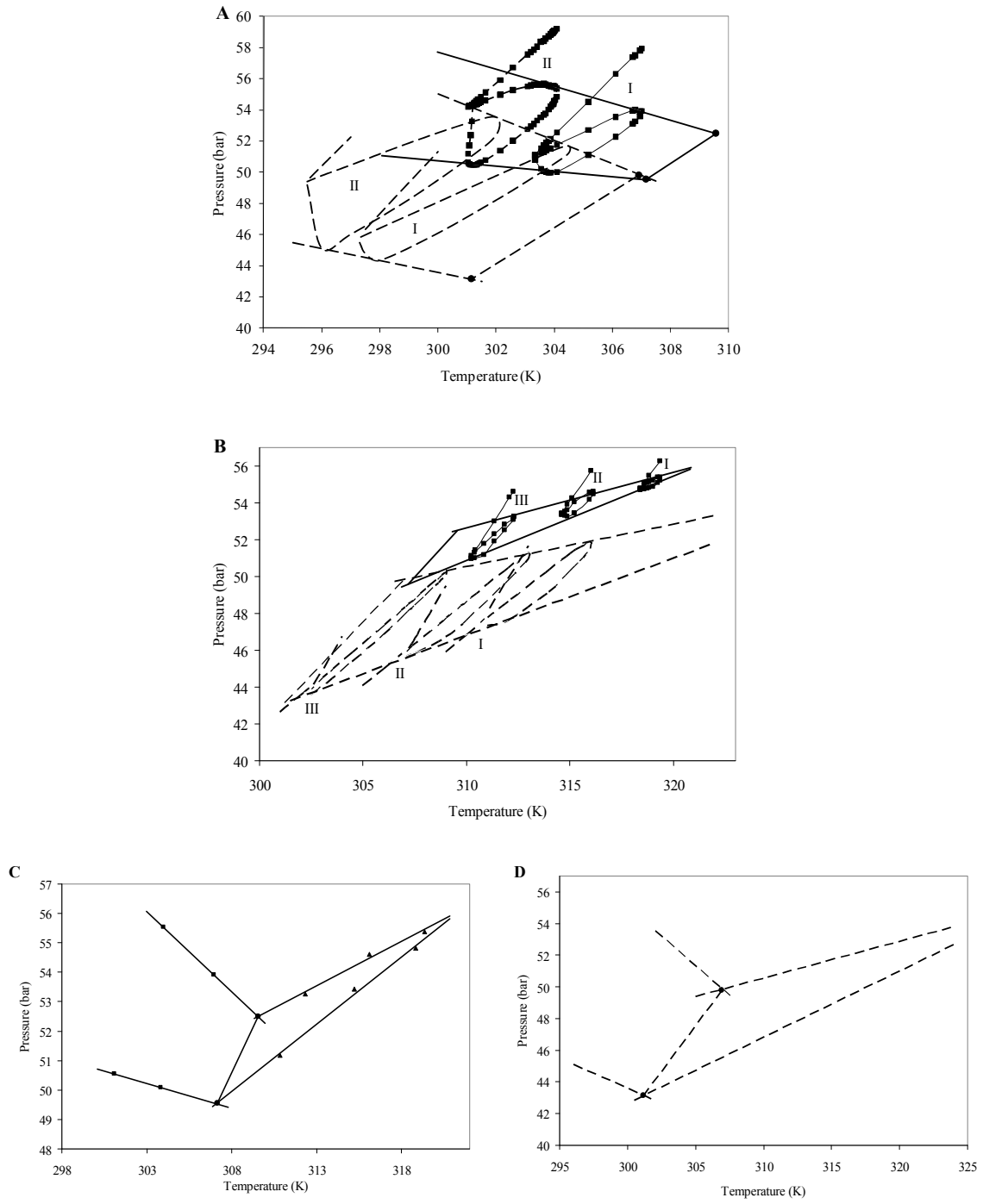

Figure 3.6. Measured and predicted LLV phase boundaries and phase behaviour trends for ternary mixtures containing n-eicosane (■, experimental data [19-20]; ▬ ▬ ▬, Marrero and Gani GC method + the PR EOS with standard k_{ij}). A) I: ethane (95.43 mole %), methane (3.14 mole %), n-eicosane (1.43 mole %). II: ethane (92.469 mole %), methane (6.87 mole %), n-eicosane (0.661 mole %). B) I: ethane (88.502 mole %), propane (10.15 mole %), n-eicosane (1.348 mole %). II: ethane (91.733 mole %), propane (6.87 mole %), n-eicosane (1.397 mole %). III: ethane (95.84 mole %), propane (2.69 mole %), n-eicosane (1.47 mole %).C) Predicted LLV line for the binary mixture ethane + n-eicosane based on ternary LLV experimental data. D) Predicted LLV line for the binary mixture ethane + n-eicosane based on modeling results.

The Marrero and Gani based model was further tested by generating the phase behaviour trends with composition as discussed above. For the model mixtures containing n-eicosane, addition of methane to a binary mixture of ethane and n-eicosane shifts the LLV zone to lower temperatures and expands it as methane is immiscible with n-eicosane. Addition of propane, which is miscible with the two other components, shifts the three-phase region to higher temperatures and pressures and shrinks it. The three-phase region disappears at a tricritical point (L1=L2=V). Similar trends were observed experimentally and computationally by Gregorowicz et al. [19-20]. The LLV line for the binary mixture of ethane and n-eicosane is defined by the intersection of the K and L loci shown in Figure 3.6 A and B. The experimental LLV line is shown in Figure 3.6 C and the predicted one in Figure 3.6 D.

For mixtures containing n-decylbenzene, both nitrogen and carbon dioxide are immiscible with n-decylbenzene and shift the three-phase region to lower temperatures. The three-phase zones are shown in Figure 3.7 A for the ternary mixture ethane + carbon dioxide + n-decylbenzene (three compositions), and in Figure 3.7 B for the mixture ethane + nitrogen + n-decylbenzene (two compositions). The impact of the addition of each component on the shape, size and location of the LLV region is unique. Addition of nitrogen to the binary mixture of ethane and n-decylbenzene alters the size and the shape of the three-phase zone significantly and shifts its location to much higher pressures. The sizes, shapes and locations of the predicted three-phase regions agree with the experimental data. Having divergent trends for K and L loci for the mixtures again makes it possible to predict the LLV line for the binary mixture ethane + n-decylbenzene by the intersection of the loci as shown in Figure 3.7 C and D. Extrapolation of experimental ternary loci yields critical end points for the binary that are in close agreement with data available in the literature. Predicted critical end points fall within a few bars and a few degrees of measurements.

As is evident from Figure 3.7 A, the K and L point loci are not rectilinear in P-T co-ordinates but are only approximately so. Linear extrapolation at low

concentrations of the third component provides a good estimate of the LLV line for the binary. For heavy oil or bitumen fractions + light hydrocarbon mixtures, such extrapolations are a potential check on whether the heavy hydrocarbon itself comprises an immiscible mixture, and if so where in pressure-temperature space the K and or L points occur. For such mixtures, K points typically arise under conditions where the mixtures are thermally unstable or under conditions where phase behaviour measurements are normally difficult to realize.

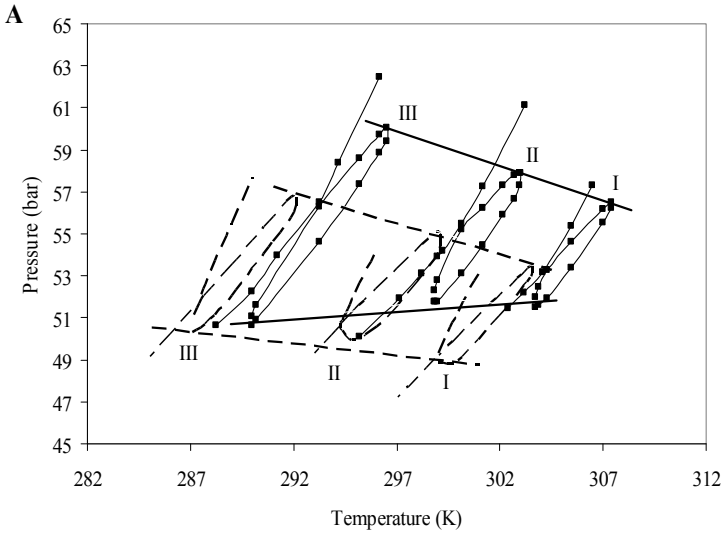

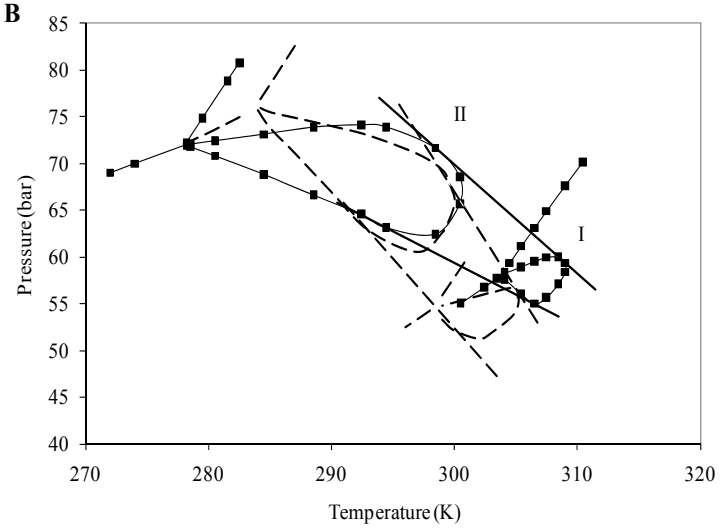

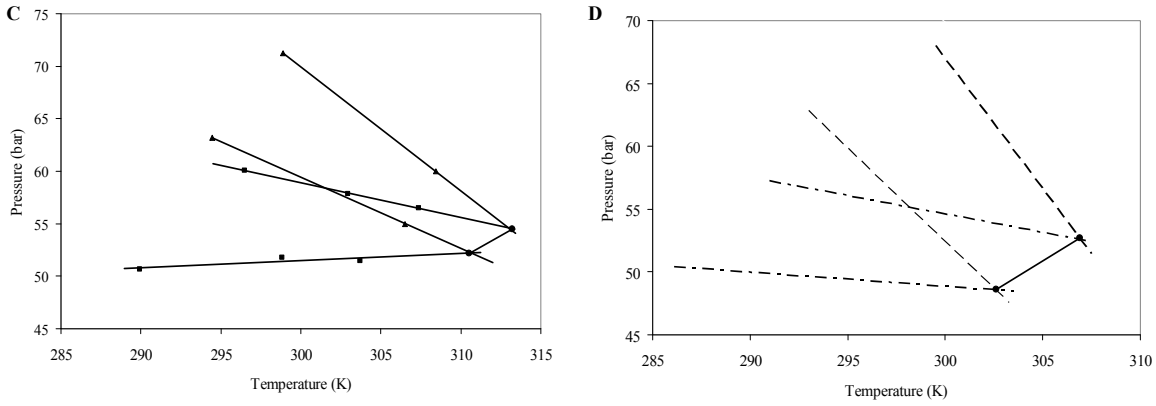

Figure 3.7. Measured and predicted LLV phase boundaries and phase behaviour trends for ternary mixtures containing n-decylbenzene (■, experimental data; ▬ ▬ ▬, Marrero and Gani GC method with standard k_{ij}). A) I : ethane (88.2 mole %), carbon dioxide (10 mole %), n-decylbenzene (1.8 mole %). II: ethane (78.4 mole %), carbon dioxide (20 mole %), n-decylbenzene (1.6 mole %). III: ethane (58.8 mole %), carbon dioxide (40 mole %), n-decylbenzene (1.2 mole %). B) I: ethane (94.09 mole %), nitrogen (3 mole %), n-decylbenzene (2.91 mole %). II: ethane (87.3 mole %), nitrogen (10 mole %), n-decylbenzene (2.7 mole %). C) LLV line for the binary mixture ethane + n-decylbenzene interpolated from experimental ternary K and L loci. D) LLV line for the binary mixture ethane + n-decylbenzene interpolated from predicted ternary K and L loci.

3.4.4 General Discussion

The reliability of a thermodynamic model with respect to the prediction of three-phase region location, shape and size is a rigorous test for its overall performance for asymmetric mixtures. The PR EOS provides reasonable results for mixtures containing n-decylbenzene, but fails to predict correct phase behaviours for n-eicosane containing mixtures without mixture specific tuning and modification. As we plan to model ill-defined hydrocarbon fluids comprising both molecularly specified constituents such as light hydrocarbons and pseudo components specified on the basis of boiling range, a reliable group contribution method must be included in the EOS model. The group contribution based PR EOS proposed by Crampon et al. [12] does not generate incorrect phase diagrams, but the differences between the predicted size, shape and location of multiphase regions in PT-X diagrams compared to the experimental data is beyond an acceptable range of error. As a result, reasonable phase behaviour predictions are not obtained by the method of Crampon et al. [12]. Tuning of the binary interaction parameters requires data and the resulting improvement is not

warranted based on the prediction improvement realized. By contrast, the phase behaviour predictions obtained using the group contribution method proposed by Marrero and Gani are promising. This method generates reliable phase diagrams for model mixtures containing n-decylbenzene and n-eicosane without any modification of k_{ij} values available in the literature, i.e.: their approach outperforms the PR EOS where all input parameters have been measured experimentally and are available in the literature. The phase behaviour trends predicted for mixtures containing n-eicosane and n-decylbenzene agree with experimental data and relevant theory. This result was unexpected and is fortuitous, as it allows us to make use of the large body of regressed phase equilibrium data that underlies group contribution methods.

Characterization of molecules present in bitumen and heavy oil presents formidable experimental and theoretical challenges. However, group contribution computational approaches are likely to play a central role in phase behaviour and thermophysical property prediction. Quantification of functional groups in molecules, and definition of mean molar mass, for boiling fractions, or whole crudes remain key challenges. For example, Jaffe et al. [33] identified more than 150 molecular substructures in petroleum residues. However, Sheremata et al. [34] proposed molecular representations for bitumen vacuum residue using a Monte Carlo construction method, which are consistent with the available ^{13}C-NMR, molecular weight, aromaticity, and SARA fractionation data by building molecular models on the basis of just ten substructures, only seven of which were drawn from the work of Jaffe et al. [33]. For asphaltenes, the situation is worse. There is little agreement on the nature of the molecular substructures they comprise. Pericondensed [35] and archipelago type molecular structures [34,36] have both been proposed for the same material. Clearly over all molecular structures and molar masses remain ambiguous but there is greater agreement on the functional groups and the types of carbon they comprise, with the possible exception of asphaltenes. Thus group contribution methods have much to offer as many of the groups can be measured and quantified experimentally using more than one technique.

In addition to EOS parameters for individual pseudo components, interaction parameters among components may also be calculated on the basis of group contributions. For example, Jaubert et al.'s k_{ij} calculation method (PPR78) [37-43] relies on knowledge of the different forms of carbon present in molecules to estimate binary interaction coefficients. For heavy oil mixtures, such data is frequently available if contradictory. Inclusion of group contribution for k_{ij}'s may increase the reliability of phase behaviour predictions for heavy oils and bitumen because k_{ij} values are not available, and modeling mixtures which include these constituents by setting all k_{ij} values to zero can result in significant deviations from experimental data. For the mixtures discussed in this paper, the k_{ij} values for n-eicosane and n-decylbenzene with the light hydrocarbons were estimated based on the method of Jaubert et al. [39-41]. The k_{ij} values obtained are listed in Table 3.4. Phase equilibrium calculations were repeated using these values for two cases and the results are shown in Figure 3.8 A and B. For both cases, the phase boundary results are superior to those obtained using standard k_{ij} values. The combination of these two group contribution methods make a powerful tool for phase behaviour prediction, which extends the findings of Jaubert and Mutelet [23] to multiphase behaviour and phase composition prediction. Consequently, phase behaviour modeling of heavy oil mixtures based on the methods of Marrero and Gani [11] and Jaubert et al. [40] will be the subject of the following chapter.

Table 3.4. Temperature dependent binary interaction coefficients – PPR78 (Jaubert et al. [40])

Temperature (K)	$k_{(ethane,\ n\text{-}eicosane)}$	$k_{(methane,\ n\text{-}eicosane)}$	$k_{(ethane,\ n\text{-}decylbenzene)}$	$k_{(carbon\ dioxide,\ n\text{-}decylbenzene)}$
295	0.0135	0.0531	0.0243	0.0880
296	0.0133	0.0529	0.0243	0.0879
297	0.0132	0.0527	0.0243	0.0879
298	0.0130	0.0525	0.0242	0.0878
299	0.0128	0.0523	0.0242	0.0878
301	0.0125	0.0518	0.0241	0.0876
302	0.0123	0.0516	0.0241	0.0875

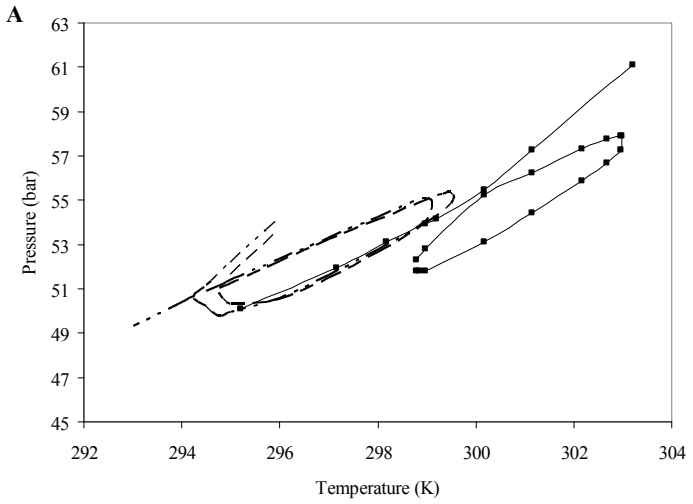

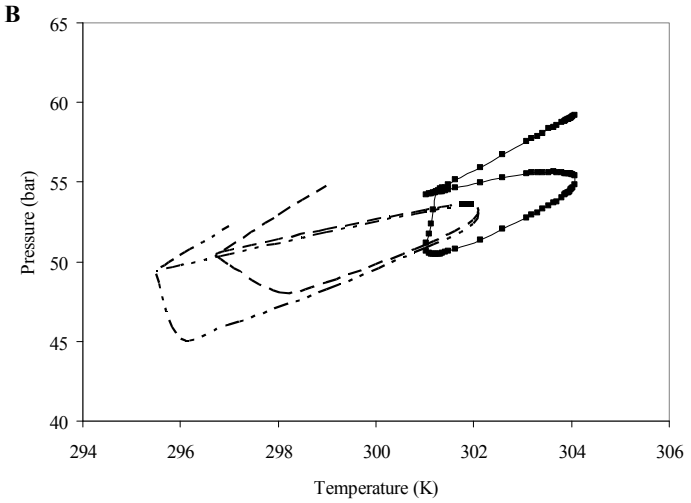

Figure 3.8. Experimental and predicted LLV phase boundaries for two ternary mixtures (■, experimental data [10,19-20] ; ▬ ▬ ▬, Marrero and Gani GC method + the PR EOS + k_{ij} values based on the method of Jaubert et al. [40] (PPR78), ▬ - - ▬ Marrero and Gani GC method + the PR EOS with standard k_{ij}) A: ethane (78.4 mole %), carbon dioxide (20 mole %), n-decylbenzene (1.6 mole %). B: ethane (92.469 mole %), methane (6.87 mole %), n-eicosane (0.661 mole %).

3.5 Conclusions

The reliability of two group contribution based thermodynamic models for predicting multiphase behaviour for model mixtures containing n-eicosane and n-decylbenzene was tested. The phase diagrams and phase behaviour trends obtained were compared to the experimental results available in the literature and to molecular based EOS calculations where available. The combination of the Peng-Robinson equation of state with the group contribution method of Marrero and Gani [11] outperformed the PR EOS, even for cases where all molecular based inputs are available. This result was surprising, particularly so for mixtures containing n-eicosane where the Peng-Robinson equation of state predicts the wrong phase diagrams. The combination of the Peng-Robinson equation of state with the group contribution method of Marrero and Gani [11] + a group contribution interaction parameter estimation method has the potential to predict complex phase behaviour of ill-defined mixtures containing bitumen and heavy oil where critical constants for constituents, among other properties, are routinely unavailable.

3.6 Nomenclature

a or a(T)	temperature dependent equation of state energy parameter
a_c	parameter in Peng-Robinson Equation of State
b	equation of state co-volume parameter
$f_i(m)$	function used in the estimation of parameter a (i = 1,2)
k_{ij}	binary interaction coefficient
M	number of first order groups
m	shape parameter
N	number of second order groups
N_j	number of groups of type j
O	number of third order groups
P	pressure
P_C	critical pressure
pc	contribution to critical pressure
R	universal gas constant
T	temperature
T_b	boiling point temperature
T_C	critical temperature
tc	contribution to critical temperature
V	total volume
v	molar volume
V_{Wj}	contribution of the j^{th} group to the van der Waals volume

Greek letters

α	temperature-dependent equation of state parameter
ε_i	(i=1) first and (i=2) second order contributions to acentric factor

ω	acentric factor
δV_{WK}	correction to van der Waals volume

3.7 Abbreviations

EOS	Equation of State
GC	Group Contribution
K	K-point, three-phase critical point
L	L-point, three-phase critical point
L1	lighter liquid phase
L2	denser liquid phase
L1V	liquid-vapour
L2V	liquid-vapour
L1L2	liquid-liquid
LLV	liquid-liquid-vapour
PR	Peng-Robinson
SLLV	solid-liquid-liquid-vapour
T	T-point, tricritical point
V	vapour

3.8 References

[1] N. Saber and J. M. Shaw, *Fluid Phase Equilibria* **264** (2008) 137-146.

[2] M. L. Michelsen, *Fluid Phase Equilib.* **9** (1982) 1-19.

[3] M. L. Michelsen, *Fluid Phase Equilib.* **9** (1982) 21-40.

[4] M. L. Michelsen, *Comput. Chem. Eng.* **17** (1993) 431-439.

[5] D. R. Jones, C. D. Perttunen, and B. E. Stuckman, *JOTA* **79** (1993) 157-181.

[6] I. Polishuk, J. Wisniak, and H. Segura, *Fluid Phase Equilib.* **164** (1999) 13-47.

[7] I. Polishuk, J. Wisniak, and H. Segura, *Chem. Eng. Sci.* **56** (2001) 6485-6510.

[8] J. Gregorowicz and T. W. de Loos, *Ind. Eng. Chem. Res.* **40** (2001) 444-451.

[9] J. Gregorowicz and T. W. deLoos, *Fluid Phase Equilib.* **118** (1996) 121-132.

[10] J. M. Shaw, T. W. de Loos, and J. de Swaan Arons, *Fluid Phase Equilib.* **84** (1993) 251-266.

[11] J. Marrero and R. Gani, *Fluid Phase Equilib.* **183** (2001) 183-208.

[12] C. Crampon, L. Trassy, L. Avaullee, E. Neau, and L. Coniglio, *Fluid Phase Equilib.* **216** (2004) 95-109.

[13] L. Coniglio, L. Trassy, and E. Rauzy, *Ind. Eng. Chem. Res.* **39** (2000) 5037-5048.

[14] R. A. McFarlane, M.Sc. Thesis, University of Alberta, 2007.

[15] K. G. Joback and R. C. Reid, *Chem. Eng. Commun.* **57** (1987) 233-243.

[16] G. M. Wilson, Jasperson, L.V., presented at the AIChE spring meeting, New Orleans, LA, 1996 (unpublished).

[17] L. Coniglio and A. Nouviaire, *Ind. Eng. Chem. Res.* **40** (2001) 1781-1790.

[18] A. Van Waeyenberghe, M.Sc. Thesis, University of Alberta, 2006.

[19] J. Gregorowicz, T. W. de Loos, and J. de Swaan Arons, *Fluid Phase Equilib.* **84** (1993) 225-250.

[20] J. Gregorowicz, P. J. Smits, T. W. de Loos, and J. de Swaan Arons, *Fluid Phase Equilib.* **85** (1993) 225-238.

[21] J. Shin, M. S. Shin, W. Bae, Y. W. Lee, and H. Kim, *J. Supercrit. Fluids* **44** (2008) 260-265.

[22] T. Fang, Y. Shimoyama, T. Abeta, Y. Iwai, M. Sasaki, and M. Goto, *J. Supercrit. Fluids* **47** (2008) 140-146.

[23] J.-N. Jaubert and F. Mutelet, *Fluid Phase Equilib.* **224** (2004) 285-304.

[24] L. Constantinou, R. Gani, and J. P. O'connell, *Fluid Phase Equilib.* **103** (1995) 11-22.

[25] A. Bondi, *Physical Properties of Molecular Crystals, Liquids and Glasses*. (John Wiley & Sons, New York, 1968).

[26] L. E. Baker, A. C. Pierce, and K. D. Luks, *SPEJ* **22** (1982) 731-742.

[27] M. L. Michelsen, *Comput. Chem. Eng.* **18** (1994) 545-550.

[28] K. D. Luks, *Fluid Phase Equilib.* **29** (1986) 209-224.

[29] J. M. Shaw and E. Behar, *Fluid Phase Equilib.* **209** (2003) 185-206.

[30] J. M. Shaw and X. Y. Zou, *J. Pet. Sci. Technol.* **22** (2004) 773-786.

[31] C. Crampon, L. Trassy, L. Avaullee, E. Neau, and L. Coniglio, *Fluid Phase Equilib.* **216** (2004) 95-109.

[32] R. L. Scott, *Phys. Chem. Phys. Chem.* (1999) 4225-4231.

[33] S. B. Jaffe, H. Freund, and W. N. Olmstead, *Ind. Eng. Chem. Res.* **44** (2005) 9840-9852.

[34] J. M. Sheremata, M. R. Gray, H. D. Dettman, and W. C. McCaffrey, *Energy Fuels* **18** (2004) 1377-1384.

[35] S. Zhao, L. S. Kotlyar, J. R. Woods, B. D. Sparks, K. Hardacre, and K. H. Chung, *FUEL* **80** (2001) 1155-1163.

[36] J. Murgich, J. A. Abanero, and O. P. Strausz, *Energy Fuels* **13** (1999) 278-286.

[37] R. Privat, F. Mutelet, and J.-N. Jaubert, *Ind. Eng. Chem. Res.* **47** (2008) 10041-10052.

[38] R. Privat, J.-N. Jaubert, and F. Mutelet, *Ind. Eng. Chem. Res.* **47** (2008) 7483-7489.

[39] J.-N. Jaubert, S. Vitu, F. Mutelet, and J.-P. Corriou, *Fluid Phase Equilib.* **237** (2005) 193-211.

[40] S. Vitu, R. Privat, J. N. Jaubert, and F. Mutelet, *J. Supercrit. Fluids* **45** (2008) 1-26.

[41] S. Vitu, J.-N. Jaubert, and F. Mutelet, *Fluid Phase Equilib.* **243** (2006) 9-28.

[42] F. Mutelet, S. Vitu, R. Privat, and J.-N. Jaubert, *Fluid Phase Equilib.* **238** (2005) 157-168.

[43] R. Privat, J.-N. Jaubert, and F. Mutelet, *Ind. Eng. Chem. Res.* **47** (2008) 2033-2048.

Chapter 4
On the Phase Behaviour of Athabasca Vacuum Residue + n-Decane[1]

4.1 Introduction

Reliable prediction of thermodynamic properties and phase behaviour of heavy oil and bitumen is essential for engineering calculations linked to the production, transport, and refining of these hydrocarbon resources. Experimental data are not usually available for these materials because they are difficult and costly to obtain. For mixtures containing light hydrocarbons such as n-alkanes in addition to constituents of bitumen and heavy oil, interpolation and extrapolation of sparse and incomplete data sets is necessary. Successful phase behaviour and phase composition prediction for mixtures including such ill-defined fluid constituents can play a major role in process design, process development, and process operation optimization, e.g.: for paraffinic deasphalting, a primary refining operation.

Three key challenges must be addressed to guarantee reliable phase behaviour prediction for ill-defined fluids, namely: creation of a robust phase equilibrium computational tool, characterization of ill-defined constituents like Athabasca bitumen vacuum residue (AVR), and implementation of a reliable thermodynamic model. The computational challenge has been discussed in Chapter 2 in detail [1]. It is based on the development of a reliable and rapid stability test employing the DIRECT global minimization method [2], which mitigates false convergence that can occur during flash calculations when the Gibbs free energy surface is non-convex [3-4]. Local minimization methods are then used in flash calculations. Reliable stability test results, in conjunction with local minimization methods for flash calculations, converge to correct phase behaviours and phase compositions.

[1]This chapter with minor modifications has been published in the journal of Fluid Phase Equilibria: Saber, N. and Shaw, J. M. (2010) *Fluid Phase Equilibria*.doi:10.1016/j.fluid.2010.09.038

Characterization of molecules present in ill-defined hydrocarbons is a challenging task both experimentally and theoretically. Quantification of functional groups in molecules, and definition of mean molar mass, for boiling fractions, or whole crudes remain key challenges. For example, Jaffe et al. [5] identified more than 150 molecular substructures in petroleum residues. Sheremata et al. [6] proposed molecular pseudo components for Athabasca bitumen vacuum residue using a Monte Carlo construction method. Only ten substructures were used to build these molecules. Based on the same substructures, Sheremata [7] recently proposed a set of 17 molecular pseudo components that are consistent with experimental simulated distillation data as well. However, there is little agreement on the nature of the molecular substructures that comprise Athabasca Bitumen vacuum residue. Asphaltenes, for example, make up approximately 30 wt.% of this residue, depending on the asphaltene definition employed. Pericondensed [8] and archipelago type molecular pseudo components [6,9] have both been proposed for Athabasca asphaltenes. The ambiguity may be linked to the molecule construction algorithms [10]. While molecular structures and molar masses remain ambiguous, there is greater agreement on the functional groups present and the types of carbon they comprise. Therefore, group contribution methods are appropriate candidates for generating thermodynamic properties as many of the groups are measured and quantified experimentally using more than one technique. As proposed molecular pseudo components, irrespective of molecular type, are based on these functional groups, they have the potential to generate accurate thermodynamic properties, and were chosen as a computational basis for the present work.

In Chapter 3, the applicability of the combination of the Peng-Robinson equation of state [11] and group contribution methods for predicting the phase behaviour for asymmetric mixtures containing the known molecular constituents nitrogen, carbon dioxide, methane, ethane, propane, n-decylbenzene, and n-eicosane was investigated [12]. Two different thermodynamic models were used to predict phase diagrams with a focus on the three-phase region. The phase diagrams and phase behaviour trends obtained showed that the combination of the

Peng-Robinson equation of state with the group contribution method of Marrero and Gani [13] generated the most reliable results and this thermodynamic model is also used here. Binary interaction coefficient values, appearing in this model, are not available for bitumen constituents. The group contribution based method of Jaubert et al. [14-17], which improved the quality of the predicted phase diagrams in the previous work, and a correlation proposed by Gao et al. [18] are used to estimate interaction coefficient values.

In this contribution, phase diagrams and phase behaviour trends are computed and compared with available experimental data for AVR, and AVR + n-decane [19-21]. Several attempts have been made to predict the bubble pressures for these mixtures [22-23]. However, the outcomes were not accurate due to the shortcomings in the thermodynamic models, phase equilibrium calculations and phase equilibrium data. For example, the effect of multiphase behaviour was not considered in prior works. Consequently, the range of applicability of calculations is limited to mixtures containing less than ~10 wt.% AVR. Key objectives of this contribution are to illustrate a computational approach applicable to ill-defined hydrocarbons and in particular to extend the phase behaviour prediction of AVR + n-alkane mixtures to industrially relevant compositions, pressures and temperatures. Validation of predicted phase composition results is beyond the scope of this work.

4.2 Thermodynamic Model

The parameters appearing in the Peng-Robinson equation of state (PR EOS), Equation 4.1a:

$$P = \frac{RT}{v-b} - \frac{a(T)}{v(v+b)+b(v-b)} \tag{4.1a}$$

are calculated based on Equations 4.1b-f. The temperature dependencies shown in Equations 4.1d and 4.1e for the energy parameter, α, are used.

$$a = a_c \alpha(T) \tag{4.1b}$$

$$a_c = \frac{0.45724 R^2 T_c^2}{P_c} \tag{4.1c}$$

$$\alpha = \left[1 + (0.37464 + 1.54226\omega - 0.26992\omega^2)(1 - \left(\frac{T}{T_c}\right)^{\frac{1}{2}})\right]^2 \text{ for } \omega \leq 0.49 \tag{4.1d}$$

$$\alpha = \left[1 + (0.3796 + 1.485\omega - 0.1644\omega^2 + 0.01667\omega^3)(1 - \left(\frac{T}{T_c}\right)^{\frac{1}{2}})\right]^2 \text{ for } \omega > 0.49 \tag{4.1e}$$

$$b = \frac{0.0778 R T_c}{P_c} \tag{4.1f}$$

The van der Waals mixing rules are employed to calculate the equation of state parameters for mixtures.

The group contribution method of Marrero and Gani [13] estimates the critical properties that are used to calculate equation of state parameters. The equations for estimating critical temperature (K) and pressure (bar) are:

$$exp(\frac{T_c}{231.239}) = \sum_i N_i tc_i + \sum_j M_j tc_j + \sum_k O_k tc_k \tag{4.2}$$

$$(P_c - 5.9827)^{-\frac{1}{2}} - 0.108998 = \sum_i N_i pc_i + \sum_j M_j pc_j + \sum_k O_k pc_k \tag{4.3}$$

where N_i, M_j, O_k are the numbers of the 1st, 2nd and 3rd order groups, respectively; tc_i, tc_j, tc_k are the 1st, 2nd and 3rd order group contributions to T_c; and pc_i, pc_j, pc_k are the 1st, 2nd and 3rd order group contributions to P_c.

The group contribution method of Constantinou et al. [24] was selected to estimate the acentric factors for molecules with molecular weight of less than 500 g/gmol. The group contribution method for estimating acentric factor is given in Equation 4.4:

$$\omega = 0.4085\left[ln\left(\sum_i N_i\varepsilon_{1i} + A\sum_j M_j\varepsilon_{2j} + 1.1507\right)\right]^{\frac{1}{.5050}} \quad (4.4)$$

N_i and M_j in Equation 4.4 are the numbers of the 1st and 2nd order groups, ε_{1i} and ε_{2j} are the 1st and 2nd order group contributions to ω, and A is either 0 or 1 depending on whether or not there is a defined 2nd order contribution.

The predictive method of Nji et al. [25] estimates the acentric factors for the structures with molecular weight of more than 500 g/gmol as the previous group contribution method does not generate reasonable values for heavier structures. In this method, the following perturbation equation predicts the acentric factor for any hydrocarbon based on the acentric factor of the n-paraffin with the same carbon number:

$$\omega = \omega^0\left[\frac{(1+2f)}{(1-2f)}\right]^2 \quad (4.5)$$

where ω^0 is the acentric factor of the n-paraffins, and ω is the acentric factor of a hydrocarbon of interest. The perturbation function *f* can be calculated as follows:

$$f = 0.8467\Delta SG^2 + 0.3069\Delta SG + 0.2557\Delta MW^2 + 0.0015\Delta MW + 0.3128\Delta SG\Delta MW \quad (4.6)$$

where

$$\Delta SG = ln\frac{SG^0}{SG} \quad (4.7)$$

$$\Delta MW = ln\frac{MW^0}{MW} \quad (4.8)$$

In these equations SG is the specific gravity and MW is the molecular weight.

The adjustable parameters of this thermodynamic model, the binary interaction coefficients (k_{ij}s), have a significant impact on the accuracy of the predicted phase behaviour. As their values are not available in the literature, two predictive methods were selected and evaluated. Jaubert et al.'s k_{ij} calculation method (PPR78) [14-17] estimates interaction parameters among components on the basis of group contributions. This predictive method relies on knowledge of the different forms of carbon present in molecules to estimate binary interaction coefficients. This method is described in detail elsewhere [17]. The second method is a simple equation that estimates k_{ij} values for the Peng-Robinson equation of state based on critical temperatures and critical compressibility factors. This correlation was proposed by Gao et al. [18] , Equation 4.9.

$$k_{ij} = 1 - \left[\frac{2\left(Tc_i Tc_j\right)^{0.5}}{(Tc_i + Tc_j)}\right]^{\left(\frac{Zc_i + Zc_j}{2}\right)} \tag{4.9}$$

where T_c is the critical temperature and z_c is the critical compressibility factor.

4.3 Multiphase Equilibrium Calculations

Baker [3] and Michelsen [4] proved that stability analysis is the necessary and sufficient condition for phase equilibrium. A global minimization computational technique called DIRECT was adopted for stability analysis [1]. It provides a good balance between reliability and computational speed. Two-phase and three-phase flash calculations routines are based on successive substitution and the objective functions proposed by Michelsen [26]. The equilibrium calculations start with the stability analysis performed on a feed composition. If the stability analysis shows that the mixture is unstable, two-phase flash calculations are performed to identify equilibrium phase natures and compositions corresponding to the global minimum of Gibbs free energy. The stability analysis tests the results of the two-phase flash calculations and the three-phase flash calculations are performed if required. The results of each stability analysis are used to initialize the subsequent flash calculations. The only drawback of this

computational approach is the slowness of the second stability analysis, used to validate equilibrium calculations, due to the large number of pseudo components present and the complexity of the predicted phase behaviours. VMGSim 5.0 is used to perform three-phase flash calculations. As it uses local minimization algorithms, the flash calculations are rapid.

4.4 Results and Discussion

4.4.1 Thermodynamic Properties of AVR

The AVR characterization is based on pseudo components proposed by Sheremata [7], but the mole fractions of each component were refit, using his code, to include bubble pressure data in the regression. The revised characterization remains consistent with the available ^{13}C-NMR, molecular weight, aromaticity, and SARA fractionation data, as these are constraints in the calculations. The assigned mole percents of the pseudo components are given in Table 4.1, along with the critical properties calculated using the method of Marrero and Gani [13] and their respective acentric factors. The acentric factors for molecules 1-8 were calculated using the group contribution correlation developed by Constantinou et al. [24], while the predictive method of Nji et al. [25] was used for molecules 9-16. A trial and error approach was needed because the specific gravity of the pseudo components is unknown. The specific gravity of each pseudo component was estimated as a first guess and the resulting acentric factor was calculated. The Lee-Kesler equation of state [27] was then used to recalculate the specific gravity using the critical properties and the acentric factor. The acentric factor estimates converged within 5 to 10 iterations. Binary interaction coefficient values among pairs of constituents are frequently found to impact the quality of phase equilibrium calculations. Two methods were used to estimate the k_{ij} values of the vacuum residue pseudo components. The predictive method developed by Jaubert et al. [15,17] yields small negative values, greater than -0.01726, while the correlation of Gao et al. [18] yields small positive values, less than 0.013573. Both sets of k_{ij} results and zero were used to predict vapour pressures for AVR. The choice of k_{ij} values in this range had an insignificant

effect on predicted vapour pressures and k_{ij} values for pairs of AVR constituents were set to zero for subsequent calculations.

Table 4.1. Estimated physical and thermodynamic properties for AVR pseudo components

Molecular pseudo component	Mole %	Tc (^{o}C)	Pc (bar)	Acentric Factor
1	0	419.8	27.17	0.437
2	0	475	17.88	0.473
3	15.19	536.1	18.54	0.684
4	9.49	572.1	14.95	0.654
5	7.64	605	12.97	0.67
6	1.31	642.4	12.24	0.823
7	13.86	650.1	11.35	0.698
8	13.20	696.9	11.63	0.785
9	9.51	738.8	8.29	1.055
10	7.63	804.7	7.78	1.07
11	7.48	847.2	7.41	1.06
12	6.10	920.7	7.75	1.07
13	3.63	1021.9	7.82	1.09
14	0.009	913.8	6.78	1.39
15	3.59	1043.2	6.75	1.32
16	1.36	1070.9	6.57	1.4
17	0	1153.3	6.20	-

4.4.2 AVR Bubble Pressure and Phase Behaviour

The computed bubble pressure curve for AVR is shown in Figure 4.1 along with measured values reported by Zou [20] and McFarlane [21]. The calculated bubble pressures are lower than the experimental values, but the errors are much less than those calculated by McFarlane [21,23] and Van Waeyenberghe [22] where the bubble pressure values were underestimated significantly. The maximum deviation of the predictions from the more reliable experimental data of McFarlane [21] is 80%. As bubble pressure is sensitive to the presence of trace organic impurities, water, aging and other effects linked to sample preparation and handling [28], this agreement is considered acceptable. The predicted phase behaviour indicates that AVR does not exhibit liquid-liquid or liquid-liquid-vapour phase behaviour, which is in agreement with macroscopic observations.

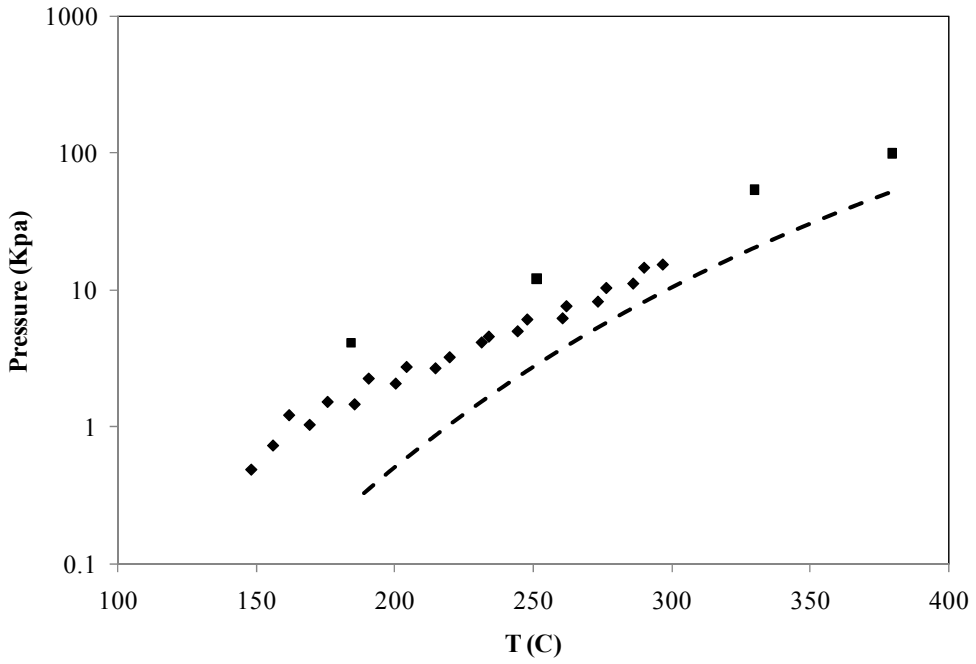

Figure 4.1. Measured and computed vapour pressures for AVR (♦, experimental data by McFarlane [21]; ■, experimental data by Zou [20]; — — —, calculations)

4.4.3 AVR + n-decane Phase Behaviour

The computed and experimental pressure-temperature phase diagrams at constant composition for n-decane + 10, 20, 30, 40, 70, and 90 wt.% AVR are presented in Figure 4.2 A-F, where L1 denotes a low density liquid phase, L2 denotes a high density liquid phase, and V denotes a vapour phase. Critical phenomena such as K-points (L1=V+L2) and L-points (L1=L2+V) are also indicated. As is clear from Figure 4.2, AVR + n-decane mixtures are highly asymmetric and they exhibit complex phase behaviours [19]. The presence of L1 and L1V regions in the experimental phase diagrams at both low and high wt.% AVR is particularly noteworthy, as it requires an L-point to be present along the L1L2V – LV phase boundary. From less than 10 wt.% to ~ 35 wt.% AVR, the L1L2V three-phase region observed experimentally extends to low temperatures and pressures. For mixtures containing ~35% to ~60% AVR, a lower temperature bound for the L1L2V region is observed experimentally. Mixtures containing higher concentrations of AVR do not exhibit LLV three-phase behaviour experimentally.

While binary interaction coefficients were estimated using the methods of Jaubert et al. (PPR78) [15,17] and Gao et al. [18], only the values obtained with the method of Gao et al. [18] were used for phase boundary calculations because the PPR78 method generated k_{ij} values that led to incorrect phase behaviour prediction. The values obtained using the method of Gao et al. [18] were tuned by multiplying all values by a constant, 7.0. Tuned k_{ij} values are shown in Table 4.2.

Table 4.2. Binary interaction coefficients for AVR pseudo components + n-decane

Compound/Molecule	1	2	3	4	5	6	7	8
n-decane	0.00305	0.00854	0.01701	0.02293	0.02884	0.03604	0.03757	0.04731
	9	10	11	12	13	14	15	16
n-decane	0.05648	0.07162	0.08172	0.09969	0.12508	0.09799	0.13049	0.13753

The phase equilibrium calculations predict the correct phase behaviour for mixtures containing less than 35 wt.% AVR, Figure 4.2 A-C. The predicted phase diagrams agree with the experimental data qualitatively and the L1L2 to L1L2V phase boundaries agree to within ~5 ^{o}C and ~5 bar. Critical point calculations are not performed, but the approximate locations of K-points and L-points were identified from relative phase volumes within the liquid-liquid-vapour region as pressure was varied at fixed temperature. These critical points are also indicated in Figure 4.2. For mixtures containing 35-60 wt.% AVR, the L1L2V region is observed to have a lower as well as an upper temperature bound experimentally. The computed composition bounds for the L1L2V region are temperature insensitive and the L1L2V regions are predicted to extend to low temperatures. The experimental results and predictions for 40 % AVR + 60 wt.% n-decane are shown in Figure 4.2 D. The location of the predicted LLV region is approximately correct but the predicted and measured phase behaviours are in qualitative disagreement below 267 ^{o}C. For 65 to 100 wt.% AVR, L1V and L1 phase behaviours are observed experimentally. The computations conform with the experiments. The L1V - L1 phase boundaries for mixtures containing 70 wt.% and 90 wt.% AVR are shown in Figure 4.2 E and F. The best quantitative

agreement between predictions and experimental data is observed between 200 and 300 ^{o}C where pressures are large enough to be measured accurately and where thermolysis reactions, which affect mixture composition and lead to high apparent bubble pressures during phase behaviour experiments [29] are insignificant.

Predicted pressure-composition phase diagrams at 200, 267, 320, and 350 ^{o}C are shown in Figure 4.3 A-D. The computed L1L2V region abuts the L1, L1V, and V regions, and the point of intersection with the L1L2V region is not visible particularly at 200 and 267 ^{o}C. The L1L2V zone extends to the middle of the diagrams but contrary to the experimental data, the composition range shrinks rather than grows as temperature increases from 200 to 267 ^{o}C. Computed L-points arise at low AVR wt.%'s. For example at 350 ^{o}C, the L point is at 5 wt.% AVR; at 320 ^{o}C the value is at 2 wt.% AVR; and at 267 ^{o}C it is at less than 1 wt.% AVR. These values appear low relative to the experimental data. K-points are present in the phase diagrams at temperatures greater than the critical temperature of n-decane (344.6 ^{o}C) as shown in Figure 4.3 D.

Finding the sources of the deviations between predicted phase boundaries and experimental data is difficult because several estimation methods were used and the contribution of each one to the overall error could not be evaluated. However, the broad qualitative and quantitative agreement between the experimental and the predicted phase boundaries illustrates the potential for group contribution equations of state to correlate and interpolate sparse phase boundary data for ill-defined hydrocarbon mixtures. In a follow up and more detailed proof of concept study, evaluation of the phase diagrams for AVR + n-pentane, and other n-alkanes is planned. In addition, artifacts in the calculations indicating incorrect trends for the composition span of the LLV region with temperature and phase compositions will be addressed.

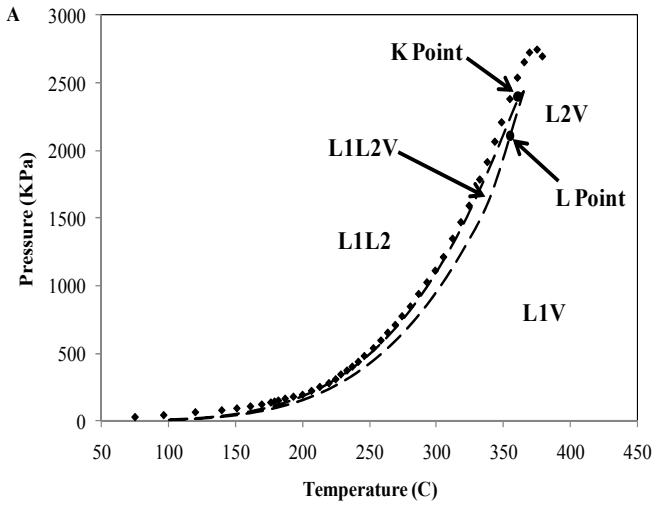
A
K Point
L2V
L1L2V
L Point
L1L2
L1V
Pressure (KPa)
Temperature (C)
3000
2500
2000
1500
1000
500
0
50
100
150
200
250
300
350
400
450

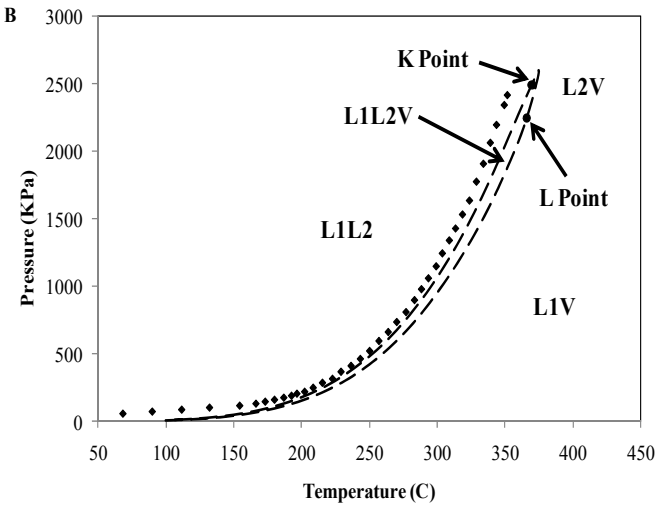
B
K Point
L2V
L1L2V
L Point
L1L2
L1V
Pressure (KPa)
Temperature (C)
3000
2500
2000
1500
1000
500
0
50
100
150
200
250
300
350
400
450

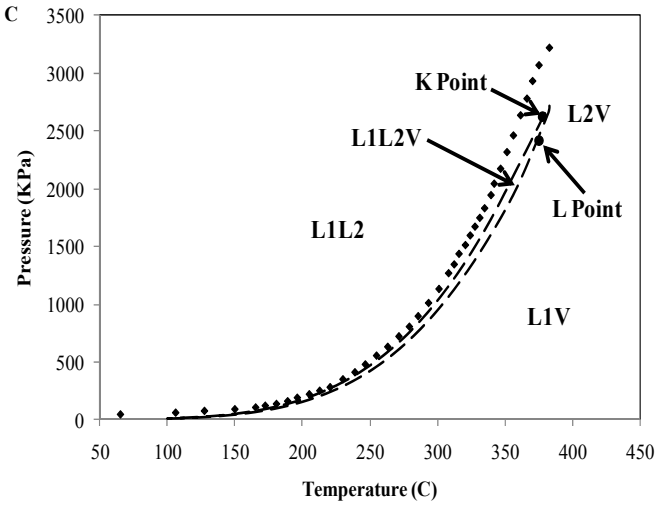
C
K Point
L2V
L1L2V
L Point
L1L2
L1V
Pressure (KPa)
Temperature (C)
3500
3000
2500
2000
1500
1000
500
0
50
100
150
200
250
300
350
400
450

D

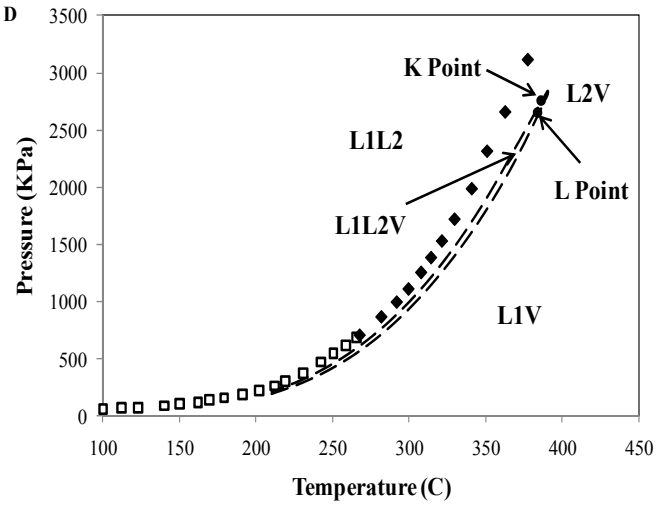
3500
3000
2500
2000
1500
1000
500
0
Pressure (KPa)
K Point
L2V
L1L2
L Point
L1L2V
L1V
100
150
200
250
300
350
400
450
Temperature (C)

E

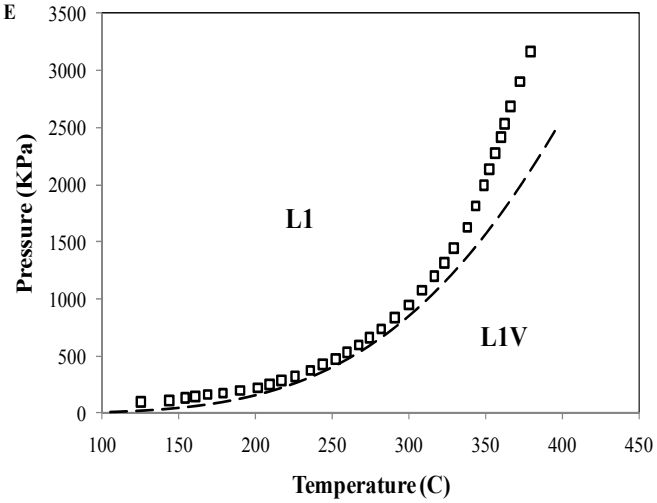
3500
3000
2500
2000
1500
1000
500
0
Pressure (KPa)
L1
L1V
100
150
200
250
300
350
400
450
Temperature (C)

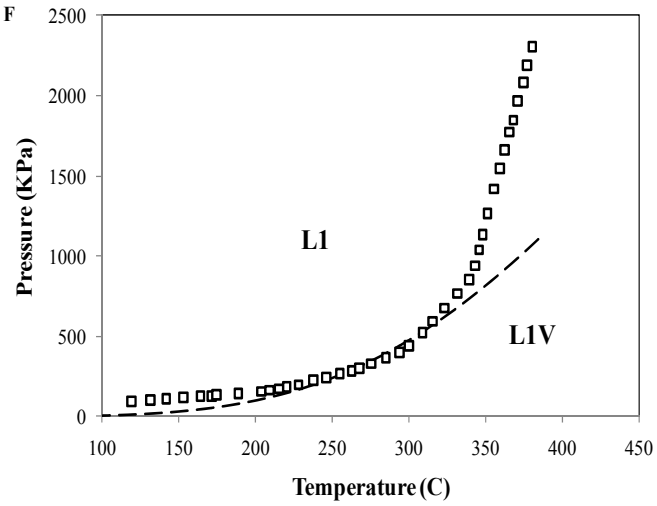

Figure 4.2. Experimental and predicted LLV phase boundaries for AVR + n-decane mixtures (♦, experimental L1L2V/L1L2 boundary [19]; ■, experimental L1V/L1 boundary [19]; ▬ ▬ ▬, computed boundary). A) 10 wt.% AVR. B) 20 wt.% AVR. C) 30 wt.% AVR. D) 40 wt.% AVR. E) 70 wt.% AVR. F) 90 wt.% AVR.

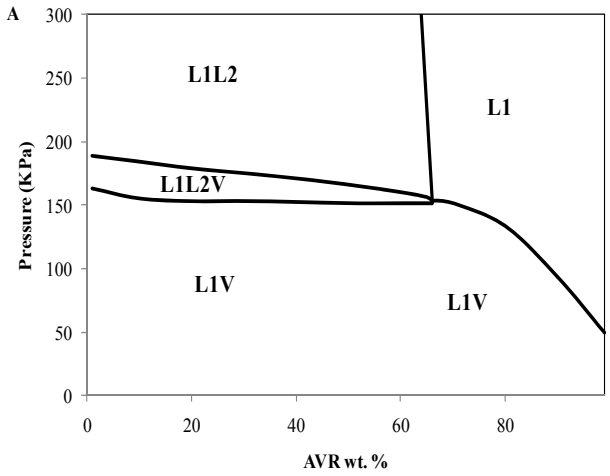
A
L1L2
L1
L1L2V
L1V
L1V
Pressure (KPa)
AVR wt. %

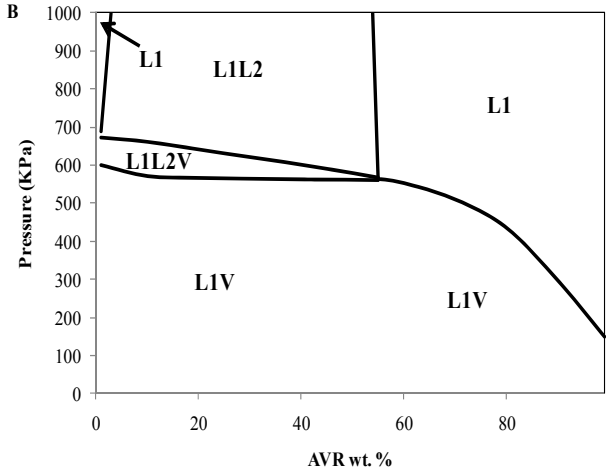
B
L1
L1L2
L1
L1L2V
L1V
L1V
Pressure (KPa)
AVR wt. %

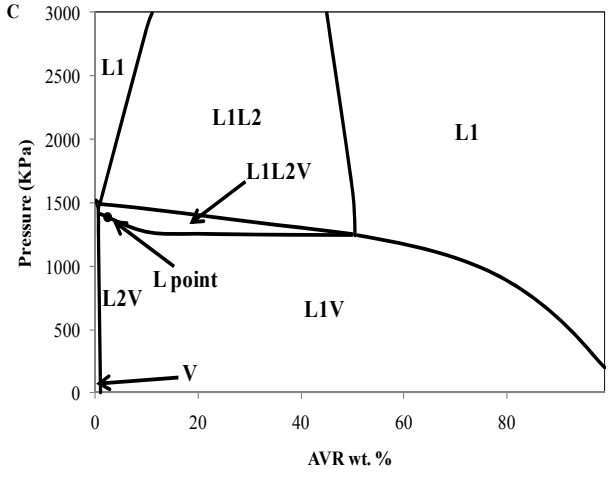
C
L1
L1L2
L1
L1L2V
L point
L2V
L1V
V
Pressure (KPa)
AVR wt. %

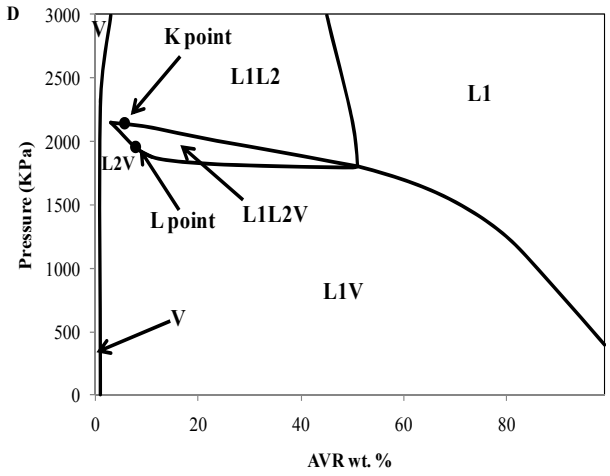

Figure 4.3. Calculated P-x diagrams for AVR + n-decane mixtures at A) 200 ^{o}C, B) 267 ^{o}C, C) 320 ^{o}C, and D) 350 ^{o}C

4.5 Conclusions

The PR EOS combined with the group contribution method of Marrero and Gani for Tc and Pc estimation presents a viable computational approach for simulating the phase behaviour of asymmetric and ill-defined hydrocarbon mixtures. Binary interaction coefficient values among residue pseudo components were set to zero. Values for coefficients between residue pseudo components and the small molecules present have a significant impact on the accuracy and correctness of the predicted phase behaviours and tuning is required to guarantee accurate results. For the specific case of Athabasca Vacuum Residue (AVR) + n-decane, the computational success represents a major advance as reliable phase behaviour computations are available for the first time, for paraffinic deasphalting processes, and distillation and refining processes for Athabasca vacuum residue. The origin of the mismatch between predicted and measured phase behaviour, over a limited range of compositions at lower temperatures, is the subject of ongoing investigation and exploration and will be discussed in the context of the phase behaviour of AVR + pentane and other n-alkanes, where limited phase boundary and phase composition data sets are also available.

4.6 Nomenclature

a or a(T)	temperature dependent equation of state energy parameter
a_c	parameter in Peng-Robinson equation of State
b	equation of state co-volume parameter
f	perturbation function
k_{ij}	binary interaction coefficient
M	number of first order groups
MW	molecular weight
N	number of second order groups
O	number of third order groups
P	pressure
P_C	critical pressure
pc	contribution to critical pressure
R	universal gas constant
SG	specific gravity
T	temperature
T_C	critical temperature
tc	contribution to critical temperature
v	molar volume

Greek letters

α	temperature-dependent equation of state parameter
ε_i	(i=1) first and (i=2) second order contributions to acentric factor
ω	acentric factor

4.7 Abbreviations

AVR	Athabasca vacuum residue
EOS	Equation of State
K	K-point, three-phase critical point
L	L-point, three-phase critical point
L1	lighter liquid phase
L2	denser liquid phase
L1V	liquid-vapour
L2V	liquid-vapour
L1L2	liquid-liquid
LLV	liquid-liquid-vapour
NMR	nuclear magnetic resonance
PPR78	predictive Peng-Robinson 78 method
PR	Peng-Robinson
SARA	saturates-aromatics-resins-asphaltenes
V	vapour

4.8 References

[1] N. Saber and J. M. Shaw, *Fluid Phase Equilibria* **264** (2008) 137-146.

[2] D. R. Jones, C. D. Perttunen, and B. E. Stuckman, *JOTA* **79** (1993) 157-181.

[3] L. E. Baker, A. C. Pierce, and K. D. Luks, *SPEJ* **22** (1982) 731-742.

[4] M. L. Michelsen, *Fluid Phase Equilib.* **9** (1982) 1-19.

[5] S. B. Jaffe, H. Freund, and W. N. Olmstead, *Ind. Eng. Chem. Res.* **44** (2005) 9840-9852.

[6] J. M. Sheremata, M. R. Gray, H. D. Dettman, and W. C. McCaffrey, *Energy Fuels* **18** (2004) 1377-1384.

[7] J. M. Sheremata, Ph.D. Thesis, University of Alberta, 2008.

[8] S. Zhao, L. S. Kotlyar, J. R. Woods, B. D. Sparks, K. Hardacre, and K. H. Chung, *FUEL* **80** (2001) 1155-1163.

[9] J. Murgich, J. A. Abanero, and O. P. Strausz, *Energy Fuels* **13** (1999) 278-286.

[10] C. Obiosa-Maife and J. M. Shaw, *Energy Fuels* **In Press** (2010) DOI:10.1021/ef1006808.

[11] D. Peng and D. B. Robinson, *I.&E.C. Fund.* **15** (1976) 59-64.

[12] N. Saber and J. M. Shaw, *Fluid Phase Equilib.* **285** (2009) 73-82.

[13] J. Marrero and R. Gani, *Fluid Phase Equilib.* **183** (2001) 183-208.

[14] J.-N. Jaubert, S. Vitu, F. Mutelet, and J.-P. Corriou, *Fluid Phase Equilib.* **237** (2005) 193-211.

[15] J.-N. Jaubert and F. Mutelet, *Fluid Phase Equilib.* **224** (2004) 285-304.

[16] S. Vitu, J.-N. Jaubert, and F. Mutelet, *Fluid Phase Equilib.* **243** (2006) 9-28.

[17] S. Vitu, R. Privat, J. N. Jaubert, and F. Mutelet, *J. Supercrit. Fluids* **45** (2008) 1-26.

[18] G. H. Gao, J. L. Daridon, H. Saintguirons, P. Xans, and F. Montel, *Fluid Phase Equilib.* **74** (1992) 85-93.

[19] X. Zhang, Ph.D. Thesis, University of Alberta, 2006.

[20] X. Y. Zou, Ph.D. Thesis, University of Toronto, 2003.

[21] R. A. McFarlane, M.Sc. Thesis, University of Alberta, 2007.

[22] A. Van Waeyenberghe, M.Sc. Thesis, University of Alberta, 2006.

[23] R. A. McFarlane, M. R. Gray, and J. M. Shaw, *Fluid Phase Equilib.* **293** (2010) 87-100.

[24] L. Constantinou, R. Gani, and J. P. O'connell, *Fluid Phase Equilib.* **103** (1995) 11-22.

[25] G. N. Nji, W. Y. Svrcek, H. Yarranton, and A. A. Satyro, *Energy & Fuels* **23** (2009) 366-373.

[26] M. L. Michelsen, *Comput. Chem. Eng.* **18** (1994) 545-550.

[27] B. I. Lee and M. G. Kesler, *Aiche J.* **21** (1975) 510-527.

[28] A. B. Bazyleva, A. Hasan, M. Fulem, M. Becerra, and J. M. Shaw, *J. Chem. Eng. Data* **55** (2010) 1389-1397.

[29] H. Y. Cai, J. M. Shaw, and K. H. Chung, *FUEL* **80** (2001) 1065-1077.

Chapter 5
On the Phase Behaviour of Athabasca Vacuum Residue + n-Alkanes

5.1 Introduction

Understanding the phase behaviour of mixtures containing n-alkanes and heavy oil constituents under reservoir and refining conditions plays a central role in the optimization and development of related industrial processes. SAGD, SA-SAGD, VAPEX, and other similar production processes have been developed or are under development for heavy oil and bitumen production [1-2]. These processes often include diluents such as light hydrocarbons to reduce viscosity and sometimes to perform in-situ separation. Deasphalting, an essential refining operation, also involves mixtures containing light hydrocarbons and heavy oil constituents. Removal of asphaltenes eliminates many undesired components that can cause significant problems such as catalyst poisoning and line plugging in refineries. Reliable phase behaviour simulation is an essential enabling technology for successful design and development of production and refining processes.

Though data are essential, the high cost and complexity of experimental phase behaviour measurements for mixtures containing heavy oil [3-4], are major barriers for the general availability of data. Phase behaviour prediction, leveraging the value of limited data sets, is the sole practical answer but only if reliable predictions or extrapolations are available. Common refinery type computational methods are not capable of handling predictions for mixtures containing heavy oil or bitumen constituents. They are limited to and based on techniques that are only reliable for conventional oil. Novel adaptations targeting heavy oil have been reported recently [5-7]. Aspects of an alternative non-refinery computational approach, the subject of this thesis, have been published recently [8-11]. This alternative approach is based on a robust phase equilibrium computational method [9,12] in combination with a reliable thermodynamic model developed

specifically for ill-defined asymmetric mixtures [10]. The thermodynamic model combines the Peng-Robinson equation of state [13] and group contribution methods [14-16] and predictive correlations [5,17], eliminating the need for measured critical properties of heavy components. This combination of equations simulates the multiphase behaviour of asymmetric mixtures where the components are well-defined quite reliably. The only adjustable parameters are binary interaction coefficients that are tuned to available phase equilibrium data based on a method proposed by Gao et al. [17]. To ensure convergence to the correct phase behaviour a global search algorithm for phase stability analysis is imbedded in the calculations [9,18].

This approach was tested successfully for mixtures containing n-decane and Athabasca Vacuum Residue (AVR) [8]. The phase behaviour type and trends were correctly simulated. Phase boundaries (LV/L and LLV/LL) were identified to within 5 ^{o}C and 5 bar. Mismatch was observed for a small range of compositions where experimental data exhibit an unexpected lower bound for the liquid-liquid-vapour (LLV) region, while the three-phase zone is predicted to extend to low temperatures and pressures. Correct phase diagrams for ~ 0 to 35 and 65 to 100 wt. % AVR, for the full range of temperatures and pressures where data are available were obtained for the first time. The composition, temperature and pressure range where mismatch arises is outside of the operating window for most envisioned industrial processes.

In this contribution, phase diagrams and phase behaviour trends for AVR + n-alkanes, from n-pentane to n-dodecane are simulated on the basis of available data for n-pentane, n-heptane, n-decane and n-dodecane. Computed phase behaviours and phase boundaries using the group contribution approach applied previously to AVR + n-decane are compared with available experimental data. The phase behaviour of these asymmetric mixtures has been studied experimentally [19-20] and computationally [21-22]. These mixtures exhibit complex phase behaviour patterns. In addition, the densities of liquid phases present in the LLV three-phase region are calculated and compared to the

available measurements for the mixture of AVR + n-decane. As the accuracy of predictions depends on the values of binary interaction parameters, a simple approach for tuning these coefficients is also presented.

5.2 Methodology

The methodology was discussed in Chapter 4 in detail. Only a brief overview is given here. The phase equilibrium calculations combine a cubic equation of state with group contribution methods. Group contribution methods permit thermodynamic models to be used for mixtures containing constituents for which thermodynamic properties (e.g. critical properties) are unavailable. The only inputs required are the molecular structures of constituents. The Peng-Robinson (PR) equation of state [13] and group contribution methods of Marrero and Gani [14], Constantinou et al. [16], and correlations by Nji et al. [5] and Gao et al. [17] define the thermodynamic model. The critical properties, used to calculate equation of state parameters, are estimated according to the group contribution method of Marrero and Gani [14]. The acentric factors for molecules with molar masses less than 500 g/mol are estimated using the group contribution method of Constantinou et al. [16] As this group contribution method does not generate reasonable values for larger molecules, the predictive method of Nji et al. [5] is used for molecules larger than 500 g/mol. The only adjustable parameters in this thermodynamic model are the binary interaction coefficients (k_{ij}s) and these are estimated using the method of Gao et al. [17].

Phase equilibrium calculations were performed using a computational tool developed by Saber and Shaw [9] where a global minimization technique called DIRECT [12] was adopted for stability analysis. The equilibrium calculations start with a stability analysis performed on a feed composition. If the stability analysis showed that the mixture is unstable, two-phase flash calculations were performed to identify the number, nature and compositions of phases corresponding to the global minimum of Gibbs free energy. The results of two-phase calculations were again subject to stability analysis and three-phase flash calculations were performed if required. The results of each stability analysis

were used to initialize subsequent flash calculations. Due to the large number of pseudo components present and the complexity of the predicted phase behaviours, the VMGSim process simulation engine (Version 5.012) was used to perform the three-phase flash calculations.

AVR characterization was based on molecular representations proposed by Sheremata [23], which are consistent with available ^{13}C-NMR, molecular weight, aromaticity, SARA fractionation, and simulated distillation data. Molecular representations and molar masses are not unique. Boek et al. [24] proposed alternative representations and molar masses based on the same input data. It is clear from recent quantum mechanical calculations [25] that ^{13}C-NMR provides no information at molecular length scales. Small changes in the molecule construction algorithms lead to radically different molecular representations. However, there is a better agreement at the functional group level, where there is a closer link with the ^{13}C-NMR data and the results appear to be robust. The properties generated using Sheremata's representations were used to model AVR containing mixtures. These properties along with the mole percent of pseudo components are tabulated in Table 5.1. The binary interaction parameters between pseudo components were set to zero as explained elsewhere [8,11]. The vapour pressure curve for AVR based on this approach agrees with the experimental data and the predicted phase behaviour type is consistent with experimental observation [19,22,26].

5.3 Results and Discussion

Binary interaction coefficients have a great impact on the accuracy of phase boundary placement and must be tuned to guarantee agreement between experimental and simulated phase behaviour. A simple predictive approach for tuning binary interaction coefficients was introduced in our recent contribution [8]. The k_{ij} values are first estimated using the method of Gao et al. [17] and are then tuned by multiplying them by a constant that depends solely on the carbon number of the n-alkane based on our observation. As a rough rule of thumb, the value of this constant is the carbon number minus 3. The tuned values based on

this approach generated reliable results for n-alkanes from n-C_5 up to n-C_{12}. Implementation of this approach is not recommended outside this range. Two observations can be made based on the tuned k_{ij} values. The first observation is that the values of k_{ij}s between pseudo components 1-7 and all of the n-alkanes are similar. The sensitivity of the phase boundary results to these k_{ij} values was probed. The binary interaction coefficients between pseudo components 1-7 and n-decane were used for the other n-alkanes and phase boundary calculations were performed. The simulations were found to be insensitive to this modification. Changes in phase boundary pressures at fixed temperature were insignificant (~0.1 to a maximum of ~5 kPa). Therefore, the same k_{ij} values can be used between pseudo components 1-7 and all n-alkanes without compromising precision. However, phase boundary results were found to be sensitive to the k_{ij} values between the heavier pseudo components and n-alkanes, which leads to a second observation. The values of binary interaction coefficients between n-alkanes and pseudo components 8-16 become larger as the carbon number of n-alkane increases, while the reverse was anticipated from the typical behaviour of asymmetric mixtures. The correct phase behaviour types and trends are not captured otherwise. The tuned binary interaction coefficients are tabulated in Table 5.2.

5.3.1 AVR + n-pentane Phase Behaviour

Figure 5.1 A-G presents the predicted and experimental pressure-temperature phase diagrams at constant composition for mixtures of n-pentane + AVR at 10, 20, 30, 40, 60, 70, and 80 wt.% AVR. In this figure, L1, L2, L3, and V denote a low density liquid phase, an intermediate density liquid phase, a high density liquid phase, and a vapour phase respectively. K-points (L1=V+L2) are also indicated. From Figure 5.1, AVR + n-pentane mixtures are highly asymmetric and exhibit expected complex phase behaviour at a below the critical temperature of pentane and unexpected complex phase behaviours - three-phase zone at high temperatures and pressures for compositions between ~40 and ~ 60 wt.% AVR [20,27]. From less than 10 wt.% to ~ 35 wt.% AVR, the L1L2V three-

phase region observed experimentally extends to low temperatures and pressures. The L2V to V phase boundaries move to higher pressures as more AVR is added to the mixture. For mixtures containing ~35 wt.% to ~60 wt.% AVR, a L2L3V three-phase zone is observed in addition to the L1L2V region that extends to lower temperatures and pressures. Mixtures containing higher concentrations of AVR do not exhibit LLV three-phase behaviour experimentally. As more AVR is added to the mixture, solids become more of an issue even at higher temperatures. Experimental data for the LV to L phase boundaries are not available for 70 and 80 wt.% AVR and only some liquid-vapour equilibrium data are measured inside the LV region.

Figure 5.1 A-C show that phase equilibrium calculations simulate the phase behaviour for mixtures containing less than 35 wt.% AVR. The predicted phase diagrams agree with the experimental data qualitatively. The L1L2 to L1L2V phase boundaries agree quantitatively with the experimental data and exhibit insignificant errors. The L2V to V phase boundaries are within an acceptable range of error, but the deviation increases as more AVR is added to the mixture. The maximum deviation of ~30 % is observed for the mixture containing 30 wt.% AVR. Critical point calculations were not performed, but the approximate locations of K-points were identified from relative phase volumes within the LLV region as pressure was varied at fixed temperature. These critical points are also indicated in Figure 5.1. For mixtures containing ~35-60 wt.% AVR, the L1L2V region is still present and another L2L3V zone is observed at higher temperature and pressures for which a lower as well as an upper temperature bound are obtained experimentally. The computations do not anticipate this upper three-phase zone. The experimental results and predictions for 40 % AVR + 60 wt.% n-pentane are shown in Figure 5.1 D. The location of the predicted LLV region is correct but the predicted and measured phase behaviours are not in qualitative agreement above 220 ^{o}C. The experimentally observed LLV-LL and LLV-LV phase boundaries are miss predicted as an LV-V phase boundary. For 60 to 100 wt.% AVR, L3V and L3 phase behaviours are observed experimentally. The computations conform with the experiments. The

computed LV - L phase boundaries for mixtures containing 60 , 70, and 80 wt.% AVR are shown in Figure 5.1 E-G. The experimental phase boundaries are only available for 60 wt.% AVR, where the computed results show a maximum of ~30 % deviation from the experimental data. For the other two compositions, experimental phase boundaries are not available and only some equilibrium data are given in the literature. Acceptable agreement is observed for the mixture containing 60 wt.% AVR and the same level of accuracy is expected for the mixtures containing 70 and 80 wt.% AVR. The best quantitative agreement between predictions and experimental data is observed at lower temperatures. At higher temperatures the experimental phase boundary shows an unusual trend where pressures along the boundary seem to be underestimated.

Table 5.1. Estimated physical and thermodynamic properties for AVR pseudo components

Molecular pseudo component	Mole %	Tc (^{o}C)	Pc (bar)	Acentric Factor
1	0	419.8	27.17	0.437
2	0	475	17.88	0.473
3	15.19	536.1	18.54	0.684
4	9.49	572.1	14.95	0.654
5	7.64	605	12.97	0.67
6	1.31	642.4	12.24	0.823
7	13.86	650.1	11.35	0.698
8	13.20	696.9	11.63	0.785
9	9.51	738.8	8.29	1.055
10	7.63	804.7	7.78	1.07
11	7.48	847.2	7.41	1.06
12	6.10	920.7	7.75	1.07
13	3.63	1021.9	7.82	1.09
14	0.009	913.8	6.78	1.39
15	3.59	1043.2	6.75	1.32
16	1.36	1070.9	6.57	1.4
17	0	1153.3	6.20	-

Table 5.2. Binary interaction coefficients for AVR pseudo components + n-pentane, n-heptane, and n-dodecane

Compound/Molecule	1	2	3	4
n-pentane/ n-heptane/n-dodecane	0.00305	0.00854	0.01701	0.02293
	5	6	7	8
n-pentane/ n-heptane/n-dodecane	0.02884	0.03604	0.03757	0.034/0.045/0.045
	9	10	11	12
n-pentane/ n-heptane/n-dodecane	0.038/0.052/0.055	0.044/0.063/0.073	0.048/0.070/0.085	0.056/0.082/0.105
	13	14	15	16
n-pentane/ n-heptane/n-dodecane	0.066/0.099/0.136	0.056/0.081/0.104	0.067/0.102/0.142	0.090/0.110/0.150

The predicted pressure-composition phase diagram at 160 ^{o}C is shown and compared with the experimental data in Figure 5.2. The location of the phase boundaries agrees with the experimental data, but there is qualitative disagreement from ~ 40 to 60 wt.% AVR where the existence of the L3 phase observed experimentally is not predicted. Outside this composition range there is qualitative and quantitative agreement between the predictions and experiments.

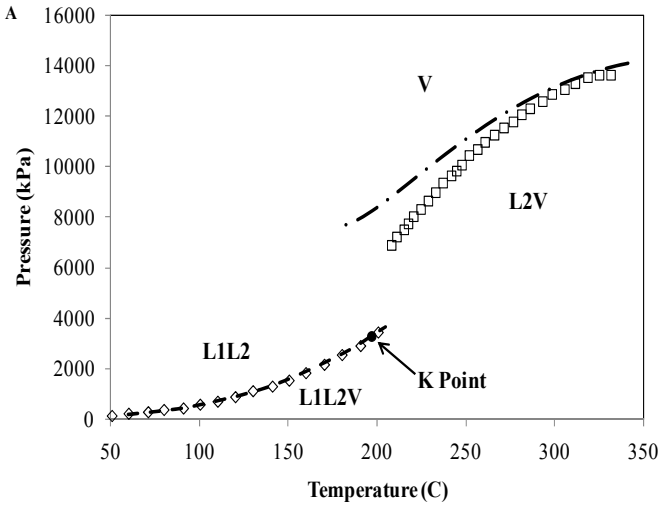
A
16000
14000
12000
10000
8000
6000
4000
2000
0
Pressure (kPa)
V
L2V
L1L2
L1L2V
K Point
50
100
150
200
250
300
350
Temperature (C)

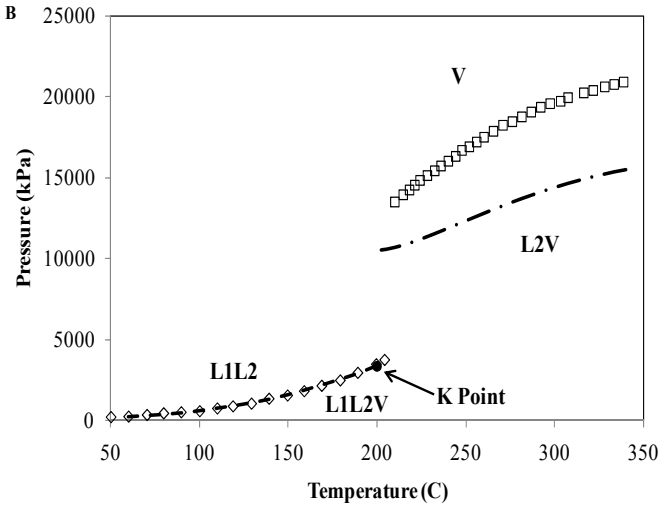
B
25000
20000
15000
10000
5000
0
Pressure (kPa)
V
L2V
L1L2
L1L2V
K Point
50
100
150
200
250
300
350
Temperature (C)

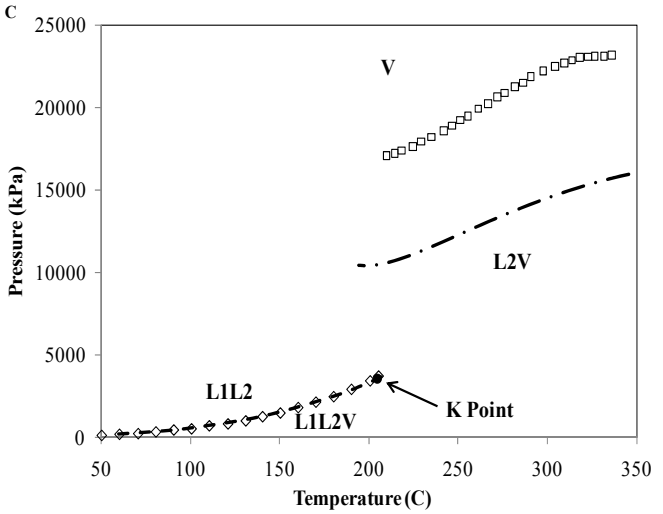
C
25000
20000
15000
10000
5000
0
Pressure (kPa)
V
L2V
L1L2
L1L2V
K Point
50
100
150
200
250
300
350
Temperature (C)

D

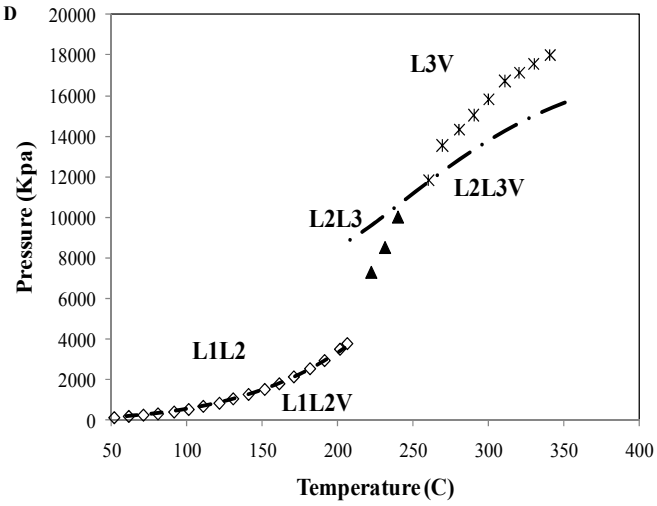
Pressure (Kpa)
Temperature (C)
L3V
L2L3V
L2L3
L1L2
L1L2V

E

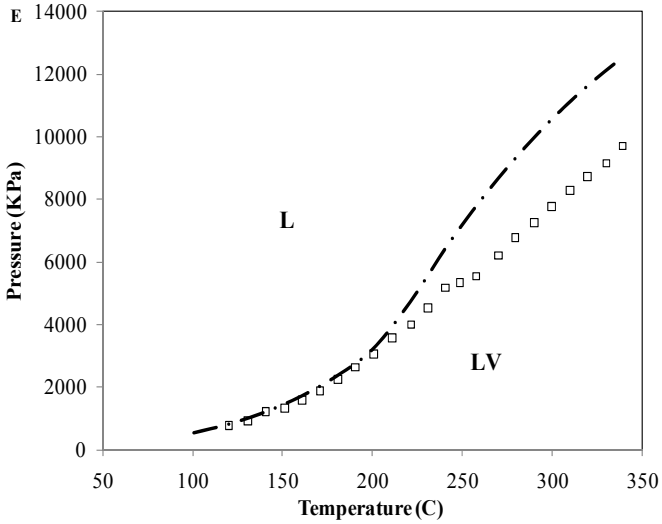
Pressure (KPa)
Temperature (C)
L
LV

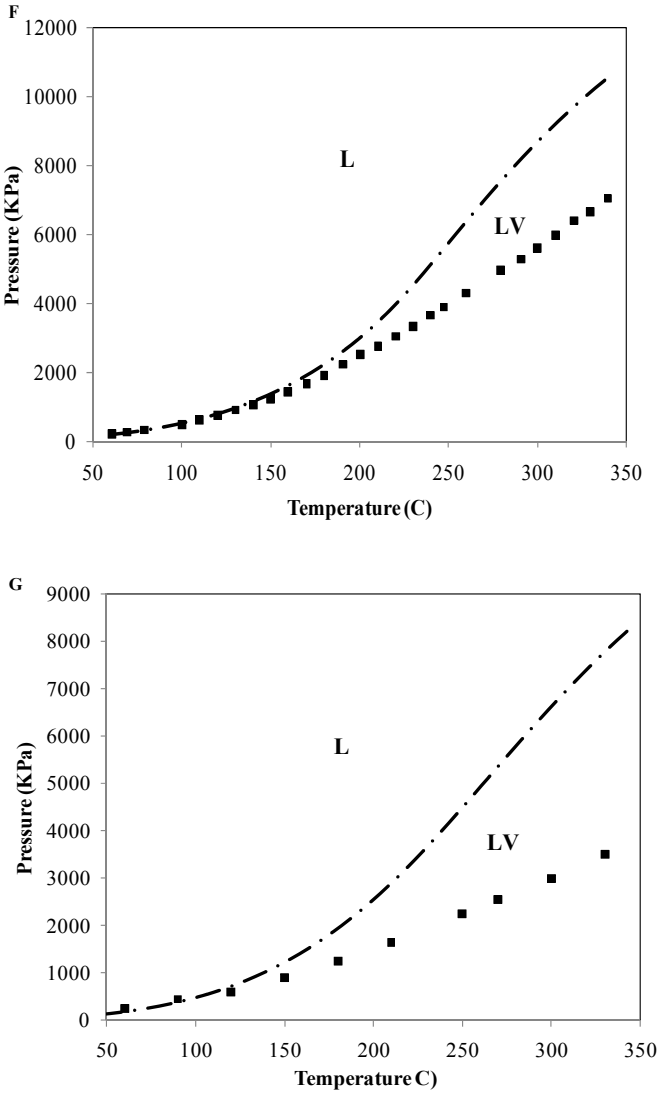

Figure 5.1. Experimental and predicted LLV phase boundaries for AVR + n-pentane mixtures (◊, experimental L1L2V/L1L2 boundary; □, experimental L1V/L1 boundary; ▲, experimental L2L3V/L2L3 boundary; *, experimental L2L3V/L3V boundary ■, experimental LV data [20]; ——, computed L1L2V/L1L2 boundary; — - —, computed LV/L or V boundary). A) 10 wt.% AVR. B) 20 wt.% AVR. C) 30 wt.% AVR. D) 40 wt.% AVR. E) 60 wt.% AVR F) 70 wt.% AVR. G) 80 wt.% AVR.

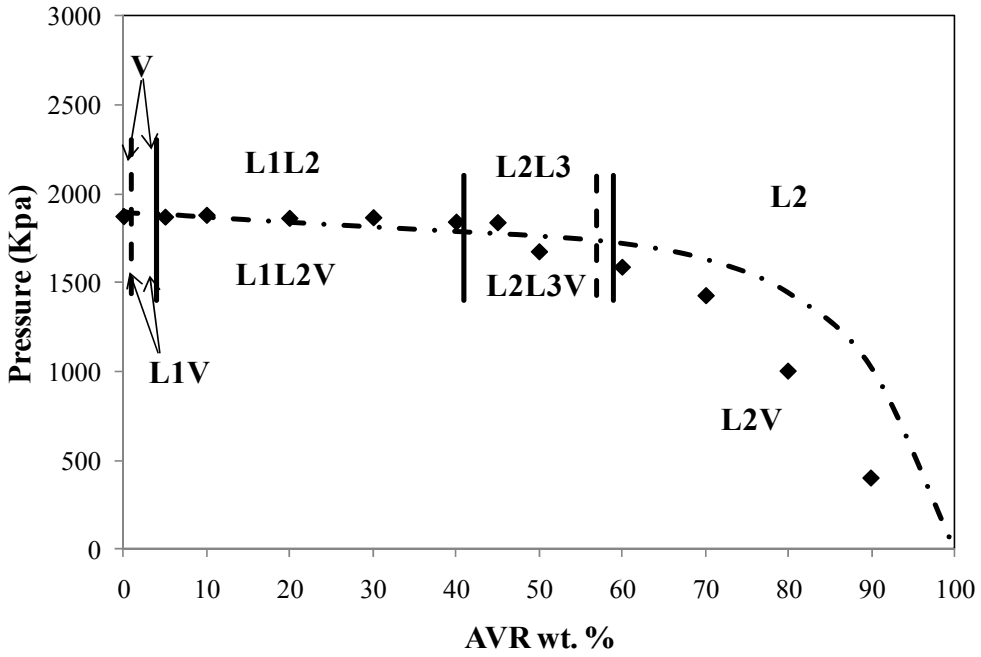

Figure 5.2. Calculated and measured P-x diagram for AVR + n-pentane mixtures at 160 ^{o}C

5.3.2 Phase Behaviour of AVR + n-heptane and n-dodecane

Experimental data for mixtures of n-heptane + AVR and n-dodecane + AVR are only available for one composition [27] making precise comparisons more difficult. However, the phase behaviour type can be deduced based on this limited data set and both mixtures exhibits Type III phase behaviour. Figure 5.3 and Figure 5.4 show the predicted and measured LLV phase boundaries for the mixtures of 25 wt.% AVR + 75 wt.% n-heptane and 25 wt.% AVR + 75 wt.% n-dodecane respectively. As depicted in these figures, the observed phase behaviours conform with Type III and predictions are in qualitative and quantitative agreement with experiments.

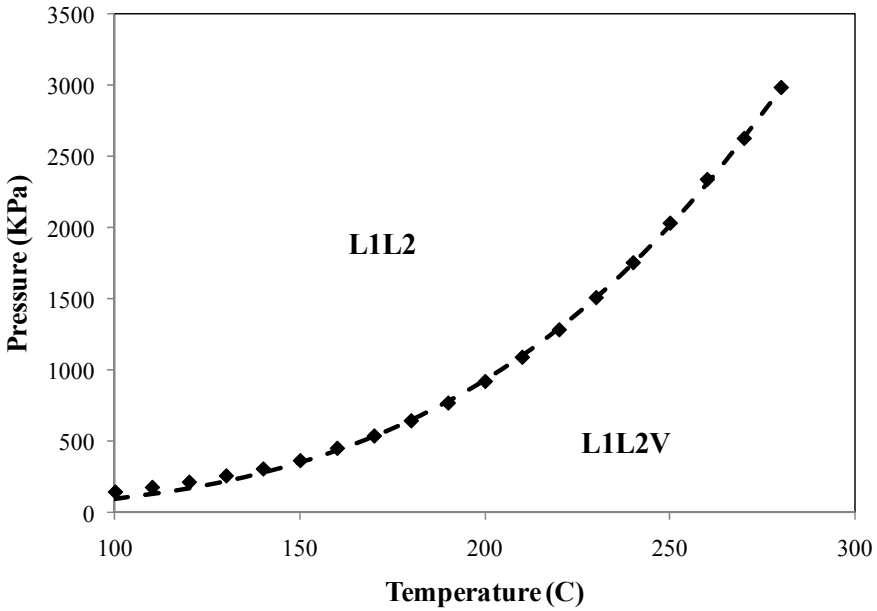

Figure 5.3. Experimental and predicted LLV phase boundaries for the mixture of 25 wt.% AVR + 75 wt.% n-heptane (♦, experimental L1L2V/L1L2 boundary [27]; — — —, computed L1L2V/L1L2 boundary)

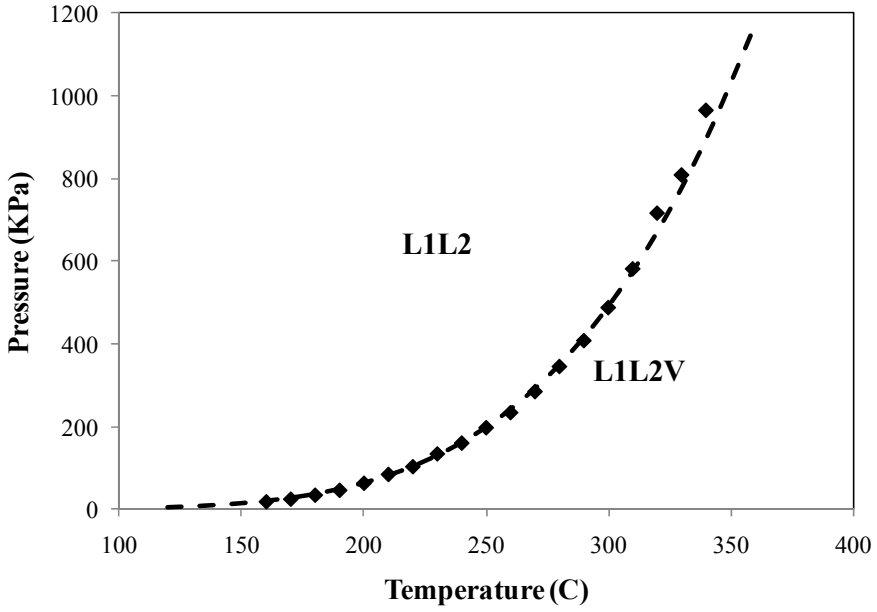

Figure 5.4. Experimental and predicted LLV phase boundaries for the mixture of 25 wt.% AVR + 75 wt.% n-dodecane (♦, experimental L1L2V/L1L2 boundary [27]; — — —, computed L1L2V/L1L2 boundary)

5.3.3 Phase Densities for the Mixture of AVR + n-decane

In this section, density versus temperature curves are generated for the previously studied [8,11] mixture of AVR + n-decane. Although the Peng-Robinson equation of state is not the most suitable thermodynamic model for estimating liquid densities, the objective of performing such calculations is to investigate the accuracy of the predicted compositions for the phases in equilibrium. The densities of L1 and L2 phases are calculated in the three-phase region and close to the LLV/LL phase boundary where experimental data are available. As predicted pressures along the phase boundary are lower than the measurements, densities are estimated at pressures that make the mass fractions of L1, L2, and V phases as close as possible to the experimental data with an emphasis on the fraction of the vapour phase.

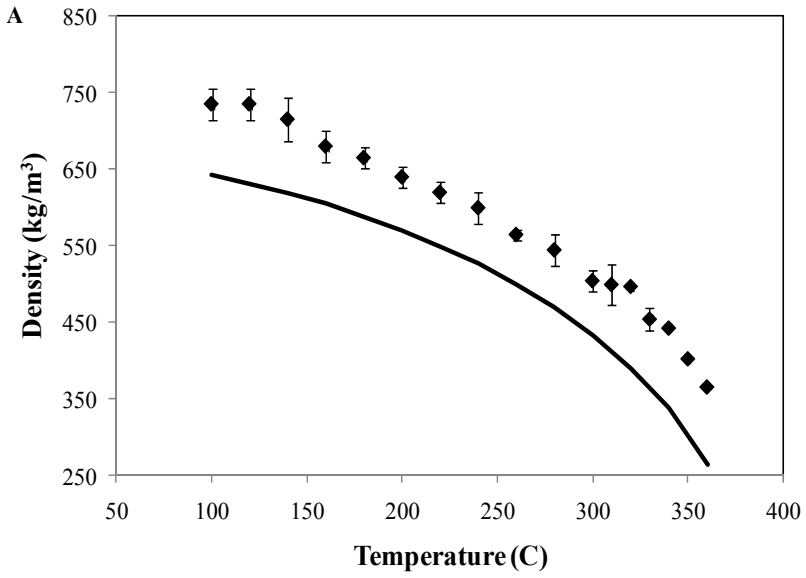

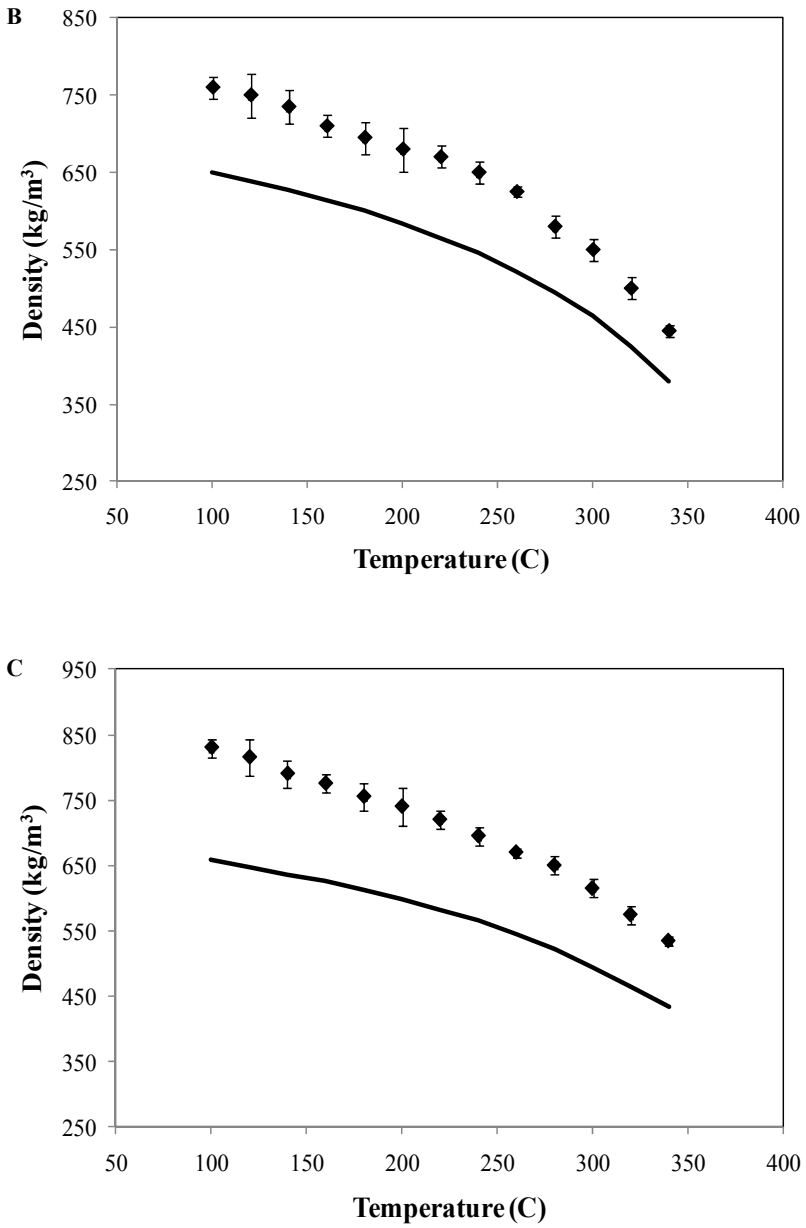

Figure 5.5. Experimental and predicted L1 phase densities for the mixture of A) 10 wt.% AVR. B) 20 wt.% AVR. C) 30 wt.% AVR + n-decane. (♦, experimental data [19]; ▬, computed densities)

The computed and measured L1 and L2 phase densities for the mixtures of 10, 20, and 30 wt.% n-decane + AVR are shown and compared in Figure 5.5 and Figure 5.6 respectively. The L1 phase densities follow the same trend as the experimental data, but the measured and calculated L2 phase densities do not agree qualitatively. If the volume correction is added to the thermodynamic

model, the L1 densities can be estimated within an acceptable range of error from the experimental data, but this is not the case for the L2 phase. The L1 and L2 phases predominantly consist of n-decane and AVR respectively. While solubility of AVR in n-decane seems to be predicted correctly, the solubility of n-decane in the AVR-rich phase seems to be underestimated, which is the reason for the observed increase of calculated densities with temperature. The measured density values increase abruptly at higher temperatures due to the sudden decrease in solubility of n-decane in AVR around its critical temperature.

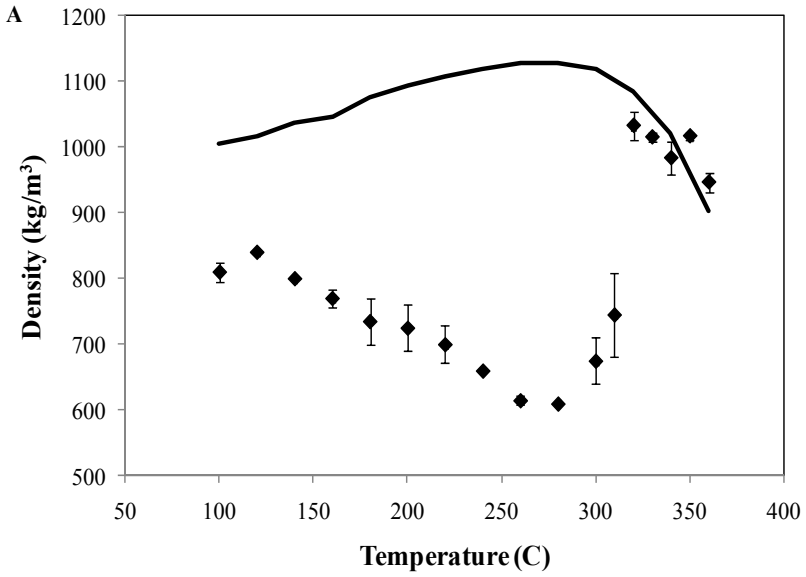

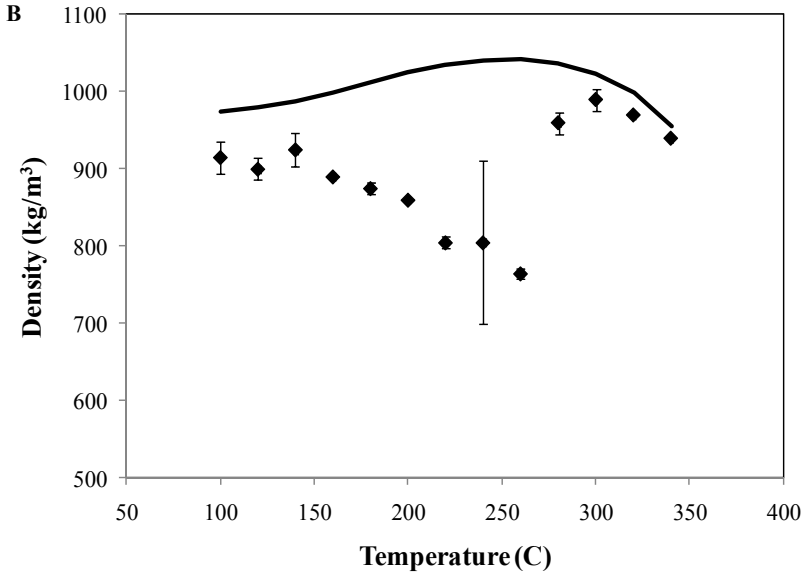

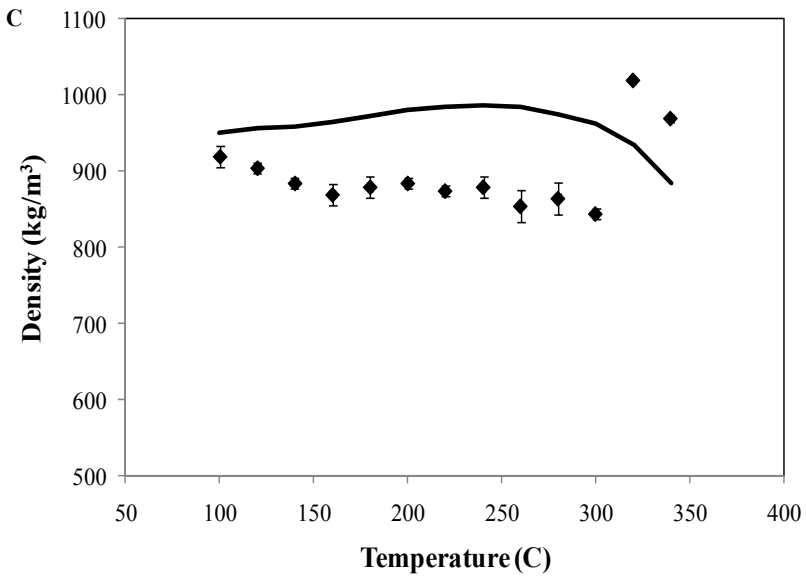

Figure 5.6. Experimental and predicted L2 phase densities for the mixture of A) 10 wt.% AVR. B) 20 wt.% AVR. C) 30 wt.% AVR + n-decane. (♦, experimental data [19]; ▬, computed densities)

There are many factors that can contribute to the observed errors and finding the sources of the deviations between predicted phase boundaries and experimental data is not trivial. For instance, the reason for underestimation of pressures along the L2V-V phase boundary for mixtures containing 10-30 wt. % AVR + n-pentane can lie in the inaccuracy of the correlations and methods used for characterization or the equation of state parameters employed for calculations. The contribution of each portion of the thermodynamic model to the overall error could not be evaluated because several estimation methods were combined. This is assuming that the available experimental data are completely reliable while some inaccuracies can be involved. Therefore, different factors can contribute to the mismatch over a small range of composition for the AVR + n-pentane and AVR + n-decane mixtures. Computational errors are the major source for the former case while measurement inaccuracies should be the main contributor to the overall error for the latter case. For the AVR + n-pentane mixtures, the type of the predicted phase behaviour does not match the experimental data, which may be due to the errors involved in the thermodynamic model. For the AVR + n-decane mixtures, the correct type of phase behaviour is predicted, but an unexpected

lower bound for the three phase region is observed experimentally, which does not conform with Type III phase behaviour. There could be a small amount of a second liquid phase present at lower temperatures and pressures that had been missed due to the limitations of the experimental technique.

Despite the observed mismatch over a small range of compositions, the broad qualitative and quantitative agreement between the experimental and the predicted phase boundaries illustrates the capability of group contribution based equations of state to correlate and interpolate sparse phase boundary data for ill-defined hydrocarbon mixtures. The predictive capability of the computational tool is extended to a wide range of compositions, pressures and temperatures and reliable results that can be employed in relevant industrial processes are obtained for the first time. The proposed thermodynamic approach has the potential to be applied to other heavy oil containing mixtures through which it can be generalized and evaluated further. The generalization procedure can be initiated by applying the approach to bitumen containing mixtures where the mole fractions of the same pseudo components should be optimized to include the bitumen vapour pressure data instead of AVR. For other heavy oils that are less similar to bitumen and its constituents, the mole fraction optimization will include elemental analysis and aromaticity in addition to vapour pressure data. The reliability of the thermodynamic model should also be further tested by validating the predicted phase compositions. In the absence of more relevant experimental data, comparing computational and experimental density data examines the accuracy of the predicted phase compositions to some extent, but does not necessarily reveal the exact shortcomings and virtues of the computed phase compositions. Elemental analysis is one of the available techniques that can be applied to the phases in equilibrium and provide a much better basis for comparison.

5.4 Conclusions

The group contribution based thermodynamic model, developed previously for AVR + n-decane, was extended successfully to a range of n-alkanes. Binary interaction coefficient values between residue pseudo components and n-alkanes are shown to have a significant impact on the accuracy and correctness of the predicted phase behaviours. A tuning procedure was introduced and interaction parameter values were refined. Successful computational results for the phase behaviour of AVR + n-alkanes from n-pentane to n-dodecane are presented. These results comprise a major advance as reliable phase behaviour predictions are available for the first time. The model will provide a reliable basis for the simulation of paraffinic deasphalting processes, distillation and refining processes for Athabasca vacuum residue, and bitumen solvent assisted production and pipelining processes. The model will be subject to further development and experimental validation as the origin of the mismatch between predicted and measured phase behaviour, over a limited range of compositions temperatures and pressures is explored in more detail. Shortcomings in the model and the experimental data both require resolution, both with respect to the patterns of phase behaviour and phase composition. For example, the computed densities of the liquid phases present in the three-phase region are compared against experimental measurements. The computed results suggest the possible underestimation of solubility of n-decane in the AVR-rich phase below the critical temperature of n-decane.

5.5 Abbreviations

AVR	Athabasca vacuum residue
K	K-point, three-phase critical point
L	L-point, three-phase critical point
L1	low density liquid phase
L2	intermediate density liquid phase

L3	high density liquid phase
L1V/ L2V/ L3V	liquid-vapour
L1L2	liquid-liquid
LLV/L1L2V/L2L3V	liquid-liquid-vapour
NMR	nuclear magnetic resonance
SARA	saturates-aromatics-resins-asphaltenes
V	vapour

5.6 References

[1] S. K. Das and R. M. Butler, *J. Pet. Sci. Eng.* **21** (1998) 43-59.

[2] R. M. butler, *Thermal recovery of oil and bitumen* (Prentice Hall, Englewood Cliffs, N.J., 1991).

[3] S. J. Abedi, H. Y. Cai, S. Seyfaie, and J. M. Shaw, *Fluid Phase Equilib.* **160** (1999) 775-781.

[4] J. M. Shaw and E. Behar, *Fluid Phase Equilib.* **209** (2003) 185-206.

[5] G. N. Nji, W. Y. Svrcek, H. Yarranton, and A. A. Satyro, *Energy Fuels* **23** (2009) 366-373.

[6] G. N. Nji, W. Y. Svreek, H. W. Yarranton, and M. A. Satyro, *Energy Fuels* **22** (2008) 3559-3559.

[7] M. A. Satyro and H. Yarranton, *Energy Fuels* **23** (2009) 3960-3970.

[8] N. Saber and J. M. Shaw, *Fluid Phase Equilib.* **In Press**

[9] N. Saber and J. M. Shaw, *Fluid Phase Equilib.* **264** (2008) 137-146.

[10] N. Saber and J. M. Shaw, *Fluid Phase Equilib.* **285** (2009) 73-82.

[11] N. Saber and J. M. Shaw, *On the Phase Behaviour of Athabasca Vacuum Residue + n-Decane*, Suzhou, China, 2010.

[12] D. R. Jones, C. D. Perttunen, and B. E. Stuckman, *JOTA* **79** (1993) 157-181.

[13] D. Peng and D. B. Robinson, *I.&E.C. Fund.* **15** (1976) 59-64.

[14] J. Marrero and R. Gani, *Fluid Phase Equilib.* **183** (2001) 183-208.

[15] L. Constantinou and R. Gani, *Aiche J.* **40** (1994) 1697-1710.

[16] L. Constantinou, R. Gani, and J. P. O'connell, *Fluid Phase Equilib.* **103** (1995) 11-22.

[17] G. H. Gao, J. L. Daridon, H. Saintguirons, P. Xans, and F. Montel, *Fluid Phase Equilib.* **74** (1992) 85-93.

[18] L. E. Baker, A. C. Pierce, and K. D. Luks, *SPEJ* **22** (1982) 731-742.

[19] X. Zhang, Ph.D. Thesis, University of Alberta, 2006.

[20] X. Y. Zou, Ph.D. Thesis, University of Toronto, 2003.

[21] A. Van Waeyenberghe, M.Sc. Thesis, University of Alberta, 2006.

[22] R. A. McFarlane, M.Sc. Thesis, University of Alberta, 2007.

[23] J. M. Sheremata, Ph.D. Thesis, University of Alberta, 2008.

[24] E. S. Boek, D. S. Yakovlev, and T. F. Headen, *Energy Fuels* **23** (2009) 1209-1219.

[25] C. Obiosa-Maife, M.Sc. Thesis, University of Alberta, 2009.

[26] R. A. McFarlane, M. R. Gray, and J. M. Shaw, *Fluid Phase Equilib.* **293** (2010) 87-100.

[27] X. Y. Zou, X. Zhang, and J. M. Shaw, *SPE Production & Operations* **22** (2007) 265-272.

Chapter 6
Conclusions and Recommendations

6.1 Conclusions

A general computational approach for predicting multiphase behaviour of ill-defined asymmetric mixtures was developed and validated. The method consists of two key building blocks: a phase equilibrium calculation routine and a thermodynamic model. The reliability of the phase equilibrium algorithm is guaranteed by including a robust phase stability analysis. The phase equilibrium approach addresses the numerical shortcomings involved in traditional equilibrium calculations used in both commercial and academic simulators that can cause severe problems in industrial applications. The thermodynamic model presents a practical approach for predicting the phase behaviour of asymmetric and ill-defined hydrocarbon mixtures.

The computational tool was validated by simulating the phase behaviour of mixtures containing Athabasca Vacuum Residue (AVR) and n-alkanes. The results show a broad agreement between computational and experimental phase diagrams and reliable simulations are obtained over industrially relevant ranges of compositions, pressures and temperatures. This computational success is a major advance as reliable phase behaviour predictions are available for the first time for an important class of mixtures. The results can be employed in paraffinic deasphalting, distillation and refining processes for Athabasca vacuum residue and solvent-assisted production processes of bitumen and play a significant role in the advancement of design, development and troubleshooting of these processes.

The following conclusions are drawn from different parts of this thesis:

1. Stability analysis is the necessary and sufficient condition for phase equilibrium and is the key to successful phase behaviour predictions. Stability analysis not only provides the ideal initialization for flash calculations, but also is the ultimate test of correctness of the predicted

phase behaviours. Conventional computational techniques that are employed in commercial simulators and are not based on a reliable stability analysis are prone to failure. Commercial simulators are shown to converge to false phase behaviours even for simple binary mixtures of industrial importance. In this regard:

a. A robust stability analysis based on the DIRECT global minimization method guarantees convergence to correct phase behaviours. The algorithm converges to the global minimum of the tangent plane distance function using significantly fewer function evaluations than other available approaches in the literature.
b. Flash calculation routines based on local minimization methods can be used reliably as long as they are initiated and checked using a robust stability analysis.

2. Even if all equations are solved correctly and all the numerical issues are addressed, incorrect phase behaviours can still be predicted due to shortcomings in a thermodynamic model. The incorrectness of predictions can range from misestimation of phase boundary pressures to misprediction of the type of phase behaviour. The thermodynamic model should not only be reliable enough to address such issues, but should also accommodate ill-defined hydrocarbons for which thermodynamic properties like critical temperatures are not available, e.g. bitumen containing mixtures. To this end:
    a. The combination of the Peng-Robinson equation of state and the group contribution method of Marrero and Gani proved to be a superior choice. This model outperforms the group contribution method of Coniglio et al. and the standard Peng-Robinson equation of state for asymmetric mixtures containing n-decylbenzene and n-eicosane. This model combined with a predictive method for estimation of binary interaction coefficients can be applied to bitumen and heavy oil containing mixtures.

b. The PPR78 predictive method for estimation of binary interaction coefficients improved the quality of predicted phase behaviours for n-eicosane containing mixtures. However, this method was not successful for Athabasca Vacuum Residue (AVR) containing mixtures and was replaced with the predictive method of Gao et al.

3. The thermodynamic model was first benchmarked against phase diagrams for the mixture of AVR + n-decane. AVR was characterized using molecular representations proposed by Sheremata, which are not unique at the molecular level. Over all molecular structures and molar masses remain ambiguous for bitumen. However, there is greater agreement on the functional groups and the types of carbon they comprise. Thus group contribution methods have much to offer as many of the groups can be measured and quantified experimentally using more than one technique. Mole fractions for Sheremata's pseudo components were re-optimized to provide better agreement with experimental vapour pressure data for AVR.
    a. Simulated P-T and P-x diagrams are in good qualitative and quantitative agreement with the experimental data over a broad range of temperatures, pressures, and compositions. This agreement includes the pressure-temperature-composition placement of liquid-liquid, liquid-vapour, and liquid-liquid-vapour regions. Mismatch is only observed for the composition range of ~35 to ~60 wt. % AVR.
    b. The origin of this mismatch is perceived to be the inaccuracies of the measured phase behaviours, where possibly a small amount of L2 phase present at lower temperatures and pressures is missed due to measurement technique limitations.
    c. A simple tuning procedure based on the method of Gao et al. is used to estimate k_{ij} values between the AVR pseudo components and n-decane. These coefficients have a significant impact on the accuracy of phase behaviour calculations. The same procedure is

then applied to mixtures of AVR + other n-alkanes, which results in successful predictions. This tuning approach is recommended for mixtures of AVR + n-alkanes form C5 to C12.

4. The proposed thermodynamic model is further validated by generating computational results for phase behaviour of mixtures of AVR + n-alkanes from n-pentane to n-dodecane.
    a. There is broad agreement between predicted and measured phase behaviours. For the mixture of n-pentane + AVR, mismatch is observed over the limited composition range of ~40 to ~60 wt. % AVR.
    b. The origin of the mismatch between predicted and measured phase behaviours, over this range of composition, is perceived to be the shortcomings in the thermodynamic model for the case of n-pentane.
    c. The densities of the liquid phases present in the three-phase region are compared against the experimental measurements. The computational results suggest the possible underestimation of solubility of n-decane in the AVR-rich (L2) phase by the employed model.

6.2 Recommendations for Future Work

The following recommendations for the extension of this research project are made based on the present study:

1. The group contribution based thermodynamic model can be generalized as a universal heavy oil modeling tool. Initially and to test the idea, the model can be applied to bitumen containing mixtures, which are similar to AVR mixtures in nature. The only required modification is that mole fractions of pseudo components be optimized to include the vapour pressure data for bitumen. Mass balance constraints on elements, carbon type and functional groups may also prove necessary.

2. The predicted phase compositions should be validated as an ultimate test of the reliability of the thermodynamic model. Performing elemental analysis, carbon type analysis or other analyses on the phases in equilibrium is the most convenient way of creating a strong basis for comparison.
3. In order to decrease the error in the experimental data, some modifications should be applied to the measurement techniques to minimize the possibility of misrepresenting the phase behaviours. Installation of a pressure transducer with higher accuracy, a camera with higher resolution, and a more accurate controller are some examples of the modifications that have been applied recently.

Appendix 1
The Procedure for Simulation of Experimental Simulated Distillation Data

Distillation assays are one of the most commonly used data for oil characterization. The experimental simulated distillation data are used along with other analytical data like ^{13}C-NMR to provide a better basis for characterization of bitumen and its constituents. Standard assay types such as the ASTM D1160 [1] vacuum distillation do not provide true boiling point (TBP) data directly and conversion procedures are required. It is unclear whether the ASTM D2887 [2] provides the TBP data or the methodology developed for converting distillation to TBP data should be used [3].

Simulated distillation data generated using the ASTM D2887 [2] are compared with the TBP data for three hydrocarbon mixtures to investigate if additional conversion procedures are required. The first two sample are mixtures of n-alkanes from n-C9 to n-C19 at two different compositions. The third sample is a mixture of n-alkanes and aromatics. The components present in these samples, their composition, and normal boiling points are tabulated in Table A1.1. The experiments to generate simulated distillation data for these mixtures are performed at CANMET Energy Technology Centre in Devon, Alberta. The experimental distillation curves are shown and compared to the TBP curves in Figure A1.1 A-C. There is an excellent agreement between experimental simulated distillation and TBP data. Therefore, it is concluded that there is no need for any conversion procedures and simulated distillation data can be modeled in terms of normal boiling points of the components in the mixture as long as their compositions are known.

Table A1.1. Compositions and normal boiling points of the prepared samples

Components	Normal boiling points [4] (^{o}C)	Sample 1- mass %	Sample 2- mass %	Sample 3- mass %
n-nonane	150.76	20.13	5.18	-
n-decane	174.12	19.35	9.44	-
n-undecane	196	16.55	8.80	-
n-dodecane	216	15.83	11.41	2.51
n-pentadecane	269	8.47	12.75	2.29
n-hexadecane	287	10.03	15.10	2.64
n-octadecane	317	5.20	15.12	1.99
n-nonadecane	330	4.44	22.21	2.15
quinoline	238	-	-	49.82
1-methylnaphthalene	242	-	-	35.81
anthracene	340	-	-	1.42
pyrene	404	-	-	1.36

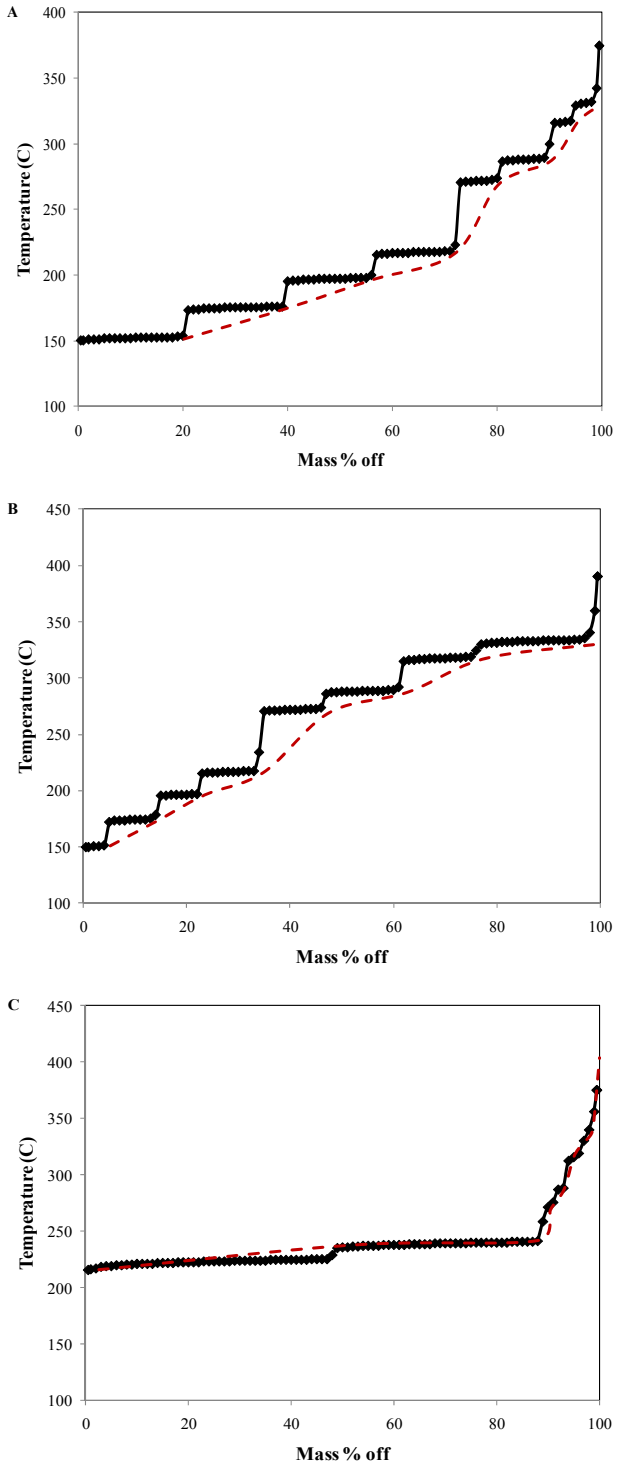

Figure A1.1. ♦, Experimental simulated distillation data; and ---, TBP curve for A) Sample 1, B) Sample 2, C)Sample 3.

References

[1] *ASTM D1160 - 06 Standard Test Method for Distillation of Petroleum Products at Reduced Pressure*, DOI: 10.1520/D1160-06 2006.

[2] *ASTM D2887-08, Standard Test Method for Boiling Range Distribution of Petroleum Fractions by Gas Chromatography*, DOI: 10.1520/D2887-08 2008.

[3] M. A. Satyro and H. Yarranton, *Energy Fuels* **23** (2009) 3960-3970.

[4] NIST, http://webbook.nist.gov/

Appendix 2
Phase Equilibrium Codes and the Procedure to Run the Codes in MATLAB

The DIRECT stability analysis for a mixture at specified temperature and pressure and based on the Peng-Robinson Equation of state can be called using the following command:

```
[fcn_minval,final_xatmin,history]=stabilityn1(nc,T,P,Z,Pc,Tc,w,kk)
```

where the inputs are:

nc: number of components in the mixture, a variable

T: specified temperature (K), a variable

P: specified pressure (bar), a variable

Z: feed composition (mole fractions), [z_1; z_2;...;z_{nc}]

Pc: critical pressures (bar), [Pc_1 Pc_2 ... Pc_{nc}]

Tc: critical temperatures (K), [Tc_1 Tc_2 ... Tc_{nc}]

w: acentric factors, [w_1; w_2;...;w_{nc}]

kk: binary interaction parameters matrix, $k_{ij} = \begin{bmatrix} k_{12} \cdots k_{1nc} \\ \vdots \cdots \vdots \\ k_{nc1} \cdots k_{ncnc} \end{bmatrix}_{nc\ xnc}$

and outputs are:

fcn_minval: returns the minimum value of the objective function

final_xatmin: returns the composition of the trial phase corresponding to the minimum of the objective function

history: returns the calculated parameters of each iteration

```
function [ret_minval,final_xatmin,history] = ...
    stabilityn1(nc,T,P,Z,Pc,Tc,w,kk,varargin)
tic
%Kijs are added to this version
R=83.14;%bar.cm3/K.mol
nn=nc-1;
bounds=zeros(nn,2);
for i=1:nn
    bounds(i,2)=1;
end
lengths = [];c = [];fc = [];
con = [];szes = [];feas_flags=[];
om_lower     = bounds(:,1);
om_upper     = bounds(:,2);
fcncounter   = 0;
perror       = 0;
itctr        = 1;
done         = 0;      n=nn;
ep        = 1e-4;
maxevals  = 50000;
maxits    = 450;
maxdeep   = 150;
testflag  = 0;
showits   = 1;
globalmin = 0;
tol       = 0.01;
theglobalmin = globalmin;
tflag        = testflag;
if tflag == 0
    lengths    = zeros(n,maxevals + floor(.10*maxevals));
    c          = lengths;
    fc         = zeros(1,maxevals + floor(.10*maxevals));
    szes       = fc;
    con        = fc;
    feas_flags = fc;
end
%Because feed composition is always the same, calculation of feed fugacity
%should not be performed in the function evaluation part

ai=zeros(1,n); m=ai; bi=ai;  lanphyz=ai; %calculation of EOS's parameters
sumbbf=0; % f stands for feed
for i=1:nc
    if w(i)<0.49
        m(i)=0.37464+1.54226*w(i)-0.26992*w(i)^2;
    else
        m(i)=0.3796+1.485*w(i)-0.1644*w(i)^2+0.01667*w(i)^3;
    end
    ai(i)=0.45724*R^2*Tc(i)^2/Pc(i)*(1+m(i)*(1-(T/Tc(i))^0.5))^2;
    bi(i)=0.07780*R*Tc(i)/Pc(i);  %the same for feed composition and trial
composition
    sumbbf=sumbbf+bi(i)*Z(i);
end
bbf=sumbbf; sumaaf=0;
for i=1:nc
    for j=1:nc
        sumaaf=sumaaf+Z(i)*Z(j)*(ai(i)*ai(j))^0.5*(1-kk(i,j));
    end
end
aaf=sumaaf; AAf=aaf*P/(R^2*T^2); BBf=bbf*P/(R*T);
% Calling roots function to find compressibility factor
[zmaxf,zminf,nphf]=roots_1(AAf,BBf);
% If there are two roots for z then the one with lower Gibbs free energy should be
used
if nphf==2
     gminf=zminf-1-log(zminf-BBf)-
(AAf/(BBf*2*2^0.5))*(log((zminf+(1+2^0.5)*BBf)/(zminf+(1-2^0.5)*BBf)));
     gmaxf=zmaxf-1-log(zmaxf-BBf)-
(AAf/(BBf*2*2^0.5))*(log((zmaxf+(1+2^0.5)*BBf)/(zmaxf+(1-2^0.5)*BBf)));
    if gminf<gmaxf
        zzf=zminf;
    else
```

```
        zzf=zmaxf;
    end
else
    zzf=zminf;
end

% Fugacity coefficient is calculated in this part
for i=1:nc
    sumzf=0;
    for j=1:nc
        sumzf=sumzf+Z(j)*(ai(i)*ai(j))^0.5*(1-kk(i,j));
    end
    lanphyz(i)=bi(i)/bbf*(zzf-1)-log(zzf-BBf)- (AAf/(BBf*2*2^0.5))*(2/aaf*sumzf-
bi(i)/bbf)* (log((zzf+(1+2^0.5)*BBf)/(zzf+(1-2^0.5)*BBf)));
%lanphyy(i)=bi(i)/bb*(zz-1)-log(zz-BB)- (AA/(BB*2*2^0.5))*(2/aa*sumpoint-bi(i)/b)*
(log((zz+(1+2^0.5)*BB)/(zz+(1-2^0.5)*BB)));
end
%-- Call DIRini ----------------------------------------------------%
[thirds , lengths, c , fc, con, feas_flags minval,xatmin,perror,...
        history,szes,fcncounter,calltype] =...
        DIRini(n,bounds(:,1),bounds(:,2),...
        lengths,c,fc,con, feas_flags, szes,...
        theglobalmin,maxdeep,tflag,ai,bi,R,T,P,Z,lanphyz,nc,kk, varargin);

ret_minval = minval;
ret_xatmin = xatmin;

%-- MAIN LOOP ------------------------------------------------------%
minval = fc(1) + con(1);
while perror > tol
   %-- Create list S of potentially optimal hyper-rectangles
   S = find_po(fc(1:fcncounter)+con(1:fcncounter),...
       lengths(:,1:fcncounter),minval,ep,szes(1:fcncounter));

   %-- Loop through the potentially optimal hrectangles -----------%
   %-- and divide -------------------------------------------------%
   for i = 1:size(S,2)
      [lengths,fc,c,con,feas_flags,szes,fcncounter,success] = ...
          DIRdivide(bounds(:,1),bounds(:,2),S(1,i),thirds,lengths,...

fc,c,con,feas_flags,fcncounter,szes,calltype,ai,bi,R,T,P,Z,lanphyz,nc,kk,varargin{
:});
   end

   %-- update minval, xatmin --------------------------------------%
   [minval,fminindex] =  min(fc(1:fcncounter)+con(1:fcncounter));
   penminval = minval + con(fminindex);
   xatmin = (om_upper - om_lower).*c(:,fminindex) + om_lower;
   if (con(fminindex) > 0)|(feas_flags(fminindex) ~= 0)
       %--- new minval is infeasible, don't do anything
   else
       %--- update return values
       ret_minval = minval;
       ret_xatmin = xatmin;
   end

   %--see if we are done --------------------------------------------%
   if tflag == 1
      %-- Calculate error if globalmin known
      if theglobalmin ~= 0
          perror = 100*(minval - theglobalmin)/abs(theglobalmin);
      else
          perror = 100*minval;
      end
   else
      %-- Have we exceeded the maxits?
      if itctr >= maxits
         disp('Exceeded max iterations. Increase maxits')
         done = 1;
      end
      %-- Have we exceeded the maxevals?
```

```
      if fcncounter > maxevals
         disp('Exceeded max fcn evals. Increase maxevals')
         done = 1;
      end
      if done == 1
         perror = -1;
      end
   end
   if max(max(lengths)) >= maxdeep
      %-- We've exceeded the max depth
      disp('Exceeded Max depth. Increse maxdeep')
      perror = -1;
   end

      %-- Store History
      maxhist = size(history,1);
      history(maxhist+1,1) = itctr;
      history(maxhist+1,2) = fcncounter;
      history(maxhist+1,3) = minval;
  %end


  %-- show iteration stats
   if showits == 1
     if  (con(fminindex) > 0) | (feas_flags(fminindex) == 1)
         fprintf('Iter: %4i   f_min: %15.16f*    fn evals: %8i\n',...
         itctr,minval,fcncounter);
     else
         fprintf('Iter: %4i   f_min: %15.16f    fn evals: %8i\n',...
          itctr,minval,fcncounter);
     end
   end
   itctr  = itctr + 1;
 end

final_xatminn=zeros(nn,1);sumx=0;final_xatminn(1)=ret_xatmin(1);
for i=2:nn
    sumx=sumx+final_xatminn(i-1);
    final_xatminn(i) = (1-sumx)*ret_xatmin(i);
end
final_xatmin=final_xatminn;

    %-- chop off 1st row of history
    history(1:size(history,1)-1,:) = history(2:size(history,1),:);
    history = history(1:size(history,1)-1,:);
%end
toc
return

%-----------------------------------------------------------------%
% Function:   DIRini                                              %
% Purpose   : Initialization of Direct                            %
%             to eliminate storing floating points                %
%-----------------------------------------------------------------%
function [l_thirds,l_lengths,l_c,l_fc,l_con, l_feas_flags,
minval,xatmin,perror,...
        history,szes,fcncounter,calltype] = DIRini(n,a,b,...
        p_lengths,p_c,p_fc,p_con, p_feas_flags, p_szes,theglobalmin,...
        maxdeep,tflag,ai,bi,R,T,P,Z,lanphyz,nc,kk,varargin)

l_lengths    = p_lengths;
l_c          = p_c;
l_fc         = p_fc;
l_con        = p_con;
l_feas_flags = p_feas_flags;
szes         = p_szes;


%-- start by calculating the thirds array
%-- here we precalculate (1/3)^i which we will use frequently
l_thirds(1) = 1/3;
```

```
for i = 2:maxdeep
   l_thirds(i) = (1/3)*l_thirds(i-1);
end

%-- length array will store # of slices in each dimension for
%-- each rectangle. dimension will be rows; each rectangle
%-- will be a column

%-- first rectangle is the whole unit hyperrectangle
l_lengths(:,1) = zeros(n,1);

%01/21/04 HACK
%-- store size of hyperrectangle in vector szes
szes(1,1) = 1;

%-- first element of c is the center of the unit hyperrectangle
l_c(:,1) = ones(n,1)/2;

%-- Determine if there are constraints
calltype = 1;

%-- first element of f is going to be the function evaluated
%-- at the center of the unit hyper-rectangle.
%om_point   = abs(b - a).*l_c(:,1)+ a;
%l_fc(1)    = feval(f,om_point,varargin{:});
[l_fc(1),l_con(1), l_feas_flags(1)] = ...
    CallObjFcn(l_c(:,1),a,b,calltype,ai,bi,R,T,P,Z,lanphyz,nc,kk,varargin{:});
fcncounter = 1;


%-- initialize minval and xatmin to be center of hyper-rectangle
xatmin = l_c(:,1);
minval   = l_fc(1);
if tflag == 1
    if theglobalmin ~= 0
        perror = 100*(minval - theglobalmin)/abs(theglobalmin);
    else
        perror = 100*minval;
    end
else
   perror = 2;
end

%-- initialize history
%if g_nargout == 3
    history(1,1) = 0;
    history(1,2) = 0;
    history(1,3) = 0;
%end
%-----------------------------------------------------------------%
% Function   :  find_po                                           %
% Purpose    :  Return list of PO hyperrectangles                 %
%-----------------------------------------------------------------%
function rects = find_po(fc,lengths,minval,ep,szes)

%-- 1. Find all rects on hub
diff_szes = sum(lengths,1);
tmp_max = max(diff_szes);
j=1;
sum_lengths = sum(lengths,1);
for i =1:tmp_max+1
    tmp_idx = find(sum_lengths==i-1);
    [tmp_n, hullidx] = min(fc(tmp_idx));
    if length(hullidx) > 0
        hull(j) = tmp_idx(hullidx);
        j=j+1;
        %-- 1.5 Check for ties
        ties = find(abs(fc(tmp_idx)-tmp_n) <= 1e-20);
        if length(ties) > 1
            mod_ties = find(tmp_idx(ties) ~= hull(j-1));
            hull = [hull tmp_idx(ties(mod_ties))];
```

```
            j = length(hull)+1;
        end
    end
end
%-- 2. Compute lb and ub for rects on hub
lbound = calc_lbound(lengths,fc,hull,szes);
ubound = calc_ubound(lengths,fc,hull,szes);

%-- 3. Find indeces of hull who satisfy
%--    1st condition
maybe_po = find(lbound-ubound <= 0);

%-- 4. Find indeces of hull who satisfy
%--    2nd condition
t_len  = length(hull(maybe_po));
if minval ~= 0
    po = find((minval-fc(hull(maybe_po)))./abs(minval) +...
        szes(hull(maybe_po)).*ubound(maybe_po)./abs(minval) >= ep);
else
    po = find(fc(hull(maybe_po)) -...
        szes(hull(maybe_po)).*ubound(maybe_po) <= 0);
end
final_pos      = hull(maybe_po(po));

rects = [final_pos;szes(final_pos)];
return
%-----------------------------------------------------------------%
% Function   :  calc_ubound                                       %
% Purpose    :  calculate the ubound used in determing potentially %
%               optimal hrectangles                               %
%-----------------------------------------------------------------%
function ub = calc_ubound(lengths,fc,hull,szes)

hull_length  = length(hull);
hull_lengths = lengths(:,hull);
for i =1:hull_length
    tmp_rects = find(sum(hull_lengths,1)<sum(lengths(:,hull(i))));
    if length(tmp_rects) > 0
        tmp_f     = fc(hull(tmp_rects));
        tmp_szes  = szes(hull(tmp_rects));
        tmp_ubs   = (tmp_f-fc(hull(i)))./(tmp_szes-szes(hull(i)));
        ub(i)        = min(tmp_ubs);
    else
        ub(i)=1.976e14;
    end
end
return
%-----------------------------------------------------------------%
% Function   :  calc_lbound                                       %
% Purpose    :  calculate the lbound used in determing potentially %
%               optimal hrectangles                               %
%-----------------------------------------------------------------%
function lb = calc_lbound(lengths,fc,hull,szes)

hull_length  = length(hull);
hull_lengths = lengths(:,hull);
for i = 1:hull_length
    tmp_rects = find(sum(hull_lengths,1)>sum(lengths(:,hull(i))));
    if length(tmp_rects) > 0
        tmp_f     = fc(hull(tmp_rects));
        tmp_szes  = szes(hull(tmp_rects));
        tmp_lbs   = (fc(hull(i))-tmp_f)./(szes(hull(i))-tmp_szes);
        lb(i)     = max(tmp_lbs);
    else
        lb(i)     = -1.976e14;
    end
end
return
%-----------------------------------------------------------------%
% Function   :  DIRdivide                                         %
% Purpose    :  Divides rectangle i that is passed in             %
```

```
%-----------------------------------------------------------------%
function [lengths,fc,c,con,feas_flags,szes,fcncounter,pass] = ...
    DIRdivide(a,b,index,thirds,p_lengths,p_fc,p_c,p_con,...

p_feas_flags,p_fcncounter,p_szes,calltype,ai,bi,R,T,P,Z,lanphyz,nc,kk,varargin)
lengths    = p_lengths;
fc         = p_fc;
c          = p_c;
szes       = p_szes;
fcncounter = p_fcncounter;
con        = p_con;
feas_flags = p_feas_flags;

%-- 1. Determine which sides are the largest
li     = lengths(:,index);
biggy  = min(li);
ls     = find(li==biggy);
lssize = length(ls);
j = 0;

%-- 2. Evaluate function in directions of biggest size
%--    to determine which direction to make divisions
oldc       = c(:,index);
delta      = thirds(biggy+1);
newc_left  = oldc(:,ones(1,lssize));
newc_right = oldc(:,ones(1,lssize));
f_left     = zeros(1,lssize);
f_right    = zeros(1,lssize);
for i = 1:lssize
    lsi               = ls(i);
    newc_left(lsi,i)  = newc_left(lsi,i) - delta;
    newc_right(lsi,i) = newc_right(lsi,i) + delta;
    [f_left(i), con_left(i), fflag_left(i)]    =
CallObjFcn(newc_left(:,i),a,b,calltype,ai,bi,R,T,P,Z,lanphyz,nc,kk,varargin{:});
    [f_right(i), con_right(i), fflag_right(i)] =
CallObjFcn(newc_right(:,i),a,b,calltype,ai,bi,R,T,P,Z,lanphyz,nc,kk,varargin{:});
    fcncounter = fcncounter + 2;
end
w = [min(f_left, f_right)' ls];

%-- 3. Sort w for division order
[V,order] = sort(w,1);

%-- 4. Make divisions in order specified by order
for i = 1:size(order,1)

   newleftindex  = p_fcncounter+2*(i-1)+1;
   newrightindex = p_fcncounter+2*(i-1)+2;
   %-- 4.1 create new rectangles identical to the old one
   oldrect = lengths(:,index);
   lengths(:,newleftindex)   = oldrect;
   lengths(:,newrightindex)  = oldrect;

   %-- old, and new rectangles have been sliced in order(i) direction
   lengths(ls(order(i,1)),newleftindex)  = lengths(ls(order(i,1)),index) + 1;
   lengths(ls(order(i,1)),newrightindex) = lengths(ls(order(i,1)),index) + 1;
   lengths(ls(order(i,1)),index)         = lengths(ls(order(i,1)),index) + 1;

   %-- add new columns to c
   c(:,newleftindex)  = newc_left(:,order(i));
   c(:,newrightindex) = newc_right(:,order(i));

   %-- add new values to fc
   fc(newleftindex)  = f_left(order(i));
   fc(newrightindex) = f_right(order(i));

   %-- add new values to con
   con(newleftindex)  = con_left(order(i));
   con(newrightindex) = con_right(order(i));

   %-- add new flag values to feas_flags
```

```
   feas_flags(newleftindex)  = fflag_left(order(i));
   feas_flags(newrightindex) = fflag_right(order(i));

   %-- store sizes of each rectangle
   szes(1,newleftindex)  =
1/2*norm((1/3*ones(size(lengths,1),1)).^(lengths(:,newleftindex)));
   szes(1,newrightindex) =
1/2*norm((1/3*ones(size(lengths,1),1)).^(lengths(:,newrightindex)));
end
szes(index) = 1/2*norm((1/3*ones(size(lengths,1),1)).^(lengths(:,index)));
pass = 1;

return
%-------------------------------------------------------------------%
% Function   :  CallObjFcn                                          %
% Purpose    :  Evaluate ObjFcn at pointed specified                %
%-------------------------------------------------------------------%
function [fcn_value, con_value, feas_flag] = ...
    CallObjFcn(x,a,b,calltype,ai,bi,R,T,P,Z,lanphyz,nc,kk,varargin)

con_value = 0;
feas_flag = 0;

%-- Scale variable back to original space
nnn=nc-1;
point=zeros(nc,1);
point(1) = abs(b(1) - a(1)).*x(1)+ a(1);
sump=0;
for i=2:nnn
    sump=sump+point(i-1);
    b(i)=1-sump;
    point(i) = abs(b(i) - a(i)).*x(i)+ a(i);
end

point(nc)=1-sum(sum(point));


%if sum(sum(point))==1
if calltype == 1
    %-- No constraints at all
sumaa=0; sumbb=0; lanphyy=zeros(1,nc);
for i=1:nc
    sumbb=sumbb+bi(i)*point(i);
    for j=1:nc
        sumaa=sumaa+point(i)*point(j)*(ai(i)*ai(j))^0.5*(1-kk(i,j));
    end
end
aa=sumaa; bb=sumbb;
AA=aa*P/(R^2*T^2); BB=bb*P/(R*T);

% Calling roots function to find compressibility factor
[zmax,zmin,nph]= roots_1(AA,BB);

% If there are two roots for z then the one with lower Gibbs free energy should be
used
if nph==2
    gmin=zmin-1-log(zmin-BB)-(AA/(BB*2*2^0.5))*(log((zmin+(1+2^0.5)*BB)/(zmin+(1-
2^0.5)*BB)));
    gmax=zmax-1-log(zmax-BB)-(AA/(BB*2*2^0.5))*(log((zmax+(1+2^0.5)*BB)/(zmax+(1-
2^0.5)*BB)));
    if gmin<gmax
        zz=zmin;
    else
        zz=zmax;
    end
else
    zz=zmin;
end

% Fugacity coefficients are calculated in this part
for i=1:nc
```

```
    sumpoint=0;
    for j=1:nc
        sumpoint=sumpoint+point(j)*(ai(i)*ai(j))^0.5*(1-kk(i,j));
    end
    lanphyy(i)=bi(i)/bb*(zz-1)-log(zz-BB)- (AA/(BB*2*2^0.5))*(2/aa*sumpoint-
bi(i)/bb)* (log((zz+(1+2^0.5)*BB)/(zz+(1-2^0.5)*BB)));
end
sumtpd=0;
%The TPD is calculated here
for i=1:nc
    sumtpd=sumtpd+point(i)*(log(point(i))+lanphyy(i)-log(Z(i))-lanphyz(i));
end
    fcn_value = sumtpd;
end
%else
    %feas_flag = 1;
    %fcn_value = 0;
%end
return
%-------------------------------------------------------------------%
% Function   :  roots_1                                             %
% Purpose    :  Evaluate Compressibility factors                    %
%-------------------------------------------------------------------%
function [zmax,zmin,nph]= roots_1(AA,BB)
    co(1) = 1;
    co(2) = -(1 - BB);
    co(3) = AA - 3 * BB ^ 2 - 2 * BB;
    co(4) = -(AA * BB - BB * BB - BB * BB * BB);
    r=roots(co);
    n=0;
    for i=1:3
        test=imag(r(i));
        test2=real(r(i));
        if (abs(test)<=1e-8 & test2>=0 & test2>=BB)
            n=n+1;
            y(n)=real(r(i));
        end
    end
    if n==1
        nph=1;
        zmax=y(n);
        zmin=zmax;
    end
    if n>1
        nph=2;
        zmax=max(y);
        zmin=min(y);
    end
```

The two-phase flash code based on the successive substitution algorithm can be called using the following command:

```
[x_phase1,x_phase2,z_compressibility,bethaa] = ...
    flashssnewtonPR(nc,T,P,Z,Pc,Tc,w,kk,x_0,index)
```

where the inputs are:

nc: number of components in the mixture, a variable

T: specified temperature (K), a variable

P: specified pressure (bar), a variable

Z: feed composition (mole fractions), [z_1; z_2;...;z_{nc}]

Pc: critical pressures (bar), [Pc_1 Pc_2 ... Pc_{nc}]

Tc: critical temperatures (K), [Tc_1 Tc_2 ... Tc_{nc}]

w: acentric factors, [w_1; w_2;...;w_{nc}]

kk: binary interaction parameters matrix, $k_{ij} = \begin{bmatrix} k_{12} \cdots k_{1nc} \\ \vdots \quad \cdots \quad \vdots \\ k_{nc1} \cdots k_{ncnc} \end{bmatrix}_{nc\ xnc}$

x_0: initial guess for phase composition: [x_1; x_2;...;x_{nc}] (the result of the stability analysis provide the best initialization)

index: 0 if x_0 is a vapour-like or 1 if x_0 is a liquid-like phase (does not have any impact on the results based on the employed approach)

and outputs are:

x_phase1: composition vector of phase 1

x_phase2: composition vector of phase 2

z_ compressibility : the compressibility factor of each phase, [Z_1 Z_2]

bethaa: the fraction of phase 1

```
function [x_phase1,x_phase2,z_compressibility,bethaa] = ...
    flashssnewtonPR(nc,T,P,Z,Pc,Tc,w,kk,x_0,index)
tic
R=83.14;%bar.cm3/K.mol

%initialization of K values
K_value=zeros(nc,1);


%Because ai and bi are always the same, their calculation
%should not be performed in the function evaluation part

ai=zeros(1,nc); m=ai; bi=ai; %calculation of EOS's parameters

for i=1:nc
    %EOS's parameters
    if w(i)<0.49
        m(i)=0.37464+1.54226*w(i)-0.26992*w(i)^2;
    else
        m(i)=0.3796+1.485*w(i)-0.1644*w(i)^2+0.01667*w(i)^3;
    end
    ai(i)=0.45724*R^2*Tc(i)^2/Pc(i)*(1+m(i)*(1-(T/Tc(i))^0.5))^2;
    bi(i)=0.07780*R*Tc(i)/Pc(i);
    %K values
    if index==1
        K_value(i,1)=Z(i,1)/x_0(i,1);
    else
        K_value(i,1)=x_0(i,1)/Z(i,1);
    end

end

%The loop starts here
error=1; iter=1;
while error>0.000001
    %inner loop for finding fraction of phase1


    init(1)=0; endd(1)=1; sumationbi(1)=1; sumationbe(1)=-1; betha(1)=0.5;

    % 6-10 bisections to have a good initial guess for newton method
    for j=1:10

        sumationb(j)=0;
        for i=1:nc
            sumationb(j)=sumationb(j)+(K_value(i,1)-
1)*Z(i,1)/(K_value(i,1)*betha(j)+(1-betha(j)));
        end
        if sumationb(j)*sumationbi(j)<0
            init(j+1)=init(j); sumationbi(j+1)=sumationbi(j);
            endd(j+1)=betha(j); sumationbe(j+1)=sumationb(j);
        else
            init(j+1)=betha(j); sumationbi(j+1)=sumationb(j);
            endd(j+1)=endd(j); sumationbe(j+1)=sumationbe(j);
        end
        betha(j+1)=(init(j+1)+endd(j+1))/2;
    end

    %Newton method for convergence
    errorr=1;bethaa=betha(11);
    while errorr>.00001
        test=bethaa;
        sumation=0; sumder=0;
        for i=1:nc
            sumation=sumation+(K_value(i,1)-1)*Z(i,1)/(K_value(i,1)*bethaa+(1-
bethaa));
            sumder=sumder+((K_value(i,1)-1)^2)*Z(i,1)/(K_value(i,1)*bethaa+(1-
bethaa))^2;
```

```
        end

        bethaa=bethaa+sumation/sumder;

        errorr=abs(test-bethaa);

    end


    %update mole fractions
    for i=1:nc
        x_phase1(i,1)=K_value(i,1)*Z(i,1)/(K_value(i,1)*bethaa+(1-bethaa));
        x_phase2(i,1)=Z(i,1)/(K_value(i,1)*bethaa+(1-bethaa));
    end

    point(:,1)=x_phase1; point(:,2)=x_phase2;
    sumaa=zeros(1,2); sumbb=sumaa; AA=sumaa; BB=sumaa; phyy=zeros(nc,2);
    for k=1:2
        for i=1:nc
            sumbb(k)=sumbb(k)+bi(i)*point(i,k);
            for j=1:nc
                sumaa(k)=sumaa(k)+point(i,k)*point(j,k)*(ai(i)*ai(j))^0.5*(1-
kk(i,j));
            end
        end
    end
    aa=sumaa; bb=sumbb;
    for k=1:2
        AA(k)=aa(k)*P/(R^2*T^2); BB(k)=bb(k)*P/(R*T);
    end
    zmax=zeros(1,2); zmin=zmax; nph=zmin; zz=zmax;

    % Calling roots function to find compressibility factor
    [zmax(1),zmin(1),nph(1)]= roots_1(AA(1),BB(1));
    [zmax(2),zmin(2),nph(2)]= roots_1(AA(2),BB(2));

    for k=1:2
        if nph(k)==2
            gmin=zmin(k)-1-log(zmin(k)-BB(k))-
(AA(k)/(BB(k)*2*2^0.5))*(log((zmin(k)+(1+2^0.5)*BB(k))/(zmin(k)+(1-
2^0.5)*BB(k))));
            gmax=zmax(k)-1-log(zmax(k)-BB(k))-
(AA(k)/(BB(k)*2*2^0.5))*(log((zmax(k)+(1+2^0.5)*BB(k))/(zmax(k)+(1-
2^0.5)*BB(k))));
            if gmin<gmax
                zz(k)=zmin(k);
            else
                zz(k)=zmax(k);
            end
        else
            zz(k)=zmin(k);
        end
    end

    % Fugacities are calculated in this part
    for k=1:2
        for i=1:nc
            sumpoint=0;
            for j=1:nc
                sumpoint=sumpoint+point(j,k)*(ai(i)*ai(j))^0.5*(1-kk(i,j));
            end
            phyy(i,k)=(P*point(i,k))*exp(bi(i)/bb(k)*(zz(k)-1)-log(zz(k)-BB(k))-
(AA(k)/(BB(k)*2*2^0.5))*(2/aa(k)*sumpoint-bi(i)/bb(k))*
(log((zz(k)+(1+2^0.5)*BB(k))/(zz(k)+(1-2^0.5)*BB(k)))));

        end
    end

    %updating K values
    for i=1:nc
        K_value(i,1)=K_value(i,1)*(phyy(i,2)/phyy(i,1));
```

```
    end

    %checking the convergence

    error=max(abs(phyy(:,1)-phyy(:,2)));
    iter=iter+1

end

z_compressibility=zz;
toc


%-------------------------------------------------------------------%
% Function   :  roots_1                                             %
% Purpose    :  Evaluate Compressibility factors                    %
%-------------------------------------------------------------------%
function [zmax,zmin,nph]= roots_1(AA,BB)
    co(1) = 1;
    co(2) = -(1 - BB);
    co(3) = AA - 3 * BB ^ 2 - 2 * BB;
    co(4) = -(AA * BB - BB * BB - BB * BB * BB);
    r=roots(co);
    n=0;
    for i=1:3
        test=imag(r(i));
        test2=real(r(i));
        if (abs(test)<=1e-8 & test2>=0 & test2>=BB)
            n=n+1;
            y(n)=real(r(i));
        end
    end
    if n==1
        nph=1;
        zmax=y(n);
        zmin=zmax;
    end
    if n>1
        nph=2;
        zmax=max(y);
        zmin=min(y);
    end
```

The command to call the three-phase flash code based on successive substitution algorithm is as follows:

```
[x_phase1,x_phase2,x_phase3,z_compressibility,mol_vol,bethaa] =...
 flash3ssnewtonPR(nc,T,P,Z,Pc,Tc,w,kk,x_1,x_2,x_3,index)
```

where the inputs are:

nc: number of components in the mixture, a variable

T: specified temperature (K), a variable

P: specified pressure (bar), a variable

Z: feed composition (mole fractions), [z_1; z_2;...;z_{nc}]

Pc: critical pressures (bar), [Pc_1 Pc_2 ... Pc_{nc}]

Tc: critical temperatures (K), [Tc_1 Tc_2 ... Tc_{nc}]

w: acentric factors, [w_1; w_2;...;w_{nc}]

kk: binary interaction parameters matrix, $k_{ij} = \begin{bmatrix} k_{12} \cdots k_{1nc} \\ \vdots \quad \cdots \quad \vdots \\ k_{nc1} \cdots k_{ncnc} \end{bmatrix}_{\text{nc xnc}}$

x_1, x_2, and x_3: initial guesss for phase compositions: [x_1; x_2;...;x_{nc}] (the result of the stability analysis plus the results of two-phase flash provide the best initialization)

index: is fixed at 1 for the three-phase flash

and outputs are:

x_phase1, x_phase2, x_phase3: composition vectors of phases 1, 2, and 3 respectively

z_ compressibility : the compressibility factor of each phase, [Z_1 Z_2 Z_3]

mol_vol: the molar volume of each phase

bethaa: a vector containing fractions of phases 1 and 2

```
function [x_phase1,x_phase2,x_phase3,z_compressibility,mol_vol,bethaa] = ...
    flash3ssnewtonPR(nc,T,P,Z,Pc,Tc,w,kk,x_1,x_2,x_3,index)
tic
R=83.14;%bar.cm3/K.mol

%initialization of K values
K_value=zeros(nc,2);


%Because ai and bi are always the same, their calculation
%should not be performed in the function evaluation part because it adds
%extra useless oprations.

ai=zeros(1,nc); m=ai; bi=ai; %calculation of EOS's parameters

for i=1:nc
    %EOS's parameters
    if w(i)<0.49
        m(i)=0.37464+1.54226*w(i)-0.26992*w(i)^2;
    else
        m(i)=0.3796+1.485*w(i)-0.1644*w(i)^2+0.01667*w(i)^3;
    end
    ai(i)=0.45724*R^2*Tc(i)^2/Pc(i)*(1+m(i)*(1-(T/Tc(i))^0.5))^2;
    bi(i)=0.07780*R*Tc(i)/Pc(i);
    %K values
    if index==1
        K_value(i,1)=x_1(i,1)/x_3(i,1);
        K_value(i,2)=x_2(i,1)/x_3(i,1);
    else
        %K_value(i,1)=x_0(i,1)/Z(i,1);
    end

end

%The loop starts here
error=1; iter=1;
while error>0.000001
    %inner loop for finding fraction of phase1


      if iter==1;
        options = optimset('Jacobian','on', 'tolfun',.00000000001);
        bethaa=fsolve(@objectivefun,[.85;.15],options,nc,K_value,Z);
      else
        options = optimset('Jacobian','on', 'tolfun',.00000000001);

bethaa=fsolve(@objectivefun,[bethaa(1,1);bethaa(2,1)],options,nc,K_value,Z);
      end


%bethaa=fminsearch(@objectivefunmin,[0.5;0.5],[],nc,K_value,Z);

    %update mole fractions
    for i=1:nc
        x_phase1(i,1)=K_value(i,1)*Z(i,1)/(1+bethaa(1,1)*(K_value(i,1)-
1)+bethaa(2,1)*(K_value(i,2)-1));
        x_phase2(i,1)=K_value(i,2)*Z(i,1)/(1+bethaa(1,1)*(K_value(i,1)-
1)+bethaa(2,1)*(K_value(i,2)-1));
        x_phase3(i,1)=Z(i,1)/(1+bethaa(1,1)*(K_value(i,1)-
1)+bethaa(2,1)*(K_value(i,2)-1));
    end

    point(:,1)=x_phase1; point(:,2)=x_phase2; point(:,3)=x_phase3;
    sumaa=zeros(1,3); sumbb=sumaa; AA=sumaa; BB=sumaa; phyy=zeros(nc,3);
```

```
    for k=1:3
        for i=1:nc
            sumbb(k)=sumbb(k)+bi(i)*point(i,k);
            for j=1:nc
                sumaa(k)=sumaa(k)+point(i,k)*point(j,k)*(ai(i)*ai(j))^0.5*(1-
kk(i,j));
            end
        end
    end
    aa=sumaa; bb=sumbb;
    for k=1:3
        AA(k)=aa(k)*P/(R^2*T^2); BB(k)=bb(k)*P/(R*T);
    end
    zmax=zeros(1,3); zmin=zmax; nph=zmin; zz=zmax;

    % Calling roots function to find compressibility factor
    [zmax(1),zmin(1),nph(1)]= roots_1(AA(1),BB(1));
    [zmax(2),zmin(2),nph(2)]= roots_1(AA(2),BB(2));
    [zmax(3),zmin(3),nph(3)]= roots_1(AA(3),BB(3));

    for k=1:3
        if nph(k)==2
            gmin=zmin(k)-1-log(zmin(k)-BB(k))-
(AA(k)/(BB(k)*2*2^0.5))*(log((zmin(k)+(1+2^0.5)*BB(k))/(zmin(k)+(1-
2^0.5)*BB(k))));
            gmax=zmax(k)-1-log(zmax(k)-BB(k))-
(AA(k)/(BB(k)*2*2^0.5))*(log((zmax(k)+(1+2^0.5)*BB(k))/(zmax(k)+(1-
2^0.5)*BB(k))));
            if gmin<gmax
                zz(k)=zmin(k);
            else
                zz(k)=zmax(k);
            end
        else
            zz(k)=zmin(k);
        end
    end

    % Fugacities are calculated in this part
    for k=1:3
        for i=1:nc
            sumpoint=0;
            for j=1:nc
                sumpoint=sumpoint+point(j,k)*(ai(i)*ai(j))^0.5*(1-kk(i,j));
            end
            phyy(i,k)=(P*point(i,k))*exp(bi(i)/bb(k)*(zz(k)-1)-log(zz(k)-BB(k))-
(AA(k)/(BB(k)*2*2^0.5))*(2/aa(k)*sumpoint-bi(i)/bb(k))*
(log((zz(k)+(1+2^0.5)*BB(k))/(zz(k)+(1-2^0.5)*BB(k)))));

        end
    end

    %updating K values
    for i=1:nc
        K_value(i,1)=K_value(i,1)*(phyy(i,3)/phyy(i,1));
        K_value(i,2)=K_value(i,2)*(phyy(i,3)/phyy(i,2));
    end

    %checking the convergence

    norm_er(1)=max(abs(phyy(:,1)-phyy(:,2)));
    norm_er(2)=max(abs(phyy(:,1)-phyy(:,3)));
    norm_er(3)=max(abs(phyy(:,2)-phyy(:,3)));
    error=max(norm_er);
    iter=iter+1;

end

z_compressibility=zz;
for i=1:3
    mol_vol(i)=z_compressibility(i)*R*T/P;
```

```
end
toc

%-------------------------------------------------------------------%
% Function   : objectivefun                                         %
% Purpose    : evaluate the objective function and its Jacobian     %
%-------------------------------------------------------------------%
function [F,J] = objectivefun(bethaa,nc,K_value,Z)

    sumation=[0;0]; sumder=zeros(2,2);
        for i=1:nc
            sumation(1,1)=sumation(1,1)+(K_value(i,1)-
1)*Z(i,1)/(1+bethaa(1,1)*(K_value(i,1)-1)+bethaa(2,1)*(K_value(i,2)-1));
            sumation(2,1)=sumation(2,1)+(K_value(i,2)-
1)*Z(i,1)/(1+bethaa(1,1)*(K_value(i,1)-1)+bethaa(2,1)*(K_value(i,2)-1));
            sumder(1,1)=sumder(1,1)+((K_value(i,1)-
1)^2)*Z(i,1)/(1+bethaa(1,1)*(K_value(i,1)-1)+bethaa(2,1)*(K_value(i,2)-1))^2;
            sumder(1,2)=sumder(1,2)+(K_value(i,1)-1)*(K_value(i,2)-
1)*Z(i,1)/(1+bethaa(1,1)*(K_value(i,1)-1)+bethaa(2,1)*(K_value(i,2)-1))^2;
            sumder(2,2)=sumder(2,2)+((K_value(i,2)-
1)^2)*Z(i,1)/(1+bethaa(1,1)*(K_value(i,1)-1)+bethaa(2,1)*(K_value(i,2)-1))^2;
        end
        sumder(2,1)=sumder(1,2);

        F= sumation;
        J=-sumder;

%-------------------------------------------------------------------%
% Function   :  objectivefunmin                                     %
% Purpose    :  An alternative formulation                          %
%-------------------------------------------------------------------%
function F = objectivefunmin(bethaa,nc,K_value,Z)

    sumation=[0;0];
        for i=1:nc
            sumation(1,1)=sumation(1,1)+(K_value(i,1)-
1)*Z(i,1)/(1+bethaa(1,1)*(K_value(i,1)-1)+bethaa(2,1)*(K_value(i,2)-1));
            sumation(2,1)=sumation(2,1)+(K_value(i,2)-
1)*Z(i,1)/(1+bethaa(1,1)*(K_value(i,1)-1)+bethaa(2,1)*(K_value(i,2)-1));
        end
    F=sumation(1,1)^2+sumation(2,1)^2;

%-------------------------------------------------------------------%
% Function   :  roots_1                                             %
% Purpose    :  Evaluate Compressibility factors                    %
%-------------------------------------------------------------------%
function [zmax,zmin,nph]= roots_1(AA,BB)
    co(1) = 1;
    co(2) = -(1 - BB);
    co(3) = AA - 3 * BB ^ 2 - 2 * BB;
    co(4) = -(AA * BB - BB * BB - BB * BB * BB);
    r=roots(co);
    n=0;
    for i=1:3
        test=imag(r(i));
        test2=real(r(i));
        if (abs(test)<=1e-8 & test2>=0 & test2>=BB)
            n=n+1;
            y(n)=real(r(i));
        end
    end
    if n==1
        nph=1;
        zmax=y(n);
        zmin=zmax;
    end
    if n>1
        nph=2;
        zmax=max(y);
        zmin=min(y);
    end
```

Appendix 3
Experimental Phase Behaviour Data

Table A3.1. LLV-LL phase boundary data for the mixture of 25 wt.% AVR + 75 wt.% n-heptane

Temperature (C)	Pressure (kPa)
20	39
30	51
40	53
50	67
60	71
70	93
80	102
90	123
100	149
110	181
120	218
130	262
140	311
150	369
160	456
170	542
180	649
190	774
200	925
210	1095
220	1288
230	1514
240	1759
250	2037
260	2344
270	2632
280	2990
290	3365

Table A3.2. LLV-LL phase boundary data for the mixture of 25 wt.% AVR + 75 wt.% n-dodecane

Temperature (C)	Pressure (kPa)
160	16.9
170	23.1
180	32.8
190	44.5
200	61.8
210	83.1
220	101.8
230	132.8
240	159.0
250	196.2
260	232.8
270	283.8
280	344.5
290	407.3
300	487.3
310	581.1
320	716.2
330	808.7
340	965.2